

AWARD NUMBER: W81XWH-20-1-0202

TITLE: Prostate-Specific Membrane Antigen-Dependent Health Disparities in Prostate Cancer

PRINCIPAL INVESTIGATOR: Leslie A. Caromile

CONTRACTING ORGANIZATION: University of Connecticut Health Center, Farmington CT

REPORT DATE: October 2021

TYPE OF REPORT: Annual Report

PREPARED FOR: U.S. Army Medical Research and Development Command  
Fort Detrick, Maryland 21702-5012

DISTRIBUTION STATEMENT: Approved for Public Release;  
Distribution Unlimited

The views, opinions and/or findings contained in this report are those of the author(s) and should not be construed as an official Department of the Army position, policy or decision unless so designated by other documentation.

# REPORT DOCUMENTATION PAGE

Form Approved  
OMB No. 0704-0188

Public reporting burden for this collection of information is estimated to average 1 hour per response, including the time for reviewing instructions, searching existing data sources, gathering and maintaining the data needed, and completing and reviewing this collection of information. Send comments regarding this burden estimate or any other aspect of this collection of information, including suggestions for reducing this burden to Department of Defense, Washington Headquarters Services, Directorate for Information Operations and Reports (0704-0188), 1215 Jefferson Davis Highway, Suite 1204, Arlington, VA 22202-4302. Respondents should be aware that notwithstanding any other provision of law, no person shall be subject to any penalty for failing to comply with a collection of information if it does not display a currently valid OMB control number. PLEASE DO NOT RETURN YOUR FORM TO THE ABOVE ADDRESS.

<b>1. REPORT DATE</b> October 2021			<b>2. REPORT TYPE</b> Annual Report		<b>3. DATES COVERED</b> 30Sep2020-29Sep2021	
<b>4. TITLE AND SUBTITLE</b>  Prostate-Specific Membrane Antigen-Dependent Health Disparities in Prostate Cancer					<b>5a. CONTRACT NUMBER</b> W81XWH-20-1-0202	
					<b>5b. GRANT NUMBER</b>	
					<b>5c. PROGRAM ELEMENT NUMBER</b>	
<b>6. AUTHOR(S)</b> Leslie A. Caromile, PhD  E-Mail:caromile@uchc.edu					<b>5d. PROJECT NUMBER</b>	
					<b>5e. TASK NUMBER</b>	
					<b>5f. WORK UNIT NUMBER</b>	
<b>7. PERFORMING ORGANIZATION NAME(S) AND ADDRESS(ES)</b> University of Connecticut Health Center 263 Farmington Ave, Farmington CT 06030					<b>8. PERFORMING ORGANIZATION REPORT NUMBER</b>	
<b>9. SPONSORING / MONITORING AGENCY NAME(S) AND ADDRESS(ES)</b>  U.S. Army Medical Research and Development Command Fort Detrick, Maryland 21702-5012					<b>10. SPONSOR/MONITOR'S ACRONYM(S)</b>	
					<b>11. SPONSOR/MONITOR'S REPORT NUMBER(S)</b>	
<b>12. DISTRIBUTION / AVAILABILITY STATEMENT</b>  Approved for Public Release; Distribution Unlimited						
<b>13. SUPPLEMENTARY NOTES</b>						
<b>14. ABSTRACT</b> According to published data, African American (AA) men AA men are 1.6 times more susceptible to develop prostate cancer, and about 2 times more likely to die from this disease than men of European (EUR) decent. In fact, even when environmental factors are corrected for, the disparity in mortality rate between AA and EUR men is higher for prostate cancer than that for any other malignancy thus suggesting a molecular component. The Caromile lab is investigating if germ line single nucleotide polymorphisms, or SNPS, within certain components of the PSMA signaling pathway might contribute to the increased risk of prostate cancer in AA men vs that of EUR men. Investigation into these molecular mechanisms not only has the potential to improve the outcomes of all men with lethal prostate cancer but also has the capability to reduce prostate cancer disparities by improving detection, morbidity and mortality of lethal prostate cancer in AA and other at-risk populations through the identification of unique, tailored treatment and prevention strategies for each patient.						
<b>15. SUBJECT TERMS</b> Prostate cancer, prostate specific membrane antigen (PSMA), single nucleotide polymorphism (SNP), germline, genomic, bioinformatics, health disparity						
<b>16. SECURITY CLASSIFICATION OF:</b>			<b>17. LIMITATION OF ABSTRACT</b>  Unclassified	<b>18. NUMBER OF PAGES</b>  43	<b>19a. NAME OF RESPONSIBLE PERSON</b> USAMRMC	
<b>a. REPORT</b>  Unclassified	<b>b. ABSTRACT</b>  Unclassified	<b>c. THIS PAGE</b>  Unclassified			<b>19b. TELEPHONE NUMBER</b> (include area code)	

## **TABLE OF CONTENTS**

	<u>Page</u>
<b>1. Introduction</b>	<b>5</b>
<b>2. Keywords</b>	<b>6</b>
<b>3. Accomplishments</b>	<b>7</b>
<b>4. Impact</b>	<b>12</b>
<b>5. Changes/Problems</b>	<b>12</b>
<b>6. Products</b>	<b>12</b>
<b>7. Participants &amp; Other Collaborating Organizations</b>	<b>12</b>
<b>8. Special Reporting Requirements</b>	<b>12</b>
<b>9. Appendices</b>	<b>12</b>

## **1. Introduction:**

According to published data, African American (AA) men are 1.6 times more susceptible to develop prostate cancer, and about 2 times more likely to die from this disease than men of European (EUR) descent. In fact, even when environmental factors are corrected for, the disparity in mortality rate between AA and EUR men is higher for prostate cancer than that for any other malignancy thus suggesting a molecular component. The Caromile lab is investigating if germ line single nucleotide polymorphisms, or SNPS, within certain components of the PSMA signaling pathway might contribute to the increased risk of prostate cancer in AA men vs that of EUR men. Investigation into these molecular mechanisms not only has the potential to improve the outcomes of all men with lethal prostate cancer but also has the capability to reduce prostate cancer disparities by improving detection, morbidity and mortality of lethal prostate cancer in AA and other at-risk populations through the identification of unique, tailored treatment and prevention strategies for each patient.

**2. Key Words:** Prostate cancer, prostate specific membrane antigen (PSMA), single nucleotide polymorphism (SNP), germline, genomic, bioinformatics, health disparity

### 3. Accomplishments:

Over the past year – I was able to get some of my proposed work started but due to loss of scientific supply chain (especially for pipet tips, gloves, serological pipets and both PCR and sequencing reagents), loss of workforce, cut back on core facility services and trimmed back administrative services – I haven't got as much done as I normally would. I am located in Connecticut and state employees just recently returned to the office (August, 2021)! I know that everyone is in the same boat, so in this report I will be discussing results from the parts of the project that I was able to collect as well as what I plan on doing in the future to catch up with this loss of productivity. I do want to preface this report by mentioning that since I could not get the supplies that I needed to approach many aspects of this project, I waited as long as I could to initiate the funding. I did not exhaust my salary.

**Major Activities:** All of the activities in this report were part of Aim 1 and Aim 2.

### Major Goals of the project:

Below is the statement of work as presented in the grant:

Specific Aim 1(specified in proposal)	Timeline	Site 1
<b>Determine whether AA men have a higher risk of a known panel of SNPs vs that of CA men and the effect of these SNPs on clinical metabolites.</b>		
Genotype archived tissue of AA and CA PC patients for polygenic risk of a known panel of SNPs.	1-18	Post Doctoral Fellow ~700 de-identified, FFPE patient samples
Statistical Analysis of MAF, Haplotype and Risk. Associate the levels of glutamate or folate to the SNPs in the PSMA dependent pathway	1-6	Dr. Kuo and Post Doctoral Fellow
Whole-exome sequencing to discover additional SNPs that influence PC in EUR vs AA Men.		Dr. Caromile and Post-Doctoral Fellow
Mathematically model PSMA-dependent crosstalk and the effects of SNPs on the pathway components:	25-30	Dr. Caromile, Dr. Laubenbacher
<i>Milestones: Comprehensive data revealing a panel of PSMA pathway related SNPs the correlate with PC risk. Validation of mathematical models ability to predict outcomes of intervention; publication of peer-reviewed papers.</i>		
<b>Specific Aim 2 (Specified in Proposal)</b>		
<b>Comprehensively characterize functional effects of a known panel of SNPs on intracellular crosstalk among PSMA dependent pathways and their effects on PC tumor growth <i>in vivo</i>.</b>	1-18	
Generate molecular and phenotypic data from a panel of PC cell lines treated with and without pathway specific inhibitors.	1-12	Dr. Caromile and Post Doctoral Fellow
Evaluate molecular and phenotypic effects on PC lines engineered to express bar coded SNPs	1-18	Dr. Caromile and Post Doctoral Fellow
In vivo evaluation of PC cell lines engineered to express unique barcoded SNPs on a tumor growth and dissemination mouse model.	6-12	Dr. Caromile and Post Doctoral Fellow ~200 mice
<i>Milestone: Identify SNPs, single or in combination or that have a functional effects in vivo and in vitro as well as in tumor progression.</i>		
Local IACUC Approval for proposed methods.	12	Dr. Caromile

**Specific objectives and Significant Results:**

Aim 1: Determine whether AA men have a higher risk of a known panel of SNPs vs that of CA men and the effect of these SNPs on clinical metabolites.

a. *Obtained patient samples and stratified by them by National Cancer Comprehensive Network resource stratification criteria:*

Through the UCONN Health Research Biorepository, we obtained our first set of 100 de-identified, formalin-fixed paraffin-embedded (FFPE) from consented AA and EUR patients who have self-identified as either European/non-Hispanic or African American/non-Hispanic, whom were confirmed to have PC and have undergone radical prostatectomy at UCONN Health. Pathology reports were provided for all patient samples. Patient samples were then stratified into *highly aggressive* where the GS sum  $\geq 8$ , or PSA  $>20$  ng/ml and  $>10\%$  probability of pelvic lymph node involvement; *low aggressive* where GS sum  $\leq 7$ , or PSA  $\leq 20$ ng/ml and  $< 10\%$  probability of pelvic lymph node involvement. All of our stratification was verified by our in-house pathologist, Mary Melinda Sanders, MD.

*Significant Data from Section a:*

In this sample set, we found that a higher number of EUR individuals whom have had prostatectomies at UCONN Health, had primary prostate tumors that were of a higher grade than that of AA individuals. Attached is a samples of a pathology report that we received for 16 patents.

	EUR	AA
<b>Average Age</b>	<b>62.6</b>	<b>61</b>
<b>Highly Aggressive (Gleason Score <math>\geq 8</math>)</b>	<b>14</b>	<b>20</b>
<b>Low Aggressive (Gleason Score <math>\leq 7</math>)</b>	<b>40</b>	<b>30</b>

b. *PSMA verification and localization in patient tissue:*

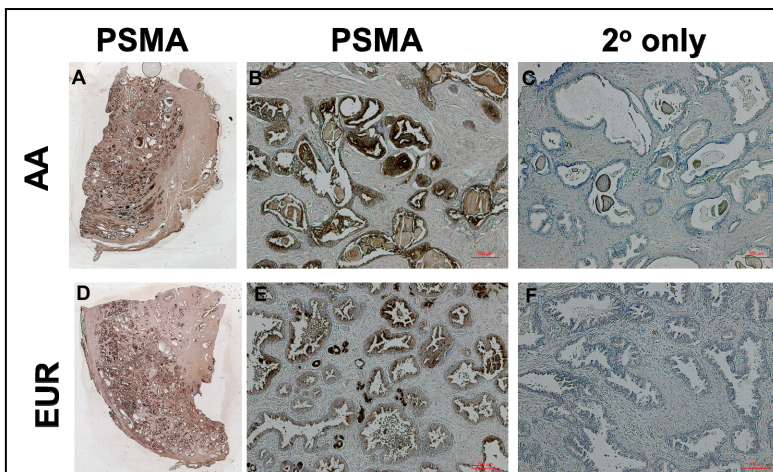
Although PSMA is present in ~80-90% of all PC primary tumors the presence and localization of PSMA will be verified in each patient sample by the following methods:

i. *Immunohistochemistry (IHC):*

PSMA presence and localization within the PC tumor was validated on sections of FFPE tissue from each patient. Secondary antibody only control was used to assess non-specific background staining.

*Significant Data from Section i:*

Our data showed that all our patient samples had varying levels of PSMA protein staining via IHC. The below image is an example of our results: A, D Is a slide scan of 2 patient’s entire tumor sample. They are stained for PSMA protein expression (brown). B, E Are the same samples stained with PSMA antibody (Cell Signaling D718E). PSMA is localized to the glandular area (5x), C, F is a secondary antibody only control indicating negligible background staining (5x). Samples were counterstained with hematoxylin.

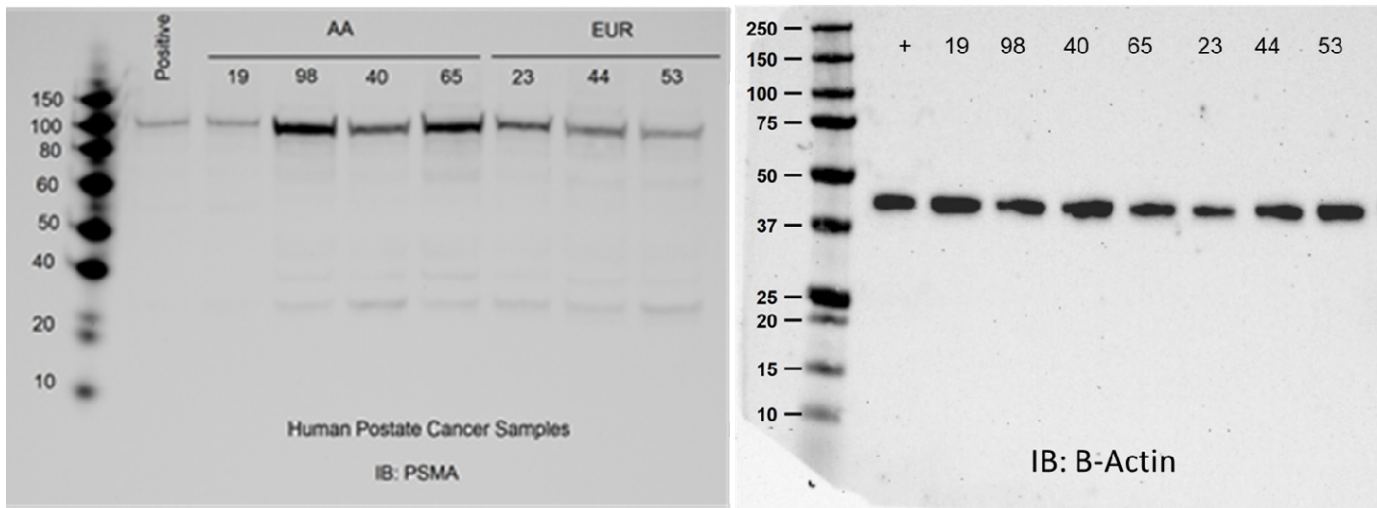


ii) *Western blot analysis*

PSMA protein expression in patient tissue samples was verified by western blot protein expression using PSMA antibody (Cell Signaling D718E) and normalizing to a  $\beta$ -actin loading control (Cell Signaling D6A8).

*Significant Data from Section ii:*

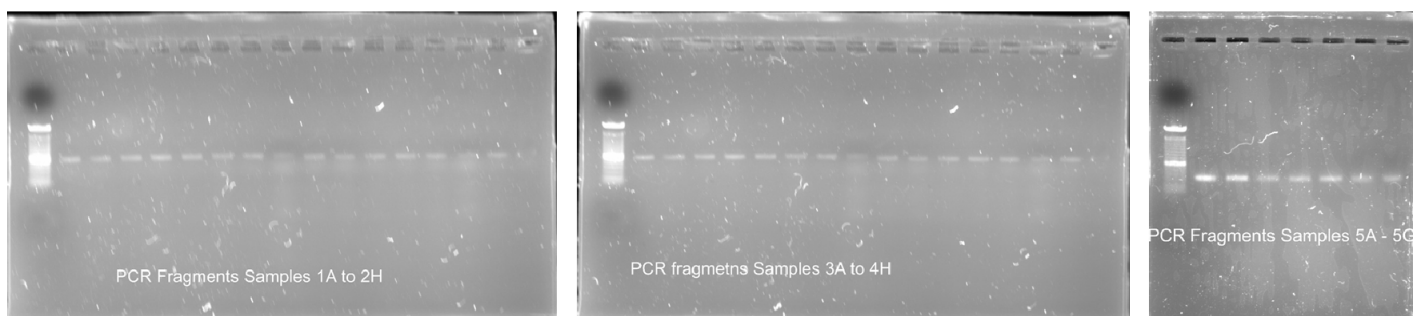
The representative western blot image below shows that PSMA is detectable in protein extracted from our FFPE patient tissue samples. We used an immortalized human prostate cancer cell line LnCaP as a positive control.



**c. SNP Verification in gDNA from Patient Tissue:**

To start to approach this objective, we used the Applied Biosystems SeqStudio Genetic Analyzer and Data Collection Software to verify if the SNPs in the below panel were present in the genome of each patient. Commercially available and validated, M13 labeled primers were used to perform Sanger sequencing analysis. Using the Big Dye Kit, we ran both the PCR step and the cycle sequencing step seen below and then sent our samples to be cleaned and analyzed by the UCONN Sequencing Core.

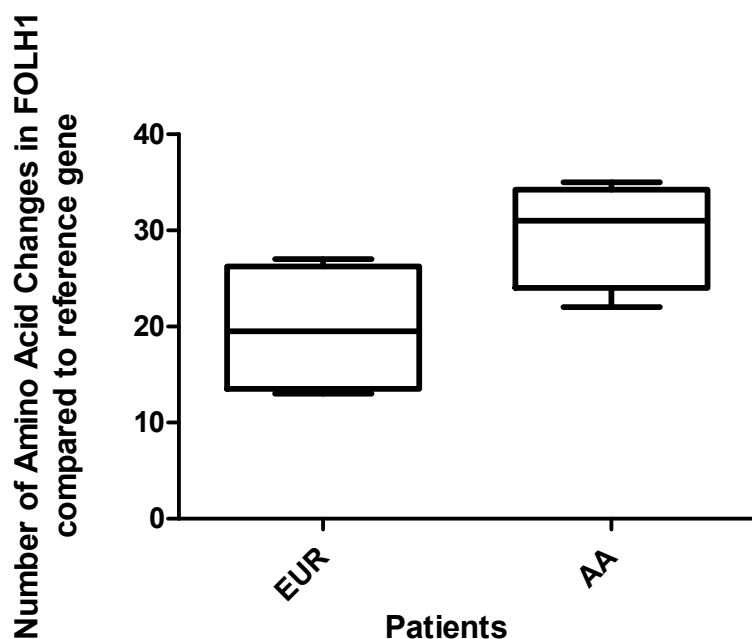
<b>PCR/Sanger Sequencing Primer Pairs</b>						
<u>Gene</u>	<u>Coding SNP</u>	<u>Amino Acid Coordinate</u>	<u>Location</u>	<u>Alleles (Ancestral /MAF)</u>	<u>Amplicon Length (BP)</u>	<u>Assay ID</u>
FOLH1	rs202676	Y75H	Chromosome 11: 49,206,018-49,206,118	A/G	274	Hs00648640_CE
FOLH1	rs202680	A111A	Chromosome 11: 49,200,283-49,200,383	T/A	274	Hs00594720_CE
FOLH1	rs182169	D244E	Chromosome 11: 49,185,713-49,185,813	A/C/G	500	Hs00329578_CE
FOLR3	rs1802609	R26W	Chromosome 11: 72,135,984-72,136,084	C/A/T	498	Hs00108820_CE
SLC7A11	rs6838248	A224A	Chromosome 4: 138,219,290 - 138,219,390	G/C/T	496	Hs00254036_CE
GRM1	rs6923492	S993P	Chromosome 6: 146,434,138 - 146,434,238	T/C	499	Hs00282287_CE
GRM5	rs61741175	T453R/M	Chromosome 11: 88,604,704-	G/A/C	274	Hs00675325_CE



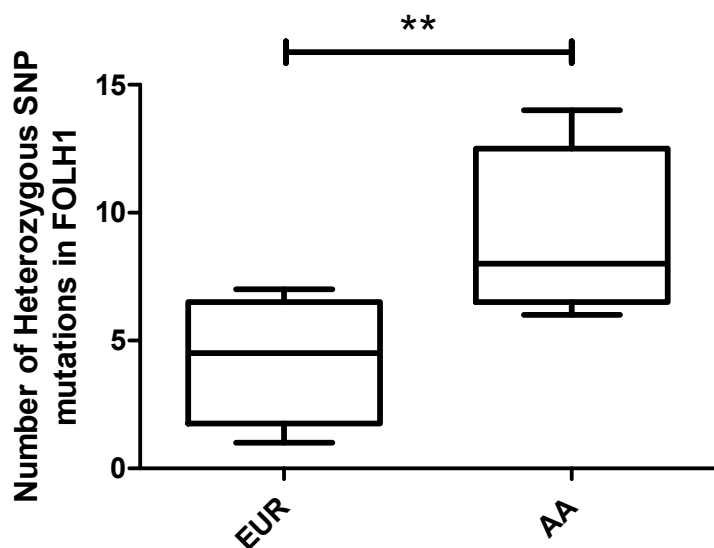
### *Significant Data from Section c:*

At this point, we had exhausted our supply of sequencing reagents. Due to the closure of our UCONN Health Histology Core, the UCONN Health Biorepository Core and the UCONN Sequencing Facility during COVID shutdown, we were unable to obtain more patient samples at this time or section the FFPE blocks that we had in the lab and the UCONN Sequencing Core was no longer accepting orders. Additionally, graduate students, lab personnel and administrative personnel were not allowed to be in the laboratory at this time and the lab was shuttered. Therefore, while working from home, we were able to do some data analysis.

Using Sequencher Software, we created a variance table that summarized all the differences between each consensus sequence and its corresponding gene reference sequence. We then validated our data by linking each cell in our data analysis to a base call. This made it easy to find out if the SNPs in our patient panel was present. We were also able to identify novel SNPs and ones that were not in our panel. This data is extremely comprehensive and I cannot include it here, however, as an example, we were able to show that in our patient sample set, our AA data set contained nearly twice as many amino acid changes in FOLH1 (the gene that encodes PSMA), than our EUR patient set. See below graph.



We also analyzed our data for the presence of heterozygous SNPs by modifying the base caller settings to analyze polymorphic positions which show both nucleotides simultaneously. Our data showed that of all the SNPs identified in this data set, our AA data set contained significantly more heterozygous SNPs in FOLH1 than our EUR patient set. See below graph.



Once key personnel were allowed to return to the lab, and we still could not get sequencing reagents, I made the decision to switch to directions and begin to address the questions in Aim 2 so that the project could continue to have forward momentum. Below we used a combination of wet lab and *in silico* techniques to gather data.

**Aim 2: Comprehensively characterize functional effects of a known panel of SNPs on intracellular crosstalk among PSMA dependent pathways and their effects on PC tumor growth *in vivo*.**

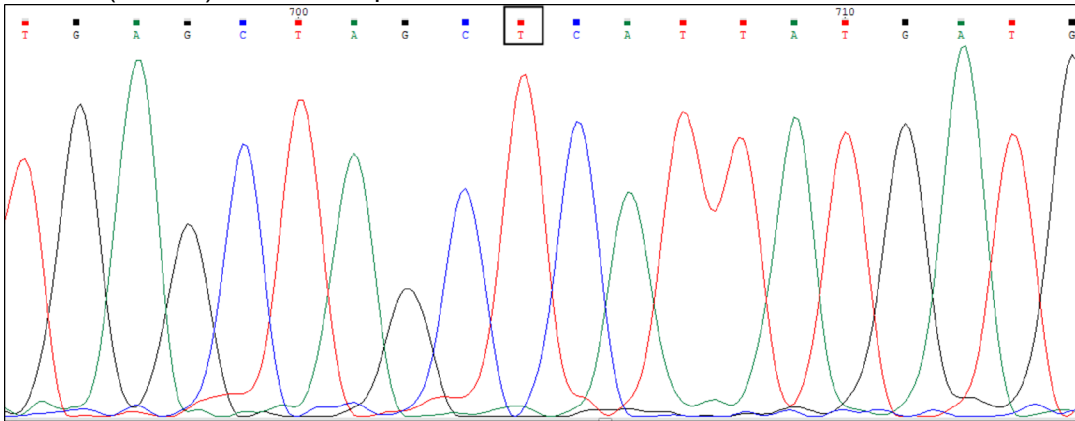
a. *Prediction of biological effects of SNPs*

Using PredictSNP analysis, which predicts the biological effects of one SNP at a time, we saw that not all SNPs were deleterious when expressed alone (see below an example of Predict SNP on SNPs in FOLH1). However, when the SNP's were expressed in combination, we believe that there will be a more amplified biological effect.

RESULTS		neutral	deleterious	XX % expected accuracy				
Annotation	Mutation	PredictSNP	MAPP	PhD-SNP	PolyPhen-1	PolyPhen-2	SIFT	SNAP
	Y75H	83 %	71 %	78 %	67 %	87 %	75 %	77 %
*	V108A	74 %	73 %	58 %	67 %	73 %	90 %	71 %
*	P160S	74 %	74 %	66 %	67 %	41 %	61 %	67 %
*	Y176H	87 %	43 %	88 %	74 %	81 %	53 %	89 %
*	R190W	61 %	64 %	58 %	59 %	40 %	79 %	50 %
*	G206R	87 %	91 %	86 %	74 %	81 %	53 %	87 %
	D244E	83 %	71 %	55 %	67 %	87 %	71 %	77 %
*	G245S	65 %	80 %	58 %	67 %	56 %	67 %	67 %
*	G250R	61 %	64 %	77 %	74 %	65 %	79 %	50 %
*	E424Q	72 %	71 %	82 %	74 %	81 %	79 %	72 %
*	H475Y	83 %	71 %	83 %	67 %	87 %	90 %	83 %
*	D520E	87 %	43 %	77 %	74 %	60 %	79 %	81 %

b. *Design and production of SNPs by site directed mutagenesis and cloning:*

We recreated all of the hPSMA SNPs in our panel above in both the hPSMA PBM-Puro Myc/His and hPSMA pQCXIP-F-luc Myc/His plasmids by site directed mutagenesis (GeneArt Site-Directed Mutagenesis PLUS System, Thermo Fisher, Cat# A14604 ). I have attached a chromatograph for the silent SNP rs202680 in FOLH1 (A111A) as an example. Codon GCC was mutated to GCT.



We then transduced the following cell lines with our SNPs. Information on hPSMA knockout CRISPR 22Rv1 and hPSMA knockout CRISPR C4-2B can be found in recent publications by Leslie A. Caromile. These publications are in the appendix.

Hosts:

hPSMA knockout CRISPR LnCaP  
hPSMA knockout CRISPR 22Rv1  
hPSMA knockout CRISPR C4-2B  
hPSMA knockout CRISPR MDA PCa 2b  
PC-3, Du145 and RWPE1

All of these cell lines are currently being analyzed for phenotypic and metabolic changes.

*b. Animal protocol and IBC:*

An animal protocol and IBC were submitted for this project and took close to 8 months to be approved due to staffing shortage and subsequent backlog.

**Training and professional development opportunities:**

Although this project was not intended to provide training and professional development, it did so in the following ways: I was invited to be an occasional reviewer for the Journal for Ethnic and Racial Health Disparities. This is ongoing and a wonderful opportunity for me to learn more about the field in general. Additionally, I have recently been in contact with the UCONN professional science master's program in Applied Genomics. The students are required to complete a semester internship as part of their curriculum. I will be hosting a student in my lab early next year and they will be very helpful with analysis of the sequencing and phenotypic data.

**How were the results disseminated to communities of interest?** Nothing to report.

**What do you plan to do during the next reporting period to accomplish the goals?**

As mentioned throughout this section, COVID significantly impacted our ability to reach the milestones that were set in the statement of work. There are many ways that I will be addressing this in the next funding cycle. Since the supply chain is picking up a little bit and the UCONN Core facilities are now open, we can move forward with the sequencing and genotyping. During this reporting period, I was the only person working on the project. Our statistician, Dr. Kuo, did not have data to analyze and therefore did not draw salary. Besides the supply chain issues that occurred over the last year, there is an ongoing labor shortage and I truly believe that this made an additional impact on my research. However, I currently have 1 master's student, Romoye Sohan, who will be working on Aim 1. Romoye is in a program called Young Innovative Investigator Program (<https://health.uconn.edu/connecticut-convergence-institute/young-innovative-investigator-program/>) and her salary is 100% and supplies are covered through her program. I had an extremely difficult time finding

a postdoc for this project as we still cannot offer positions to individuals in countries that have high rates of COVID transmission (attached advertisement). I advertised for 8 months through UCONN Health postdoctoral association, SACNAS, Minority Postdoc, LinkedIn, Handshake (included 19 universities) and Indeed. Overall, I had 3 qualified applicants. I am happy to say that I recently hired a postdoc, Amir Yarahmadi, who will be working on Aim 2. As previously mentioned, I have recently been in contact with the UCONN professional science master's program in Applied Genomics. The students are required to complete a semester internship as part of their curriculum. I will be hosting a student, Ghaida Alahmadi, in my lab early next year and they will be very helpful with analysis of the sequencing and phenotype data. They will be receiving class credit and therefore will not be compensated. I will also be taking 1 rotation student from the UCONN PhD in the Biomedical Sciences Program. I truly believe, with all this extra help, we will be able to make up for lost time.

**4. Impact:** Nothing to report.

**5. Changes and Problems:**

*a. Changes in approach and reasons for change*

Due to the COVID related loss of scientific supply chain (especially for pipet tips, gloves, serological pipets and both PCR and sequencing reagents), loss of workforce, cut back on core facility services and trimmed back administrative services, we had to be creative when it came to approaching the project. However, once we had exhausted our supply of reagents, continuing wet lab work became difficult and we did switch to data analysis. Additionally, graduate students, lab personnel and administrative personnel were not allowed to be in the laboratory at this time and the lab was shuttered. Once key personnel was allowed to return to the lab, I made the decision to switch to directions and begin to address the questions that could be answered with reagents that were available. We are still behind as all PCR and sequencing related products are currently being prioritized for clinical use due to COVID. We have recently ordered PCR plates from BioRad (October 19, 2021) and there is currently a 20 week wait. However, reagents are starting to trickle in and I'm confident that we can begin to steam ahead. Due to the lab closures, loss of scientific supply chain, loss of workforce, cut back on core facility services and trimmed back administrative services, we spent a lot less than anticipated. In fact, I waited as long as I could to initiate the funding and I did not exhaust my salary. Going forward, we plan to catch up on spending.

**Significant changes in use or care of human subjects, vertebrate animals, biohazards and/or select agents:** nothing to report

**6. Products:** Nothing to report.

**7. Participants & Other Collaborating Organizations:**

Individuals that have worked on the project:

Name:	<i>Leslie Caromile</i>
Project Role:	<i>PI</i>
Researcher Identifier (e.g. ORCID ID):	0000-0003-2193-5190
Nearest person month worked:	<i>4.2</i>
Contribution to Project:	<i>No change</i>
Funding Support:	<i>No change</i>

**7. Special Reporting Requirements:** Nothing to Report

**8. Appendices:** See attached

**Dr. Caromile prostate slides from UCONN Health Biorepository**

**All patients from UCONN Health**

Caucasian	African American
<p>S04-6223 - 62 M. DIAGNOSIS:</p> <p>A. (Left pelvic lymph node): Four (4) lymph nodes, negative for tumor.</p> <p>B. (Right pelvic lymph node): One (1) lymph node, negative for tumor.</p> <p>C. (Prostate, radical prostatectomy):                      Prostatic adenocarcinoma, Gleason score 3 + 4 = 7</p> <ul style="list-style-type: none"> <li>-Tumor involves sections from:                             <ul style="list-style-type: none"> <li>-right and left apex</li> <li>-right and left mid</li> <li>-right and left base</li> </ul> </li> <li>-Tumor is focally present in the right seminal vesicle.</li> <li>-Margins: Tumor is focally present at the following inked margins:                             <ul style="list-style-type: none"> <li>-right apex, posterior</li> <li>-right and left mid, anterior</li> <li>-left mid, posterior</li> <li>-right and left base, posterior</li> </ul> </li> <li>-Foci of high grade PIN are present</li> <li>-Perineural invasion: Present</li> <li>-Lymphovascular involvement: No definite involvement observed.</li> <li>-Tumor quantitation: Approximately 30% of prostatic tissue involved.</li> <li>-PTNM: pT3, pN0, pMX.</li> </ul>	<p>S06-4220 54/M. DIAGNOSIS:</p> <p>Prostate, (part C) radical prostatectomy:                      Prostatic adenocarcinoma, margins are uninvolved by tumor.</p> <p>Gleason's Grade: 3+4=7</p> <p>Lobes involved: Left and right lobes</p> <p>Percent parenchyma involved: Tumor involve approximately 15% of left lobe and 20% of right lobe</p> <p>Resection margins: Uninvolved by tumor</p> <p>Extraprostatic (extracapsular) involvement: Absent</p> <p>Seminal vesicles: Uninvolved by tumor</p> <p>Perineural invasion: Absent</p> <p>Prostatic intraepithelial neoplasia: Absent</p> <p>Non-neoplastic prostate shows: Benign nodular hyperplasia</p> <p>Lymph nodes, right pelvic (part B) excision:                      Negative for metastatic carcinoma (0/4 nodes)</p> <p>Lymph nodes, left pelvic, (part A) excision:                      Negative for metastatic carcinoma (0/2 nodes)</p> <p>Pathologic stage: pT2c pN0 pMX</p>
<p>S04-1244 A22- 61/M. DIAGNOSIS:</p> <p>A. (Prostate, radical prostatectomy): Prostatic adenocarcinoma, Gleason score 3 + 4.</p> <ul style="list-style-type: none"> <li>-Tumor involves right mid, left mid and left base of prostate gland. (Approximately 10% involvement of prostatic tissue).</li> <li>-Left seminal vesicle shows invasion by prostatic carcinoma.</li> <li>-Perineural invasion is focally present.</li> <li>-The surgical margins of resection are uninvolved.</li> <li>-Lymphovascular invasion: Not observed.</li> </ul> <p>B. (Left pelvic lymph node): One (1) lymph node, negative for tumor.</p> <p>C. (Right pelvic lymph node): Three (3) lymph nodes, negative for tumor.</p>	<p>S06-6698 C16- 66/M. DIAGNOSIS:</p> <p>A. (Specimen labeled left pelvic lymph nodes): Three reactive lymph nodes; no evidence of malignancy.</p> <p>B. (Specimen labeled right pelvic lymph nodes): Three reactive lymph nodes; no evidence of malignancy.</p> <p>C. (Specimen labeled prostate): Infiltrating adenocarcinoma of prostate (primary pattern III to IV, secondary pattern IV Gleason grade VII or VIII of maximum X occupying approximately 5% of total prostatic tissue in the area corresponding to left posterior close to the transitional base 'C16 to C18'. Focal low-grade carcinoma as well as several foci of intraepithelial prostatic neoplasia are also noted.</p> <p>The infiltrating carcinoma show perineural invasion and focally involves prostatic capsule, however, the surgical margins of resection are free of tumor.</p> <p>The seminal vesicles and vas as well as the apex and base margin are free of tumor.</p>
<p>S04-2653 A22- 64/M. DIAGNOSIS:</p> <p>A. (Specimen labeled prostate): Infiltrating adenocarcinoma of prostate, primary pattern III,</p>	<p>S04-6919 C18- 67/M. A. (Specimen labeled left pelvic lymph node): Benign reactive node.</p>

<p>secondary pattern III, Gleason grade VI of maximum X. The cancer is scattered throughout the prostate involving sections corresponding to apex, mid zone, base, both on the right and left and anterior and posterior parts in various quantities and distributions. Overall, the tumor burden is moderate and occupies approximately 35% of the entire tissue. Seminal vesicles and vas deferens are not involved. The inked margins of resection are free of tumor, one exception could be "A13" at mid posterior left zone, cancer reaches to extreme proximity of the inked margin of resection in one microscopic focus (less than 1/10th of a millimeter); otherwise the inked margins are free of tumor. In addition, however, a focus of cancer is present in sections taken as apex, however, in which the cancer is mostly in the center of the specimen, however, reaches to the red color inked margin also.</p> <p>B. (Specimen labeled left pelvic lymph node): Five reactive lymph nodes; no evidence of malignancy.</p> <p>C. (Specimen labeled right pelvic lymph node): Eight reactive lymph nodes; no evidence of malignancy.</p>	<p>B. (Specimen labeled right pelvic node): Benign reactive node.</p> <p>C. (Specimen labeled prostate): Infiltrating adenocarcinoma of prostate predominantly involving the right anterior portion of middle lobe but occasionally extending to the posterior area. The cancer involves approximately 25% of the tissue. Gleason primary grade III, secondary pattern III, total Gleason grade VI of maximum X.</p> <p>The cancer reaches to extreme proximity (less than 1/10th of a millimeter) of surgical margin of resection (red ink). Left portion of the prostate. The seminal vesicles apical, basal and the remainder of margins are free of tumor.</p> <p>Extensive prostatic hyperplasia, chronic prostatitis, focal atrophy and inflammation are noted.</p> <p>No perineural invasion or vascular invasion are present, however, the capsule is infiltrated by prostatic carcinoma.</p>
<p>S04-7234 C16- 67/M. DIAGNOSIS:</p> <p>A. (Specimen labeled left pelvic lymph nodes): Two reactive nodes; no evidence of malignancy.</p> <p>B. (Specimen labeled right pelvic lymph nodes): Two reactive lymph nodes; no evidence of malignancy.</p> <p>C. (Specimen labeled Prostate): Infiltrating adenocarcinoma of prostate; primary pattern III, secondary pattern III, Gleason grade VI of maximum X.</p> <p>The cancer infiltrates into the prostatic capsule but does not cross it. The cancer approaches the surgical margin of resection to less than 1/10th of a millimeter in several foci.</p> <p>Apical and base margins of resection are free of tumor. The seminal vesicle and cord show no prostatic carcinoma, however, left seminal vesicle shows a few areas of cribriform proliferation that is considered to be atypical. These foci show intact myoepithelial cells. Spermatic cords are unremarkable. The cancer burden is not heavy, however, a small foci of cancer are present in many sections from C12 to C20 representing the mid portion of prostate from right to left anterior and posterior areas. The heaviest area of involvement is in C16 corresponding to mid posterior lobe on the left. Perineural or vascular invasion are not noted</p>	<p>S06-6863 C19- 55/M. DIAGNOSIS:</p> <p>A. (Specimen labeled left pelvic nodes): Three reactive nodes; no evidence of malignancy.</p> <p>B. (Specimen labeled right pelvic nodes): Four reactive nodes; no evidence of malignancy.</p> <p>C. (Specimen labeled prostate): Infiltrating adenocarcinoma of prostate.</p> <p>Primary pattern III, secondary pattern IV (Grade IV prostate cancer is noted only in two small microscopic areas, C16 and C17). Gleason grade VII of maximum X.</p> <p>Cancer involves almost all sections of prostate and occupies approximately 40% of prostatic mass tissue. Prostatic capsule and periprostatic soft tissue are focally involved. Margins of resection are involved in several areas 'C1, C2, C12, C13, C15, C19, C18, C20'. C1 and C2 correspond to apex margins and C20 shows involvement of the soft tissue at the junction between prostatic ducts and seminal vesicle. The actual seminal vesicle wall is not involved. Spermatic cords are not involved.</p>
<p>S06-601 C2-63/M. DIAGNOSIS:</p> <p>A. (Specimen labeled right pelvic lymph nodes): Four lymph nodes; no evidence of malignancy.</p> <p>B. (Specimen labeled left pelvic lymph nodes): Four reactive nodes; no evidence of malignancy.</p> <p>C. (Specimen labeled prostate): - Infiltrating adenocarcinoma of prostate,</p>	<p>S06-4703 A7- 56/M. DIAGNOSIS: (Specimen labeled prostate): Infiltrating adenocarcinoma of prostate predominantly involving right posterior lobe but also focally noted in the right anterior area of the prostate. Numerous foci of carcinoma in-situ (PIN, high grade) are present.</p>

<ul style="list-style-type: none"> <li>- Grade: Primary pattern IV, secondary pattern V, grade IX of maximum X based on Gleason's classification.</li> <li>- Multiple foci of perineural invasion and a focus of lymphatic/vascular invasion is noted.</li> <li>- The tumor infiltrates into the capsule of prostate at the region at the vicinity of seminal vesicles and cord, extensively.</li> <li>- Seminal vesicle and cord are involved with cancer, more severely on the right.</li> <li>- Tumor burden is not very high comprising approximately 5% of the total prostatic tissue. However, it is of high-grade, widely invasive and extends into prostatic capsule with involvement of seminal vesicle.</li> <li>- The apical and base margins are not involved.</li> <li>- TNM classification: T3b, N0, MX.</li> </ul>	<p>Extensive perineural and periganglionic infiltration is present. Vascular invasion not noted.</p> <p>Margins of resection are free of tumor with the exception of one microscopic focus in which perineural invasion extends to extreme proximity of cauterized margin of resection (between 1/10th of a millimeter and 1/2 millimeter). The region of involvement corresponds to the right posterior lobe at the basal end of the lobe.</p> <p>Seminal vesicle and cord as well as sections of the apex and base margins are free of tumor.</p> <p>Gleason grading (primary pattern III, secondary pattern IV, total grade VII of maximum X).</p>
<p>S06-6525 C2- 57/M. DIAGNOSIS:</p> <p>A. (Specimen labeled left pelvic node): Two reactive nodes; no evidence of malignancy.</p> <p>B. (Specimen labeled right pelvic node): Two of the four lymph-nodes show complete replacement by metastatic prostatic adenocarcinoma with capsular and extranodal extension involving surrounding soft tissue.</p> <p>C. (Specimen labeled prostate): Infiltrating prostatic adenocarcinoma involving, all sections of prostate and in many occupying the bulk of prostatic tissue, (approximately 75% of the prostatic tissue is composed of prostatic carcinoma).</p> <p>Gleason grade: Primary pattern IV, secondary pattern V, Gleason grade IX of maximum X.</p> <p>Focal lymphovascular and perineural invasion are noted. Margins; Right and left apex and base show infiltration by prostatic carcinoma involving the inked margin at section C2 corresponding to right base. The remainder of involvement is within the substance of the sections and does not involve the inked margin. The margin of resection 'C13' corresponding to right posterior area show significant involvement of margin of resection. Other focal microscopic areas of involvement of the margin of resection are noted.</p> <p>The prostatic capsule and periprostatic adipose tissue show frequent microscopic involvement.</p> <p>Both right and left seminal vesicles are involved with prostatic carcinoma including intralymphatic involvement. The margin of resection of the section 'C18' including the seminal vesicle show involvement with prostatic carcinoma.</p> <p>TNM stage: pT3b, N1, MX.</p>	<p>S06-6565 F1- 76/M. DIAGNOSIS:</p> <p>A. (Specimen labeled prostate, right base): Benign prostatic hyperplasia.</p> <p>B. (Specimen labeled prostate, right mid): Benign prostatic hyperplasia.</p> <p>C. (Specimen labeled prostate, right apex): Benign prostatic hyperplasia.</p> <p>D. (Specimen labeled prostate, right transitional base): A microscopic focus of infiltrating prostatic adenocarcinoma comprising less than 1/10th of the tissue mass. (Primary pattern IV, secondary pattern III, Gleason grade VII of X).</p> <p>It is noteworthy that the amount of cancerous tissue is extremely small comprising 10 glands total and thus note adequate for accurate grading.</p>
<p>S04-6866 C22- 61/M. DIAGNOSIS:</p> <p>A. Left pelvic lymph node, biopsy:</p> <ul style="list-style-type: none"> <li>- Two lymph nodes, free of carcinoma (0/2).</li> </ul> <p>B. Right pelvic lymph node, biopsy:</p> <ul style="list-style-type: none"> <li>- Four lymph nodes, free of carcinoma (0/4).</li> </ul>	<p>S04-6794 A20-52/M. DIAGNOSIS:</p> <p>(Prostate, radical prostatectomy):</p> <p>Prostatic adenocarcinoma, Gleason score: 3 + 3 = 6</p> <p>Tumor involves sections labeled:</p> <ul style="list-style-type: none"> <li>-Right apex</li> </ul>

<p>C. Prostate, radical prostatectomy:</p> <ul style="list-style-type: none"> <li>- Prostatic adenocarcinoma, Gleason pattern 3, 3 (score = 6) involving approximately 66% of both lobes of the prostate (see comment).</li> <li>- Carcinoma approaches within 1 millimeter of the inked resection margin in the mid right posterior as well as mid left anterior resection margin (Slides C18, C22, C28).</li> <li>- No extraprostatic extension noted.</li> <li>- Perineural invasion identified.</li> </ul> <ul style="list-style-type: none"> <li>- High grade prostatic intraepithelial neoplasia present.</li> <li>- Apical as well as basal urethral resection margins, free of carcinoma.</li> <li>- Both vasa deferentia and seminal vesicles, free of carcinoma.</li> <li>- Focal acute prostatitis.</li> </ul> <p>TNM stage: pT2c pN0 pMX.</p>	<ul style="list-style-type: none"> <li>-Right mid</li> <li>-Left apex</li> <li>-Margins: Tumor is focal present at inked margins of resection at right mid posterior and right apex posterior.</li> <li>-Perineural invasion: Present</li> <li>-Lymphovascular invasion: Not observed</li> <li>-Proportion of prostatic tissue involvement: Less than 10%</li> <li>-Focal high grade PIN present</li> <li>-The right and left seminal vesicles and vas ampullary stumps are uninvolved</li> <li>-pTNM: pT2c, pNX, pMX</li> </ul>
<p>S06-4082 C13-66/M. DIAGNOSIS:</p> <p>A. Lymph nodes, left: Negative lymph nodes (3).  B. Lymph nodes, right: Negative lymph nodes (4).  C. Prostate, radical prostatectomy:  Adenocarcinoma of the prostate.  Gleason patterns: 3 and 5  Gleason score: 8  Tumor quantitation: 11 of 20 blocks are involved.  pT2c (both lobes involved); pN0 (0/7 see A and B);  pMX  Margins: Carcinoma extends to posterior margin  Periprostatic fat invasion: Single focus posteriorly.  Seminal vesicle invasion: Absent.  Perineural invasion: Present.  Lymphatic invasion: Absent.</p>	<p>S04-1440 C17-65/M. DIAGNOSIS:</p> <p>A. (Left pelvic lymph nodes): Five (5) lymph nodes, negative for tumor.  B. (Right pelvic lymph nodes): Three (3) lymph nodes, negative for tumor.  C. (Prostate, radical prostatectomy): Prostatic adenocarcinoma, Gleason score 3 + 3 = 6.  -Tumor involves right apex, right and left mid prostate. Estimated tumor volume: approximately 5%.  -Tumor is focally present at the right posterior margin. All other margins of resection are uninvolved.  -Perineural invasion: Not observed.  -Lymphovascular involvement: Not observed.  -The seminal vesicles and vas ampullary stumps are uninvolved.</p>
	<p>S07-356 C1-62/M. A. (Specimen labeled RB, right base): Benign prostatic hyperplasia and chronic prostatitis.  B. (Specimen labeled RM, right mid): Chronic prostatitis and benign fibromuscular hyperplasia.  C. (Specimen labeled RA, right apex): Infiltrating adenocarcinoma of prostate comprising approximately 80% of the core biopsy.  Prostatic capsule is not involved.  Primary pattern III, secondary pattern IV, grade VII of X.  D. (Specimen labeled LB, left base): Infiltrating adenocarcinoma of prostate comprising approximately 20% of the core tissue.  Gleason grade VII of X.</p>

Prostatic capsule is not involved.  
Perineural invasion not noted.

E. (Specimen labeled LM left mid): Microscopic focus of prostatic adenocarcinoma comprising less than 5% of the tissue (H&E 3). It is not possible to evaluate the exact location of the cancer and whether the capsule is involved or not.

# Prostate-Specific Membrane Antigen-Targeted Turn-on Probe for Imaging Cargo Release in Prostate Cancer Cells

Feyisola P. Olatunji, Emily A. Savoy, Mylan Panteah, Nooshin Mesbahi, Armina Abbasi, Crescencia M. Talley, Christine L. Lovingier, Leslie A. Caromile,\* and Clifford E. Berkman\*



Cite This: <https://doi.org/10.1021/acs.bioconjchem.1c00435>



Read Online

ACCESS |



Metrics & More

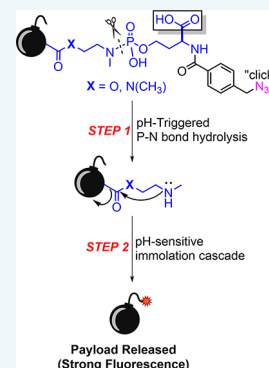


Article Recommendations



Supporting Information

**ABSTRACT:** The tunable nature of phosphoramidate linkers enables broad applicability as pH-triggered controlled-release platforms, particularly in the context of antibody- and small-molecule-drug conjugates (ADCs and SMDCs), where there remains a need for new linker technology. Herein, we explored in-depth the release of turn-on fluorogenic payloads from a homoserinyl-based phosphoramidate acid-cleavable linker. Kinetics of payload release from the scaffold was observed in buffers representing the pH conditions of systemic circulation, early and late endosomes, and lysosomes. It was found that payload release takes place in two key consecutive steps: (1) P–N bond hydrolysis and (2) spacer immolation. These two steps were found to follow pseudo-first-order kinetics and had opposite dependencies on pH. P–N bond hydrolysis increased with decreasing pH, while spacer immolation was most rapid at physiological pH. Despite the contrasting release kinetics of these two steps, maximal payload release was observed at the mildly acidic pH (5.0–5.5), while minimal payload release occurred at physiological pH. We integrated this phosphoramidate-payload linker system into a PSMA-targeted fluorescent turn-on probe to study the intracellular trafficking and release of a fluorescent payload in PSMA-expressing prostate cancer cells. Results showed excellent turn-on and accumulation of the coumarin payload in the late endosomal and lysosomal compartments of these cells. The release properties of this linker mark it as an attractive alternative in the modular design of ADCs and SMDCs, which demand selective intracellular payload release triggered by the pH changes that accompany intracellular trafficking.



## 1. INTRODUCTION

It is estimated that 608,570 individuals will die of cancer-related complications in the United States in 2021.<sup>1</sup> The types of treatment received depend exclusively on the type of cancer and how advanced it is. Many cancer patients receive conventional chemotherapy, which interferes with DNA replication or cell division, thus killing proliferating cells, which in theory are cancerous. Unfortunately, many current chemotherapeutic drugs have limited specificity and often result in deleterious effects on healthy peripheral tissues.<sup>2,3</sup> Thus, there is an obvious need for therapies with increased specificity and reduced toxicity.

Over the past two decades, antibody drug conjugates (ADCs)<sup>4–7</sup> and, to a lesser degree, small-molecule drug conjugates<sup>8–10</sup> (SMDCs) have begun to address these issues, with ADCs being the most efficacious. A successful drug conjugate (DC) comprises three design elements. First, the DC must contain a targeting molecule (e.g., antibody or high-affinity ligand) for a cell surface cancer biomarker. Once a DC is successfully bound to a cell surface cancer biomarker, it is internalized through receptor-mediated endocytosis and proceeds through a series of steps that can include (a) hydrolytic degradation under acidic conditions of subcellular organelles; (b) proteolytic degradation by lysosome-abundant proteases; or (c) disulfide cleavage by glutathione. An example of one of these

tumor-specific cell surface targets, prostate-specific membrane antigen (PSMA), has been used as a reliable clinical biomarker for the detection and localization of prostate cancer because of its specific upregulation in approximately 80% of tumor epithelial cells during prostate cancer progression, where it correlates negatively with prognosis.<sup>11–14</sup> Inhibitors (phosphoramidates and urea) of PSMA's enzymatic activity have been used as PSMA-targeting molecules for various imaging<sup>15–29</sup> and therapeutic agents.<sup>30–35</sup> Despite considerable efforts to outfit small-molecule PSMA-targeting agents with cytotoxic drugs,<sup>36</sup> a few PSMA-targeted SMDCs have been effective because of insufficient internalization into tumor cells. Regardless, many PSMA-targeted molecules are currently in clinical trials, with piflufolostat F-18<sup>37</sup> and <sup>68</sup>Ga-PSMA-11<sup>38,39</sup> recently receiving FDA approval, highlighting the continued interest in PSMA in biomedical, translational medicine, and pharmaceutical fields.<sup>40</sup>

The second element of a successful DC is that it must contain a cytotoxic payload such as the chemotherapeutic agent

Received: September 7, 2021

Revised: October 8, 2021

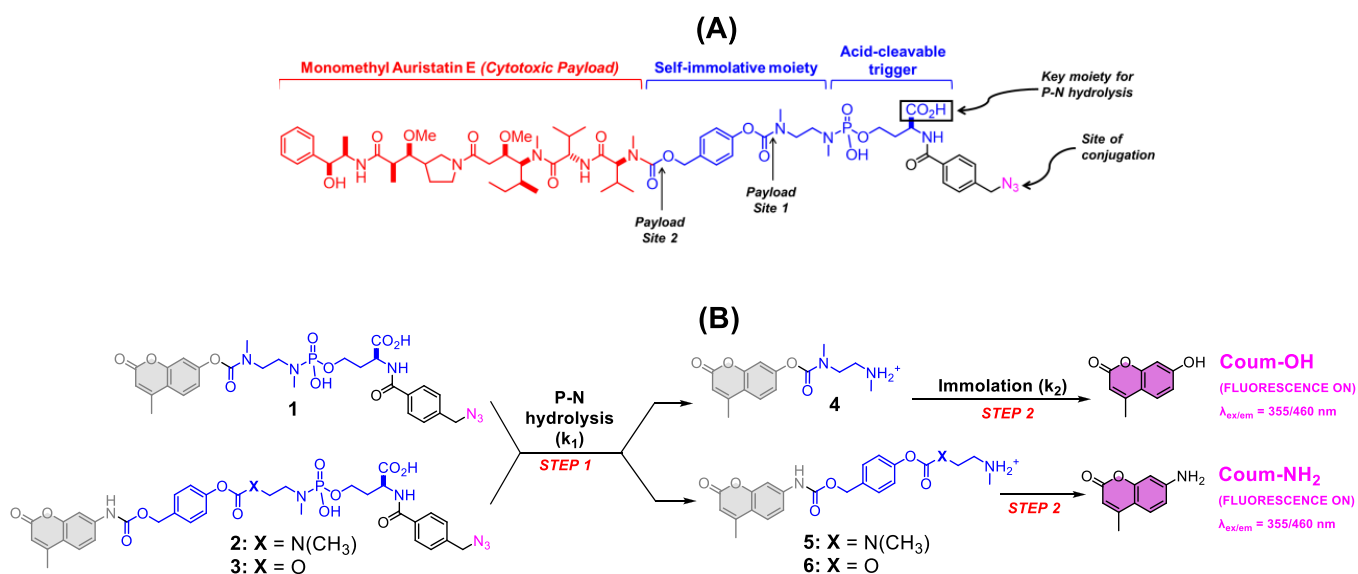
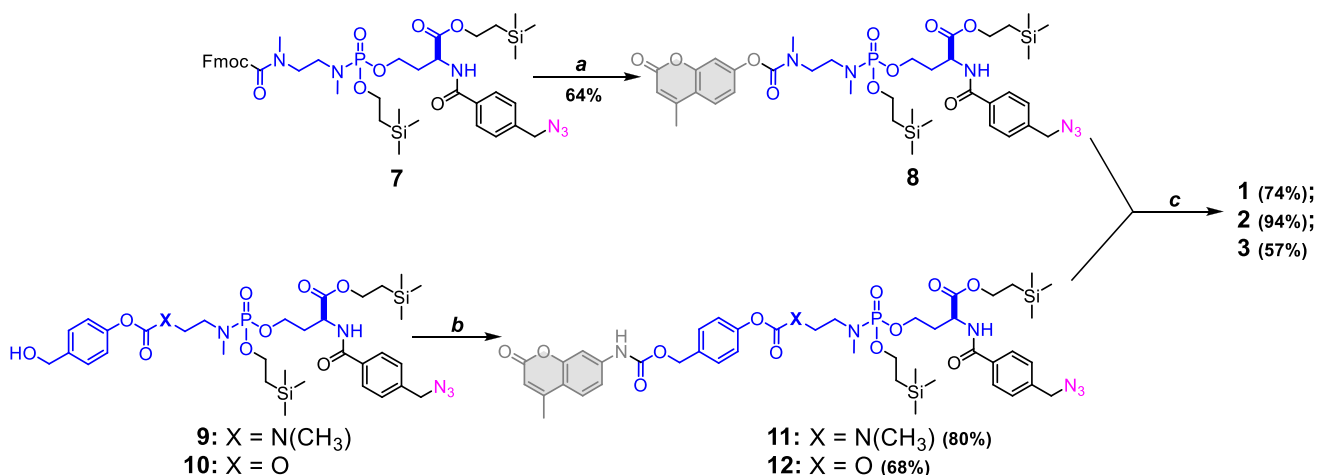


**Figure 1.** (A) Representation of the acid-cleavable phosphoramidate-payload system from prior studies. (B) Overview of the stepwise release and turn-on of latent fluorophores described in this study.  $k_1$  and  $k_2$  are rate constants for P–N bond hydrolysis and immolation, respectively.

### Scheme 1. Synthesis of 1, 2, and 3 Was Achieved via a Two-Step Procedure from Key Alcohol Intermediates<sup>a</sup>



<sup>a</sup>Reaction conditions and yields (a) **Coum-OCOCl**, cat. DBU, DIPEA, CH<sub>2</sub>Cl<sub>2</sub> (b) **Coum-NCO**, Et<sub>3</sub>N, CH<sub>2</sub>Cl<sub>2</sub> (b) CsF, 18-Crown-6, DMF.

monomethyl auristatin E (MMAE). Third, a DC must contain a cleavable linker to couple the payload to the targeting molecule for facile release of the payload in targeted cells. Acid-cleavable linkers are considered to be the most desirable yet the most challenging to incorporate into DC applications. Acid-cleavable linkers are specifically designed to remain stable at the neutral pH of serum and plasma, which is extremely important for efficient and safe drug delivery. However, these linkers can present a challenge in terms of extracellular stability within the low pH hypoxic, tumor microenvironment as they can undergo premature, spontaneous release of the cytotoxic payload and damage normal surrounding tissues as well as target cells through a bystander effect. To date, only two ADCs<sup>41–43</sup> (Mylotarg and Besponsa) utilizing an acid-degradable hydrazone linker have been approved for clinical use.

We have recently reported on the development of an acid-cleavable phosphoramidate-based linker capable of releasing MMAE (Figure 1A).<sup>44</sup> This linker contains two key structural components: (1) a biologically stable and cleavable pH-triggered phosphoramidate scaffold and (2) a self-immolative

spacer. MMAE is released when the self-immolative spacer is hydrolyzed from the phosphoramidate scaffold through exposure to acidic conditions. Once hydrolyzed, the self-immolative moiety undergoes ordered degradation, triggering a clean release of MMAE. Additionally, this linker is click-ready and water-soluble to aid bioconjugation to an array of relevant therapeutic targeting agents.

Here, we describe the versatility and potential therapeutic applicability of this phosphoramidate-based linker to effectively release amine- and alcohol-functionalized fluorogenic coumarin payloads at various acidic pH values characteristic of the endosomal and lysosomal compartments<sup>45,46</sup> encountered during receptor-mediated endocytosis. As proof of principle, we used the extracellular, enzymatic domain of the biomarker PSMA as a target to demonstrate the internalization and release of the fluorogenic coumarin payload into immortalized human prostate cancer cells via receptor-mediated endocytosis.

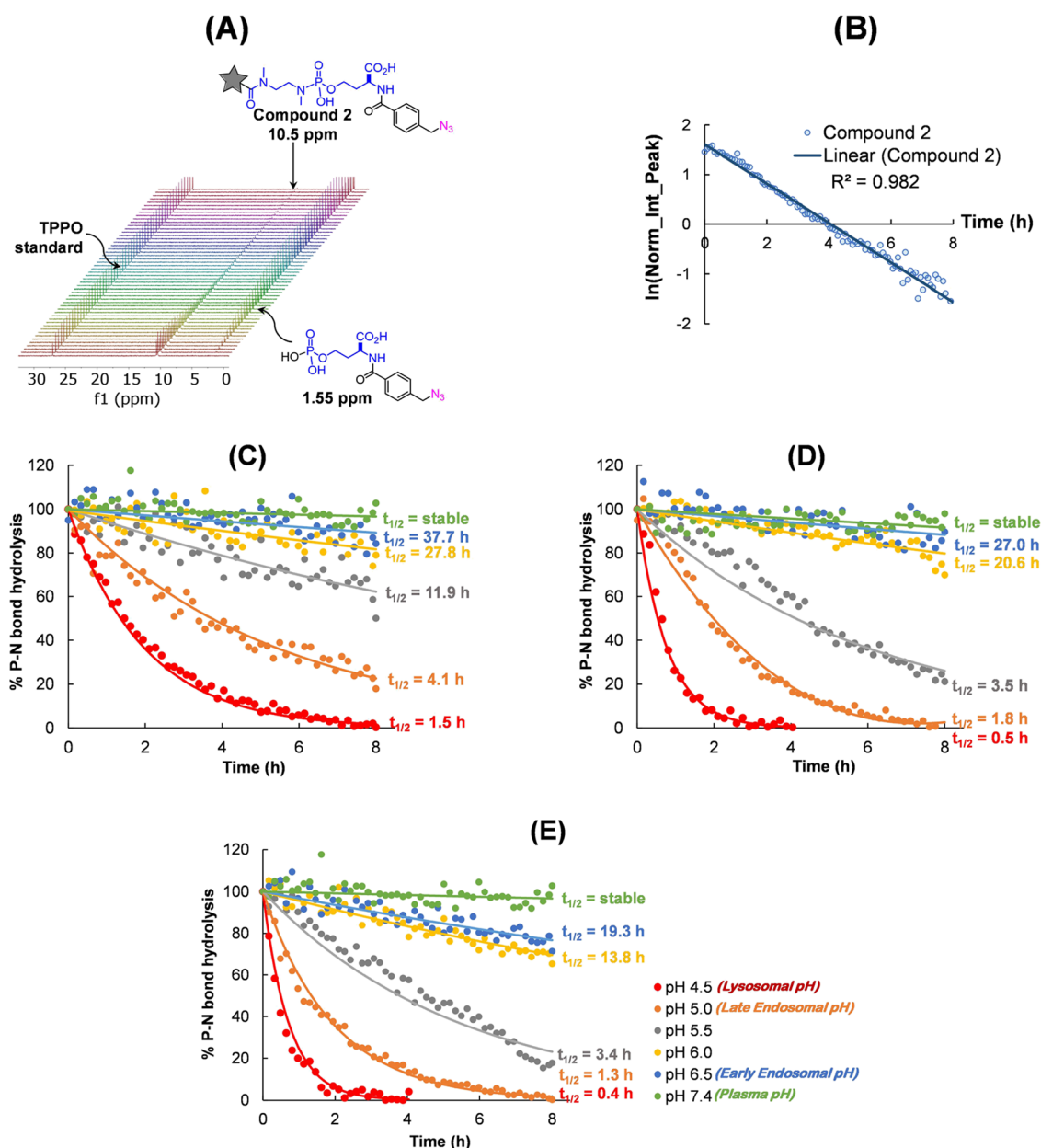


**Figure 2.** (A) Raw stacked NMR data for 2 (10.5 ppm) at pH 5.0. The peak at 1.55 ppm is the hydrolytic product. (B) Semi-log transformation of the compiled data for the area under the curve of 2 normalized to the standard, illustrating first-order kinetics. Scatter plot and their exponential fit showing %P–N bond hydrolysis (reported as half-lives) vs time at pH 4.5, 5.0, 5.5, 6.0, 6.5, and 7.4 for compound (C) 1; (D) 2; and (E) 3. Each study was carried out for 8 h.

## 2. RESULTS AND DISCUSSION

**2.1. Assembly of the Acid-Labile Turn-on Dye Modules.** The acid-labile turn-on dye modules comprised a phosphoramidate moiety coupled to a latent fluorescent payload through one or two self-immolative spacers (Figure 1B). Compound 1 was designed to explore the release of phenol-based payloads (e.g., 4-methylumbelliferone, **Coum-OH**), while compounds 2 and 3 were designed to release aniline-based payloads (e.g., 7-amino-4-methylcoumarin, **Coum-NH<sub>2</sub>**). Synthesis of 1 was achieved via the reaction of Fmoc-protected intermediate 7 in a DBU-facilitated deprotection, followed by reaction with hymecromone chloroformate all in one-pot to yield silyl-protected phosphoramidate 8. Global O-silyl deprotection of 8 afforded 1 in good yield (Scheme 1). The preparation of 2 and 3 was achieved via the reaction of alcohols 9

and 10 with 7-amino-4-methylcoumarin isocyanate, followed by global O-silyl deprotection. Of note, the rationale for substituting the carbamate N-methyl group in 2 with oxygen in compound 3 was to determine if there would be an advantage to more rapid immolation.<sup>46</sup>

**2.2. pH-Dependent Hydrolysis Kinetics of the P–N Bond in the Acid-Labile Turn-on Dye Modules.** Once prepared, the hydrolytic P–N bond degradation of turn-on dye modules 1–3 was monitored by <sup>31</sup>P NMR in buffers ranging from pH values of 4.5 (lysosomal pH), 5.0 (late endosomal pH), 5.5, 6.0, 6.5 (early endosomal pH), and 7.4 (physiological pH) over 8 h at 37 °C. The NMR array data were compiled using MNova 14.1 software, and the peak area for each compound was normalized to a constant concentration of an external standard

(triphenylphosphine oxide, TPPO), as shown for compound 2 as a representative example in Figure 2A.

As anticipated, the rate of P–N bond hydrolysis of the payload-phosphoramidate system 1–3 followed pseudo-first-order kinetics at all pH values (Figure 2B), consistent with our initial studies.<sup>44,47,48</sup> The rate constants ( $k_1$ ) are summarized in Table 1. Importantly, there was no detectable hydrolysis

**Table 1. pH-Dependent Rate Constants for P–N Bond Hydrolysis ( $k_1$ ) and Spacer Immolation ( $k_2$ )**

pH	compound 1		compound 2		compound 3	
	$k_1$ (h <sup>-1</sup> )	$k_2$ (h <sup>-1</sup> )	$k_1$ (h <sup>-1</sup> )	$k_2$ (h <sup>-1</sup> )	$k_1$ (h <sup>-1</sup> )	$k_2$ (h <sup>-1</sup> )
4.5	0.46	0.063	1.39	0.011	1.73	0.73
5.0	0.17	0.12	0.39	0.034	0.53	1.35
5.5	0.058	0.32	0.20	0.082	0.20	2.70
6.0	0.025	0.79	0.034	0.097	0.050	7.20
6.5	0.018	2.32	0.026	0.20	0.036	22.5
7.4	stable	12.6	stable	1.56	stable	unstable

observed for the modules at physiological pH (Figure 2C–E). Because the release of the payload is predicated on the initial hydrolysis of the P–N bond, the linker stability at physiological pH is expected to mitigate off-target effects typified by the premature degradation of linker-payload systems in systemic circulation. While the rates of P–N bond hydrolysis for the turn-on dye modules were generally similar across all pH values, a progressive decrease in the hydrolytic half-lives was observed as the pH dropped from 6.5 (early endosomal) to 4.5 (lysosomal). The similarities in half-lives for these three linkers indicate that the nature of the payload does not interfere with the release kinetics at the P–N bond of the phosphoramidates.

**2.3. pH-Dependent Kinetics of Fluorophore Release from Self-Immolative Spacers.** We prepared the individual spacer-dye modules (4–6) to study specifically the pH-dependence of the self-immolative release, and concomitant turn-on, of the latent fluorophores that would be independent of P–N hydrolysis. While P–N bond hydrolysis is known to be promoted by acidic conditions,<sup>44,47–50</sup> the opposite was observed to be true for the self-immolation of the *N,N'*-dimethylethylenediamine spacer. To prepare the modules (4–6) (Scheme 2), Boc-protected amine (13) and alcohols (14, 15) were reacted with activated fluorogenic payloads (Coum-OCOCl and Coum-NCO), as depicted in Scheme 2. Boc-deprotection of intermediates 16–18 with 4 N HCl in 1,4-dioxane solution provided the desired modules as amine-HCl salts. The time-dependent fluorescent turn-on kinetics of the

spacer-dye modules (4–6) were carried out for 6 h at 37 °C in buffers mimicking physiological and relevant intracellular compartment pH values, with the corresponding time course of fluorescence recorded at  $\lambda = 460$  nm (excitation at  $\lambda = 355$  nm).

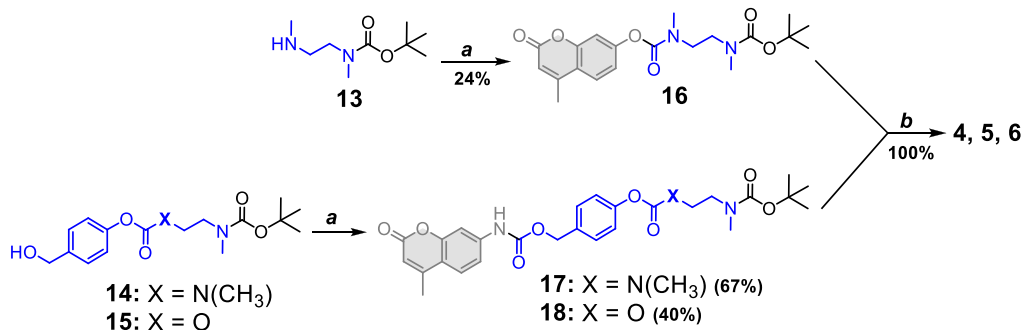
The rate of immolation for the spacer-dye modules (4–6) was found to be proportionally dependent on the pH (Figure 3). The rate constants ( $k_2$ ) are summarized in Table 1. As expected, immolation rates decreased with a decrease in pH as the acid–base equilibrium favors the non-nucleophilic conjugate acid form of the spacer-payload module, as illustrated in Scheme 3 for compound 4 as a representative example. Hence, the nucleophilicity of the *N,N'*-dimethylethylenediamine spacer is diminished and cannot initiate spontaneous cyclization that forms *N,N'*-dimethylimidazolidinone and concomitantly releases the payload. It was also noted that the pH-dependence of the immolation rate was not concentration-dependent (Figure 3A, inset). At concentrations of both 1 and 10  $\mu$ M for compound 4, the linear relationship between the immolation rate and pH was similar, suggesting first-order kinetics. This is typical for reactions with an acid–base pre-equilibrium, where only the electron-rich conjugate base undergoes the rate-determining step (Scheme 3).<sup>51</sup>

It is noteworthy that compound 5 exhibited slower release kinetics (Figure 3B) compared to that of 4 (Figure 3A). Unlike compound 4, the phenol released in compound 5 after the immolation of the *N,N'*-dimethylethylenediamine spacer undergoes an additional 1,6-elimination cascade to release para-quinone methide, CO<sub>2</sub>, and the fluorescent payload. It is likely that the slower release kinetics of compound 5 are due to this additional immolative step. Furthermore, this slower release can also be attributed to the *p*-hydroxymethyl phenol moiety in compound 5 ( $pK_a = 9.7$ ) being a poor leaving group compared to the coumarin payload ( $pK_a = 7.8$ ) found in compound 4.

Unlike compounds 4 and 5, the carbamate *N*-methyl group in the *N,N'*-dimethylethylenediamine spacer was replaced with oxygen in compound 6. This substitution, providing a more electrophilic carbonate, was expected to allow for more rapid cyclization of the *N*-methylethanolamine spacer to 3-methoxyazolidin-2-one (Figure 3C). Indeed, the payload release from 6 was found to be considerably more rapid at all pH values than that from compounds 4 and 5.

**2.4. pH-Dependent Kinetics of Fluorophore Release from the Acid-Labile Turn-on Dye Modules.** The pH-triggered release of the latent fluorogenic payloads from the turn-on dye modules 1, 2, and 3 was evaluated in buffers ranging from pH 4.5 to 7.4 at 37 °C over 18 h. The resulting fluorescence

**Scheme 2. Synthesis of 4, 5, and 6 Was Achieved via a Two-Step Procedure from Key Alcohol Intermediates<sup>a</sup>**



<sup>a</sup>Reaction conditions and yields (a) Coum-OCOCl or Coum-NCO, Et<sub>3</sub>N, CH<sub>2</sub>Cl<sub>2</sub> and (b) 4 N HCl-1,4-dioxane.

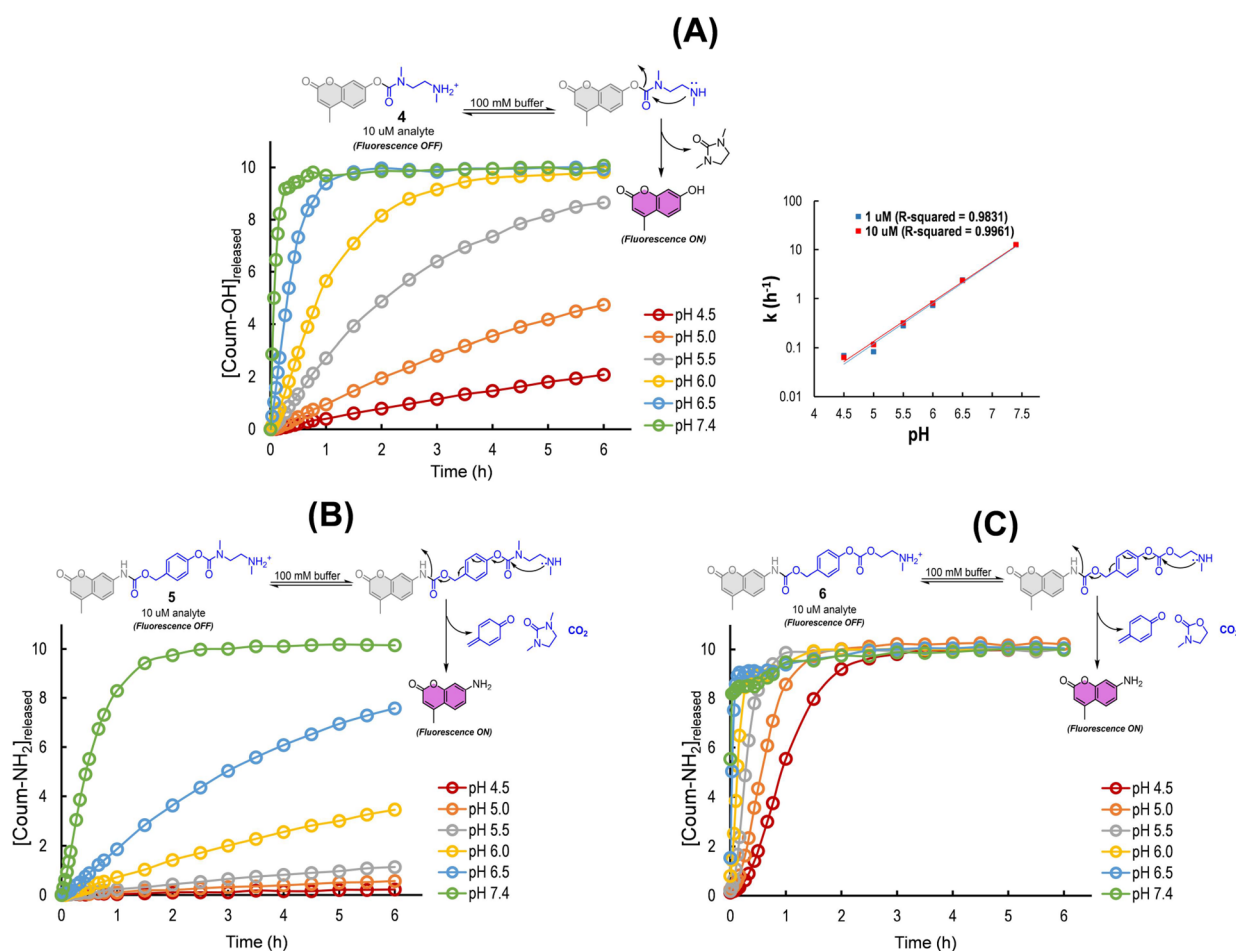
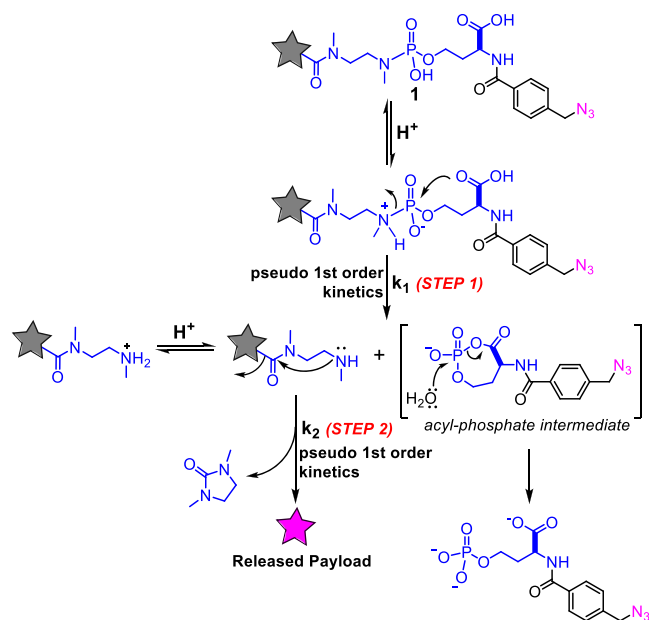


**Figure 3.** Time-dependent fluorescence studies on the spacer-payload system carried out for 6 h. pH-dependent immolation profiles of (A) Compound 4, INSET: Semi-log plot of  $k$  (h<sup>-1</sup>) vs pH. (B) Compound 5. (C) Compound 6.

### Scheme 3. Mechanism of Payload Release from Phosphoramidate-Payload System Highlighting the Two Key Steps: P–N Bond Hydrolysis and Immolation



of the released dyes was recorded at  $\lambda = 460$  nm (excitation at 355 nm). Mechanistically (Scheme 3), the release of the payload

from the acid-labile turn-on dye modules is dependent on the two consecutive reactions (P–N bond hydrolysis  $k_1$  and spacer immolation  $k_2$ ), oppositely dependent upon pH, and the amount of payload released is correlated to the contribution of the two rate constants ( $k_1$  and  $k_2$ ) associated with these two steps (Table 1). Of note, no payload release was observed for compounds 1 and 2 at physiological pH (Figure 4A,B). This was expected because despite the rapid immolation observed for the spacer units in these compounds at pH 7.4, their P–N bond was stable. Maximal dye release was observed at pH 5.0 for compound 1 and at pH 5.5 and 5.0 for compound 2. This can be explained by the observation that while at pH 4.5, P–N bond hydrolysis is rapid ( $k_1$ ), and the rate of spacer immolation to release the dye ( $k_2$ ) is sluggish.

Compound 3 exhibited a pH-dependent payload-release trend (Figure 4C) reminiscent of its P–N bond hydrolysis rates (Table 1). This is largely due to the spacer immolation rates ( $k_2$ ) for this compound being generally rapid at all pH values examined, resulting in the P–N bond hydrolysis generally being the rate-limiting step. Surprisingly, we observed dye release at pH 7.4, a condition at which the P–N bond was observed to be stable. We attributed this observation to the hydrolysis of the carbonate moiety, thus triggering the dye release prior to P–N bond hydrolysis. As such, we have concluded that the scaffold of drug conjugates as it would likely lead to premature drug release, leading to off-target effects.

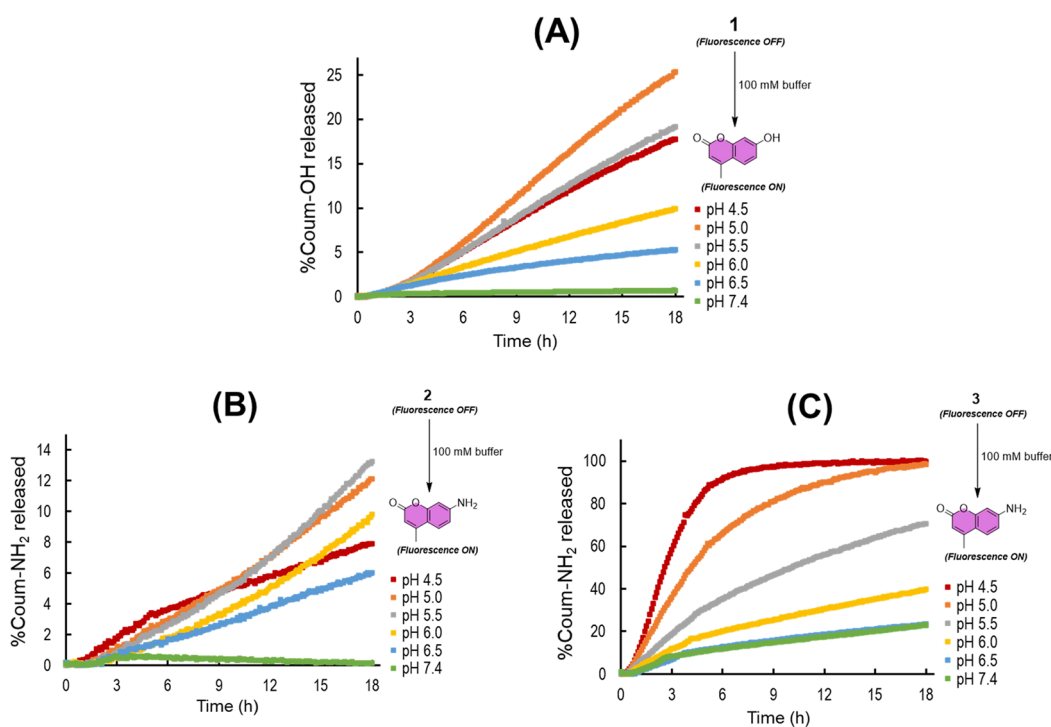


Figure 4. Scatter plots showing the percentage of payload released for (a) Compound 1, (b) Compound 2, and (c) Compound 3.

#### Scheme 4. Synthesis of PSMA-Targeting Turn-on Probe, Coum-SMDC

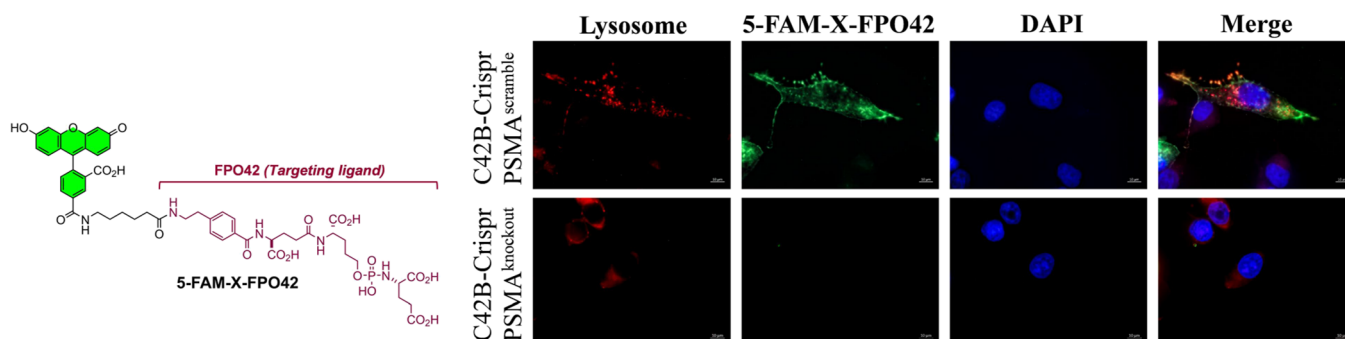
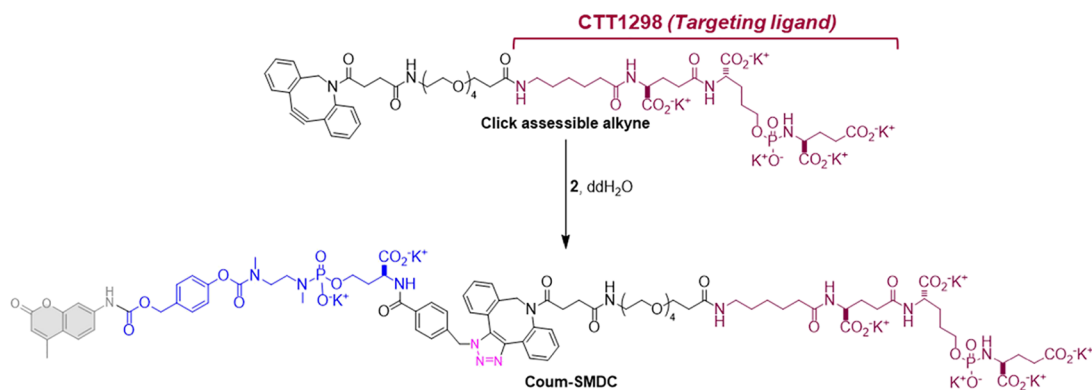
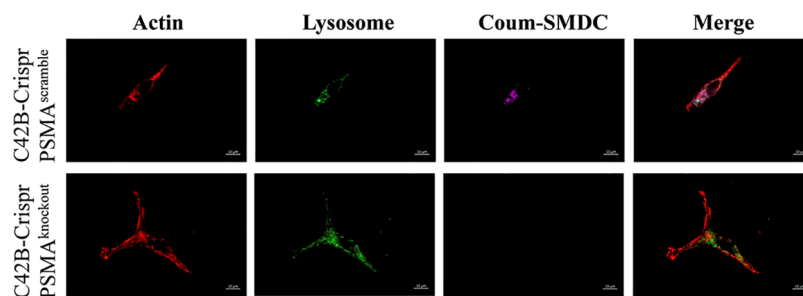


Figure 5. 5-FAM-X-FPO42 binds cell surface PSMA and is internalized via receptor-mediated endocytosis. Immunofluorescent microscopy imaging of C42B-Crispr-PSMA<sup>scramble</sup> and C42B-Crispr-PSMA<sup>knockout</sup> cells incubated with 5-FAM-X-FPO-42 and LysoTracker Red DND-99. 63x oil.

**2.5. In Vitro Evaluation of a PSMA-Targeted Turn-on Probe.** We next investigated the in vitro applicability of the acid-labile turn-on dye modules in the context of a clinically relevant biomarker-targeted probe. Using click chemistry, we coupled the acid-labile turn-on dye module 2 to the PSMA-targeting

molecule CTT1400<sup>34</sup> to form the PSMA-targeted turn-on probe Coum-SMDC (Scheme 4). CTT1400 is known to irreversibly bind to the enzymatic domain of the tumor-specific cell surface receptor PSMA on prostate tumor cells, which is then followed by rapid and extensive internalization via



**Figure 6.** Coum-SMDC releases its payload in the low pH environment of the lysosome. Immunofluorescent microscopy imaging of C42B-Crispr-PSMA<sup>Scramble</sup> (PSMA+) and C42B-Crispr-PSMA<sup>knockout</sup> (PSMA−) cells incubated with Actin, LysoTracker Green DND-26, and Coum-SMDC. 63x oil.

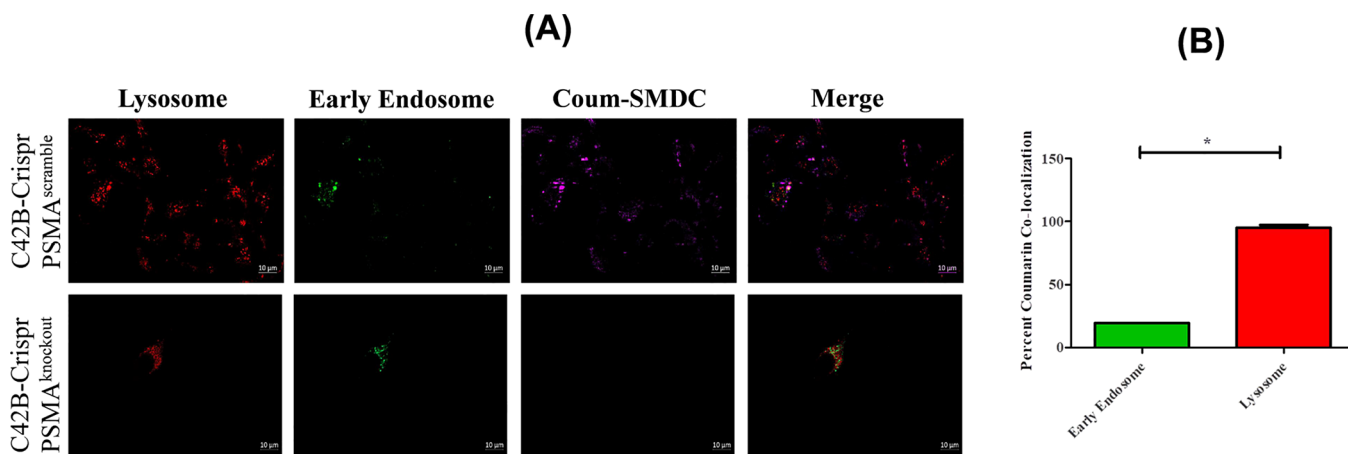


**Figure 7.** (A) Coum-SMDC releases minimal payload first in the early endosome. Immunofluorescent microscopy imaging of C42B-Crispr-PSMA<sup>Scramble</sup> and C42B-Crispr-PSMA<sup>knockout</sup> cells incubated with LysoTracker Red DND-99, CellLight Early Endosome-GFP tracker, and Coum-SMDC. 63x oil. (B) Comparison of percentage coumarin released in early endosome vs lysosome ( $n = 3$ ,  $p < 0.05$ ).

receptor-mediated endocytosis.<sup>34</sup> In addition, we have shown that PSMA is largely tolerant of various pendant groups tethered to phosphoramidate-based small-molecule ligands that target its active site.<sup>52–56</sup> Indeed, the  $IC_{50}$  for Coum-SMDC against PSMA was 1.4 nM (see Supporting Information Section S6). For proof of in vitro applicability, we created functionally manipulated PSMA CRISPR (clustered regularly interspaced short palindromic repeats) immortalized human prostate cancer C42B cell line (see Supporting Information Section S3) to use as a model. To demonstrate that the PSMA-positive C42B-Crispr-PSMA<sup>Scramble</sup> and PSMA-negative C42B-Crispr-PSMA<sup>knockout</sup> cell models were appropriate for this experiment, we first verified that the C42B-Crispr-PSMA<sup>Scramble</sup> cells expressed cell surface PSMA and that the PSMA could be internalized via receptor-mediated endocytosis. Both C42B-Crispr-PSMA<sup>Scramble</sup> and C42B-Crispr-PSMA<sup>knockout</sup> were incubated for 30 min with both the PSMA-specific SMDC 5-FAM-X-FPO-42, which binds exclusively to, and blocks, the enzymatic domain of extracellular, membrane-bound PSMA. Fluorescence microscopy indicated that the C42B-Crispr-PSMA<sup>Scramble</sup> cells were indeed positive for cell surface PSMA, and 59.81% of the 5-FAM-X-FPO-42-bound PSMA was internalized into the lysosomes (Figure 5 and Supporting Information Section S3).

In the disease state, epithelial cells located deep within a poorly vascularized tumor, such as those in advanced prostate cancer, can undergo moderate to severe hypoxia and potentially necrosis.<sup>57–60</sup> Lactic acid production and accumulation during these anaerobic conditions results in a local pH drop from 7.4 to 6.7.<sup>59</sup> Therefore, the pH sensitivity and specificity of an SMDC within the therapeutic setting is tremendously important to

prevent the untoward consequences of the bystander effect.<sup>61</sup> We previously established that the maximal dye release for compound 2 was pH 5.0 (Figure 4B). Therefore, to assess the ability of Coum-SMDC to not only bind successfully to cell surface PSMA but to also release its payload in the low pH environment of the lysosome and the late endosome (pH 4.5–5.5), C42B-Crispr-PSMA<sup>knockout</sup> and C42B-Crispr-PSMA<sup>Scramble</sup> cells were treated with Coum-SMDC and LysoTracker and incubated for 30 min. Results showed the colocalization of the fluorescent coumarin-derived signal within the lysosomes of the C42B-Crispr-PSMA<sup>Scramble</sup> but not in the C42B-Crispr-PSMA<sup>knockout</sup>, signifying that Coum-SMDC successfully bound to cell surface PSMA was trafficked to the low pH environment of the lysosome and released its fluorogenic payload (Figure 6).

To further confirm that the PSMA-targeted turn-on probe Coum-SMDC was indeed acting in a pH-specific manner in vitro and did not release its payload within the slightly acidic early endosome (pH of 5.9–6.8), which is akin to the disease-generated hypoxic microenvironment, the C42B-Crispr-PSMA<sup>knockout</sup> and C42B-Crispr-PSMA<sup>Scramble</sup> cells were incubated with CellLight Early Endosomes-GFP tracker overnight and then treated with Coum-SMDC for 30 min (Figure 7A). Results showed that 98.8% of the released fluorescent coumarin dye colocalized with the lysosomes of the C42B-Crispr-PSMA<sup>Scramble</sup>, while 19.2% colocalized with the early endosomes (Figure 7B). It should be noted that there is a 14.0% overlap in signals, which likely occurs in the endosomes that are transitioning from early to late and theoretically would have a lower pH similar to that of the lysosome. If this is indeed the

case, only 5.19% of the signal is coming from the early endosome.

### 3. CONCLUSIONS

The acidic nature of cellular compartments can be co-opted for the triggered release of cell-targeted payloads through acid-cleavable linkers. With respect to cancer therapeutic development, such applications include ADCs and SMDCs, which carry cytotoxic cargo. Herein, we have reported the utility of our acid-cleavable phosphoramidate-based linker scaffolds<sup>47–49</sup> for the pH-triggered release of both amine- and alcohol-functionalized payloads, which in this case were latent fluorogenic coumarin-based dyes. These turn-on probes (compounds **1–3**) allowed for the exploration of the key consecutive kinetic steps (P–N bond hydrolysis and spacer immolation) implicated in the eventual degradation of the linker and subsequent release of payloads. While both degradation steps were found to be pH-dependent, the individual rates of the two steps had opposite dependencies on pH. In particular, the rate of spacer immolation was greatest at pH 7.4, while the rate of P–N bond hydrolysis was slowest under this condition, but most rapid at pH 4.5.

In the context of cell-targeted payload-conjugates (such as ADCs and SMDCs), the duality of pH dependence of P–N bond hydrolysis and spacer immolation presents a conundrum in the optimization of intracellular cargo release as the pH drops from 7.4 to 4.5 through the cellular internalization process. That is, P–N bond hydrolysis increases as intracellular pH decreases, while the second step of spacer immolation and payload release begins to decrease. Therefore, the interplay between the pH-dependence of the rates for these steps has a direct implication on the amount of payload released under these various pH conditions. As such, it was observed that the greatest amount of payload release for compounds **1** and **2** was at pH 5.0–5.5 (Figure 4A,B), which, in the context of **Coum-SMDC**, was observed as expected that fluorescence turn-on would occur in the late endosomes and/or lysosomes relatively quickly.

In summary, our recently developed acid-cleavable phosphoramidate-based linker scaffold, outfitted with self-immolative spacers, demonstrates suitable stability under physiological conditions (pH 7.4), while effectively releasing cargo under the pH conditions relevant to the internalization of biomarker-targeted conjugates, that being of either lysosomes or late endosomes transitioning to lysosomes. The modularity of their assembly, amenability for click chemistry, and in vitro performance presented in this report mark this pH-triggered scaffold as an attractive platform for the development of biomarker-targeted conjugates such as ADCs and SMDCs. Indeed, the application of this pH-triggered phosphoramidate-based linker scaffold is currently being pursued in our laboratory for the development of analogous PSMA-targeted SMDCs bearing various chemotherapeutic payloads.

### 4. MATERIALS AND METHODS

**4.1. Chemical Synthesis.** All synthetic compounds and intermediates, synthetic schemes, procedures, and corresponding spectra are presented in the [Supporting Information](#).

**4.2. Kinetics Studies (<sup>31</sup>P NMR).** Following the previously described methods from our laboratory,<sup>44,47–50</sup> with minor modifications, samples were prepared using approximately 15 mg of each compound dissolved in 150  $\mu$ L of high-performance liquid chromatography (HPLC)-grade MeOH and then mixed with 400  $\mu$ L of an appropriate buffer. Buffers were chosen based

on specific pH values: 4-(2-hydroxyethyl)-1-piperazineethanesulfonic acid (HEPES, 1 M pH 7.4), 2-(*N*-morpholino)ethanesulfonic acid (MES, 0.5 M pH 6.5), and citric acid (1 M pH 6.0, 5.5, 5.0, and 4.5). Each buffer was prepared and adjusted to  $\pm 0.02$  pH with 4 M NaOH or 4 M HCl on an AB15 Accumet basic pH meter equipped with an accuTupH Ag/AgCl pH probe (Fisher Scientific, Sommerville, NJ). Stability studies were performed using <sup>31</sup>P NMR on a Varian 500 MHz instrument (Agilent Technologies, Santa Clara, CA). The instrument was equilibrated to 37 °C with an acquisition of 64 scans, a relaxation delay of 1 s, an observed pulse of 3.41  $\mu$ s at 45°, and a preacquisition delay of 185 s. The instrument was locked to an internal standard, triphenylphosphine oxide (TPPO, 40 mM in DMSO-*d*<sub>6</sub>), in an axial capillary positioned within the sample solution. Stability data were collected for 8 h or until complete decay was observed. After data acquisition was complete, all <sup>31</sup>P chemical shifts were referenced to the internal standard (TPPO, 27 ppm), and the phase was adjusted accordingly. Nuclear magnetic resonance (NMR) experiment files were loaded into the software MestReNova v14.1.2. Phase correction and baseline fitting were performed in the NMR software. Regions corresponding to the control, the starting material, and the product peak were then exported into the software OriginPro 2020 (OriginLab Corporation, Northampton, MA 01060 USA). The intensities of each peak were normalized to the intensity of the internal triphenylphosphine oxide standard. A first-order decaying linear fitting function was applied to a plot of ln(normalized intensity) of the decaying parent compound versus time. The half-life (*t*<sub>1/2</sub>) of each compound at the designated pH was then calculated as shown below:

$$t_{1/2} = \frac{\ln 2}{|\text{slope}|}$$

**4.3. Kinetic Studies (Fluorescence Spectroscopy).** A Fluostar Omega Microplate reader running Omega software version 1.02 and Mars Data Analysis Software Program version 1.10 (BMG Labtech) were used to conduct the time-dependent kinetics studies. Studies were performed in Greiner Bio-One  $\mu$ Clear Bottom 96-well 96 plates at 37 °C using hymecromone and 7-amino-4-methylcoumarin as the fluorogenic reporters, monitoring at  $\lambda_{\text{ex}} = 355$  nm and  $\lambda_{\text{em}} = 460$  nm. Assays were performed in the following 100 mM buffers: HEPES (pH 7.4), MES (pH 6.5), and citric acid (pH 6.0, 5.5, 5.0, and 4.5). Stock solutions (10 mM) of each compound (**1–6**) were prepared in ddH<sub>2</sub>O, and 10 mM stock solutions of fluorogenic reporters (**Coum-OH** and **Coum-NH<sub>2</sub>**) were prepared in EtOH. All solutions were serially diluted to 100  $\mu$ M working solutions with ddH<sub>2</sub>O. Calibration curves were carried out on the fluorogenic reporters at concentrations of 1 nM–100  $\mu$ M at each pH value, with the linear range found to be between 10 nM–10  $\mu$ M. Reactions were initiated by the addition of 20  $\mu$ L of probe (100  $\mu$ M working solution) to wells containing 180  $\mu$ L of buffer, with the total well volume of 200  $\mu$ L. Product formation was followed for 6 h, with time points recorded at 2 min intervals or for 18 h with time points recorded at 6 min intervals. The fluorescence values in each reaction well were normalized to the maximal fluorescence value in the control well (10  $\mu$ M of fluorogenic reporters). Rate constants were extracted from GraphPad Prism 9.0 by fitting the data to one phase association model.

**4.4. PSMA IC<sub>50</sub> for Coum-SMDC.** The routine determination of IC<sub>50</sub> for Coum-SMDC was performed, as most

recently described in our laboratory,<sup>62</sup> using concentrations of 100, 30, 10, 3, and 1 nM.

**4.5. Cell Imaging Studies.** Cells were plated onto coverslips at a concentration of  $1 \times 10^5$  cells/well in 1 mL of growth medium and allowed to attach overnight. Cells were then starved for 2 h in fetal bovine serum (FBS)-free RPMI and then incubated for 30 min with one or more of the following: 50 nM LysoTracker Red DND-99 (Thermo Fisher, Pittsburgh, PA), 50 nM LysoTracker Green DND-26 (Thermo Fisher, Pittsburgh, PA), and 1  $\mu$ M 5-FAM-X-FPO-42 or 1  $\mu$ M Coum-SMDC at 37 °C. To visualize early endosomes, cells were incubated for 16 h with CellLight Early Endosomes-GFP tracker according to manufacturer's instructions (Thermo Fisher, Pittsburgh, PA). For imaging, coverslips were set on ice, rinsed twice in ice-cold phosphate buffered saline (PBS), fixed in ice-cold 10% neutral buffered formalin solution for 15 min, and mounted using diamond mounting media with or without DAPI (Thermo Fisher, Pittsburgh, PA). Zeiss Zen software was used to acquire and process immunofluorescent images. Fiji Image J was used to quantify the mean gray value of the early endosome, lysosome, and coumarin release. All experiments in this study were repeated for a minimum of three independent experiments. Results are presented as mean  $\pm$  standard error of the mean (SEM). Statistical analysis was performed using the paired, two-tailed t-test. Differences were considered significant at  $P < 0.05$ .

## ■ ASSOCIATED CONTENT

### SI Supporting Information

The Supporting Information is available free of charge at <https://pubs.acs.org/doi/10.1021/acs.bioconjchem.1c00435>.

All synthetic compounds and intermediates, synthetic schemes, procedures, and corresponding spectra, as well as validation results for the cell lines used in this study (PDF)

## ■ AUTHOR INFORMATION

### Corresponding Authors

**Leslie A. Caromile** – UCONN Health-Center for Vascular Biology, Farmington, Connecticut 06030-3501, United States; Email: [caromile@uchc.edu](mailto:caromile@uchc.edu)

**Clifford E. Berkman** – Department of Chemistry, Washington State University, Pullman, Washington 99164-4630, United States; [orcid.org/0000-0003-2544-5252](https://orcid.org/0000-0003-2544-5252); Email: [cberkman@wsu.edu](mailto:cberkman@wsu.edu)

### Authors

**Feyisola P. Olatunji** – Department of Chemistry, Washington State University, Pullman, Washington 99164-4630, United States; [orcid.org/0000-0002-6429-7072](https://orcid.org/0000-0002-6429-7072)

**Emily A. Savoy** – Department of Chemistry, Washington State University, Pullman, Washington 99164-4630, United States

**Mylan Panteah** – UCONN Health-Center for Vascular Biology, Farmington, Connecticut 06030-3501, United States

**Nooshin Mesbahi** – Department of Chemistry, Washington State University, Pullman, Washington 99164-4630, United States

**Armina Abbasi** – Department of Chemistry, Washington State University, Pullman, Washington 99164-4630, United States

**Cresencia M. Talley** – Department of Chemistry, Washington State University, Pullman, Washington 99164-4630, United States

**Christine L. Lovingier** – Department of Chemistry, Washington State University, Pullman, Washington 99164-4630, United States

Complete contact information is available at: <https://pubs.acs.org/10.1021/acs.bioconjchem.1c00435>

## Notes

The authors declare no competing financial interest.

## ■ ACKNOWLEDGMENTS

This work and F.P.O. were supported by the National Institutes of Health (R21CA256382 and T32GM8336, respectively). The authors extend their gratitude for technical assistance to Dr. William Hiscox (WSU Center for NMR Spectroscopy), Dr. Gerhard Munske (WSU Laboratory of Biotechnology and Bioanalysis), and Dr. Deobald Lee (Mass Spectrometry Core Laboratory at University of Idaho). In fond memory, C.E.B. dedicates this work to James R. Keefe, a generous mentor and friend.

## ■ REFERENCES

- (1) Siegel, R. L.; Miller, K. D.; Fuchs, H. E.; Jemal, A. *Cancer Statistics*, 2021. *CA Cancer J. Clin.* **2021**, *71*, 7–33.
- (2) Pal, S. K.; Twardowski, P.; Sartor, O. Critical appraisal of cabazitaxel in the management of advanced prostate cancer. *Clin. Interv. Aging* **2010**, *5*, 395–402.
- (3) Cereda, V.; Formica, V.; Massimiani, G.; Tosetto, L.; Roselli, M. Targeting metastatic castration-resistant prostate cancer: mechanisms of progression and novel early therapeutic approaches. *Expert Opin. Investig. Drugs* **2014**, *23*, 469–487.
- (4) Khongorzul, P.; Ling, C. J.; Khan, F. U.; Ihsan, A. U.; Zhang, J. Antibody-Drug Conjugates: A Comprehensive Review. *Mol. Cancer Res.* **2020**, *18*, 3–19.
- (5) Joubert, N.; Beck, A.; Dumontet, C.; Denevault-Sabourin, C. Antibody–Drug Conjugates: The Last Decade. *Pharmaceuticals* **2020**, *13*, No. 245.
- (6) Gauzy-Lazo, L.; Sassoon, I.; Brun, M.-P. Advances in Antibody–Drug Conjugate Design: Current Clinical Landscape and Future Innovations. *SLAS DISCOVERY: Adv. Sci. Drug Discov.* **2020**, *25*, 843–868.
- (7) Drago, J. Z.; Modi, S.; Chandralapaty, S. Unlocking the potential of antibody–drug conjugates for cancer therapy. *Nat. Rev. Clin. Oncol.* **2021**, *18*, 327–344.
- (8) Zhuang, C.; Guan, X.; Ma, H.; Cong, H.; Zhang, W.; Miao, Z. Small molecule-drug conjugates: A novel strategy for cancer-targeted treatment. *Eur. J. Med. Chem.* **2019**, *163*, 883–895.
- (9) Deonarain, M. P.; Yahioğlu, G.; Stamati, I.; Pomowski, A.; Clarke, J.; Edwards, B. M.; Diez-Posada, S.; Stewart, A. C. Small-Format Drug Conjugates: A Viable Alternative to ADCs for Solid Tumours? *Antibodies* **2018**, *7*, No. 16.
- (10) Srinivasarao, M.; Galliford, C. V.; Low, P. S. Principles in the design of ligand-targeted cancer therapeutics and imaging agents. *Nat. Rev. Drug Discov.* **2015**, *14*, 203–219.
- (11) Heston, W. D. Characterization and glutamyl preferring carboxypeptidase function of prostate specific membrane antigen: a novel folate hydrolase. *Urology* **1997**, *49*, 104–112.
- (12) Israeli, R. S.; Powell, C. T.; Fair, W. R.; Heston, W. D. Molecular cloning of a complementary DNA encoding a prostate-specific membrane antigen. *Cancer Res.* **1993**, *53*, 227–230.
- (13) Pinto, J. T.; Suffoletto, B. P.; Berzin, T. M.; Qiao, C. H.; Lin, S.; Tong, W. P.; May, F.; Mukherjee, B.; Heston, W. D. Prostate-specific membrane antigen: a novel folate hydrolase in human prostatic carcinoma cells. *Clinic. cancer res.: offic. J. Amer. Ass. Cancer Res* **1996**, *2*, 1445–1451.

- (14) Murphy, G. P.; Elgamal, A. A.; Su, S. L.; Bostwick, D. G.; Holmes, E. H. Current evaluation of the tissue localization and diagnostic utility of prostate specific membrane antigen. *Cancer* **1998**, *83*, 2259–2269.
- (15) Rosenthal, S. A.; Haseaman, M. K.; Polascik, T. J. Utility of capromab pendetide (ProstaScint) imaging in the management of prostate cancer. *Tech. Urol.* **2001**, *7*, 27–37.
- (16) Bander, N. H.; Milowsky, M. L.; Nanus, D. M.; Kostakoglu, L.; Vallabhajosula, S.; Goldsmith, S. J. Phase I trial of <sup>177</sup>lutetium-labeled J591, a monoclonal antibody to prostate-specific membrane antigen, in patients with androgen-independent prostate cancer. *J. Clin. Oncol.* **2005**, *23*, 4591–4601.
- (17) Chu, T. C.; Shieh, F.; Lavery, L. A.; Levy, M.; Richards-Kortum, R.; Korgel, B. A.; Ellington, A. D. Labeling tumor cells with fluorescent nanocrystal-aptamer bioconjugates. *Biosens. Bioelectron.* **2006**, *21*, 1859–1866.
- (18) Farokhzad, O. C.; Khademhosseini, A.; Jon, S.; Hermmann, A.; Cheng, J.; Chin, C.; Kiselyuk, A.; Teply, B.; Eng, G.; Langer, R. Microfluidic system for studying the interaction of nanoparticles and microparticles with cells. *Anal. Chem.* **2005**, *77*, 5453–5459.
- (19) Foss, C. A.; Mease, R. C.; Fan, H.; Wang, Y.; Ravert, H. T.; Dannals, R. F.; Olszewski, R. T.; Heston, W. D.; Kozikowski, A. P.; Pomper, M. G. Radiolabeled small-molecule ligands for prostate-specific membrane antigen: in vivo imaging in experimental models of prostate cancer. *Clinic. cancer res.: offic. J. Amer. Ass. Cancer Res* **2005**, *11*, 4022–4028.
- (20) Gao, X.; Cui, Y.; Levenson, R. M.; Chung, L. W.; Nie, S. In vivo cancer targeting and imaging with semiconductor quantum dots. *Nat. Biotechnol.* **2004**, *22*, 969–976.
- (21) Guilarte, T. R.; McGlothlan, J. L.; Foss, C. A.; Zhou, J.; Heston, W. D.; Kozikowski, A. P.; Pomper, M. G.; Department of Environmental Health Sciences, U. S. A. Glutamate carboxypeptidase II levels in rodent brain using [<sup>125</sup>I]DCIT quantitative autoradiography. *Neurosci. Lett.* **2005**, *387*, 141–144.
- (22) Humblet, V.; Lapidus, R.; Williams, L. R.; Tsukamoto, T.; Rojas, C.; Majer, P.; Hin, B.; Ohnishi, S.; De Grand, A. M.; Zaheer, A.; Renze, J. T.; Nakayama, A.; Slusher, B. S.; Frangioni, J. V. High-affinity near-infrared fluorescent small-molecule contrast agents for in vivo imaging of prostate-specific membrane antigen. *Mol. Imaging* **2005**, *4*, 448–462.
- (23) Milowsky, M. L.; Nanus, D. M.; Kostakoglu, L.; Sheehan, C. E.; Vallabhajosula, S.; Goldsmith, S. J.; Ross, J. S.; Bander, N. H. Vascular targeted therapy with anti-prostate-specific membrane antigen monoclonal antibody J591 in advanced solid tumors. *J. Clin. Oncol.* **2007**, *25*, 540–547.
- (24) Pomper, M. G.; Musachio, J. L.; Zhang, J.; Scheffel, U.; Zhou, Y.; Hilton, J.; Maini, A.; Dannals, R. F.; Wong, D. F.; Kozikowski, A. P. 11C-MCG: synthesis, uptake selectivity, and primate PET of a probe for glutamate carboxypeptidase II (NAALADase). *Mol. Imaging* **2002**, *1*, 96–101.
- (25) Smith, M. R.; Nelson, J. B. Future therapies in hormone-refractory prostate cancer. *Urology* **2005**, *65*, 9–16 discussion 17.
- (26) Smith-Jones, P. M.; Vallabhajosula, S.; Navarro, V.; Bastidas, D.; Goldsmith, S. J.; Bander, N. H. Radiolabeled monoclonal antibodies specific to the extracellular domain of prostate-specific membrane antigen: preclinical studies in nude mice bearing LNCaP human prostate tumor. *J. Nuclear Med.* **2003**, *44*, 610–617.
- (27) Tsukamoto, T.; Wozniak, K. M.; Slusher, B. S. Progress in the discovery and development of glutamate carboxypeptidase II inhibitors. *Drug Discov. Today* **2007**, *12*, 767–776.
- (28) Ganguly, T.; Dannoon, S.; Hopkins, M. R.; Murphy, S.; Cahaya, H.; Blecha, J. E.; Jivan, S.; Drake, C. R.; Barinka, C.; Jones, E. F.; VanBrocklin, H. F.; Berkman, C. E. A high-affinity [(18)F]-labeled phosphoramidate peptidomimetic PSMA-targeted inhibitor for PET imaging of prostate cancer. *Nucl. Med. Biol.* **2015**, *42*, 780–787.
- (29) Dannoon, S.; Ganguly, T.; Cahaya, H.; Geruntho, J. J.; Galliher, M. S.; Beyer, S. K.; Choy, C. J.; Hopkins, M. R.; Regan, M.; Blecha, J. E.; Skultetyova, L.; Drake, C. R.; Jivan, S.; Barinka, C.; Jones, E. F.; Berkman, C. E.; VanBrocklin, H. F. Structure-Activity Relationship of (18)F-Labeled Phosphoramidate Peptidomimetic Prostate-Specific Membrane Antigen (PSMA)-Targeted Inhibitor Analogues for PET Imaging of Prostate Cancer. *J. Med. Chem.* **2016**, *59*, 5684–5694.
- (30) Tasch, J.; Gong, M.; Sadelain, M.; Heston, W. D. A unique folate hydrolase, prostate-specific membrane antigen (PSMA): a target for immunotherapy? *Crit. Rev. Immunol.* **2001**, *21*, 13.
- (31) Salit, R. B.; Kast, W. M.; Velders, M. P. Ins and outs of clinical trials with peptide-based vaccines. *Front Biosci.* **2002**, *7*, e204–e213.
- (32) Lu, J.; Celis, E. Recognition of prostate tumor cells by cytotoxic T lymphocytes specific for prostate-specific membrane antigen. *Cancer Res.* **2002**, *62*, 5807–5812.
- (33) Fracasso, G.; Bellisola, G.; Cingarlini, S.; Castelletti, D.; Prayer-Galetti, T.; Pagano, F.; Tridente, G.; Colombatti, M. Anti-tumor effects of toxins targeted to the prostate specific membrane antigen. *Prostate* **2002**, *53*, 9–23.
- (34) Choy, C. J.; Ling, X.; Geruntho, J. J.; Beyer, S. K.; Latoche, J. D.; Langton-Webster, B.; Anderson, C. J.; Berkman, C. E. <sup>177</sup>Lu-Labeled Phosphoramidate-Based PSMA Inhibitors: The Effect of an Albumin Binder on Biodistribution and Therapeutic Efficacy in Prostate Tumor-Bearing Mice. *Theranostics* **2017**, *7*, 1928–1939.
- (35) Ling, X.; Latoche, J. D.; Choy, C. J.; Kurland, B. F.; Laymon, C. M.; Wu, Y.; Salamacha, N.; Shen, D.; Geruntho, J. J.; Rigatti, L. H.; Windish, H. P.; Langton-Webster, B.; Berkman, C. E.; Anderson, C. J. Preclinical Dosimetry, Imaging, and Targeted Radionuclide Therapy Studies of Lu-177-Labeled Albumin-Binding, PSMA-Targeted CTT1403. *Mol. Imaging Biol.* **2020**, *22*, 274.
- (36) Wang, X.; Shirke, A.; Walker, E.; Sun, R.; Ramamurthy, G.; Wang, J.; Shan, L.; Mangadla, J.; Dong, Z.; Li, J.; Wang, Z.; Schluchter, M.; Luo, D.; Wang, Y.; Stauffer, S.; Brady-Kalnay, S.; Hoimes, C.; Lee, Z.; Basilion, J. P. Small Molecule-Based Prodrug Targeting Prostate Specific Membrane Antigen for the Treatment of Prostate Cancer. *Cancers* **2021**, *13*, No. 417.
- (37) Keam, S. J. Piflufolastat F 18: Diagnostic First Approval. *Mol. Diagn. Ther.* **2021**, 647.
- (38) Fendler, W. P.; Calais, J.; Eiber, M.; Flavell, R. R.; Mishoe, A.; Feng, F. Y.; Nguyen, H. G.; Reiter, R. E.; Rettig, M. B.; Okamoto, S.; Emmett, L.; Zacho, H. D.; Ilhan, H.; Wetter, A.; Rischpler, C.; Schoder, H.; Burger, I. A.; Gartmann, J.; Smith, R.; Small, E. J.; Slavik, R.; Carroll, P. R.; Herrmann, K.; Czernin, J.; Hope, T. A. Assessment of 68Ga-PSMA-11 PET Accuracy in Localizing Recurrent Prostate Cancer: A Prospective Single-Arm Clinical Trial. *JAMA Oncol.* **2019**, *5*, 856–863.
- (39) Hadaschik, B.; Ost, P. Re: Assessment of (68)Ga-PSMA-11 PET Accuracy in Localizing Recurrent Prostate Cancer: A Prospective Single-Arm Clinical Trial. *Eur. Urol.* **2019**, *76*, 538–539.
- (40) Dassie, J. P.; Hernandez, L. I.; Thomas, G. S.; Long, M. E.; Rocky, W. M.; Howell, C. A.; Chen, Y.; Hernandez, F. J.; Liu, X. Y.; Wilson, M. E.; Allen, L. A.; Vaena, D. A.; Meyerholz, D. K.; Giangrande, P. H. Targeted inhibition of prostate cancer metastases with an RNA aptamer to prostate-specific membrane antigen. *Mol. Ther.* **2014**, *22*, 1910–1922.
- (41) Lamb, Y. N. Inotuzumab Ozogamicin: First Global Approval. *Drugs* **2017**, *77*, 1603–1610.
- (42) Norsworthy, K. J.; Ko, C. W.; Lee, J. E.; Liu, J.; John, C. S.; Przepiora, D.; Farrell, A. T.; Pazdur, R. FDA Approval Summary: Mylotarg for Treatment of Patients with Relapsed or Refractory CD33-Positive Acute Myeloid Leukemia. *Oncologist* **2018**, *23*, 1103–1108.
- (43) Abe, Y.; Sugihara, K.; Nakada, T.; Shahidi, J.; Gallant, G. J. A., Jikoh, T., Agatsuma, T. (2019) ADCs on the Market and in Clinical Development, in *Cancer Drug Delivery Systems Based on the Tumor Microenvironment* (Matsumura, Y., Tarin, D., Eds.) pp. 155–174, Springer Japan, Tokyo, DOI: 10.1007/978-4-431-56880-3\_7.
- (44) Olatunji, F. P.; Herman, J. W.; Kesic, B. N.; Olabode, D.; Berkman, C. E. A click-ready pH-triggered phosphoramidate-based linker for controlled release of monomethyl auristatin E. *Tetrahedron Lett.* **2020**, *61*, No. 152398.
- (45) Scott, C. C.; Gruenberg, J. Ion flux and the function of endosomes and lysosomes: pH is just the start. *Bioessays* **2011**, *33*, 103–110.

- (46) Chen, E. K. Y.; McBride, R. A.; Gillies, E. R. Self-Immolative Polymers Containing Rapidly Cyclizing Spacers: Toward Rapid Depolymerization Rates. *Macromolecules* **2012**, *45*, 7364–7374.
- (47) Choy, C. J.; Ley, C. R.; Davis, A. L.; Backer, B. S.; Geruntho, J. J.; Clowers, B. H.; Berkman, C. E. Second-Generation Tunable pH-Sensitive Phosphoramidate-Based Linkers for Controlled Release. *Bioconjug. Chem.* **2016**, *27*, 2206–2213.
- (48) Backer, B. S.; Choy, C. J.; Davis, A. L.; Browne, Z. S.; Berkman, C. E. Tunable pH-Sensitive 2-Carboxybenzyl Phosphoramidate Cleavable Linkers. *Tetrahedron Lett.* **2020**, *61*, No. 151650.
- (49) Choy, C. J.; Geruntho, J. J.; Davis, A. L.; Berkman, C. E. Tunable pH-Sensitive Linker for Controlled Release. *Bioconjug. Chem.* **2016**, *27*, 824–830.
- (50) Olatunji, F. P.; Kesic, B. N.; Choy, C. J.; Berkman, C. E. Phosphoramidate derivatives as controlled-release prodrugs of l-Dopa. *Bioorg. Med. Chem. Lett.* **2019**, *29*, 2571–2574.
- (51) Müller, I. A.; Kratz, F.; Jung, M.; Warnecke, A. Schiff bases derived from p-aminobenzyl alcohol as trigger groups for pH-dependent prodrug activation. *Tetrahedron Lett.* **2010**, *51*, 4371–4374.
- (52) Liu, T.; Toriyabe, Y.; Kazak, M.; Berkman, C. E. Pseudoirreversible Inhibition of Prostate-Specific Membrane Antigen by Phosphoramidate Peptidomimetics. *Biochemistry* **2008**, *47*, 12658–12660.
- (53) Liu, T.; Wu, L. Y.; Hopkins, M. R.; Choi, J. K.; Berkman, C. E. A targeted low molecular weight near-infrared fluorescent probe for prostate cancer. *Bioorg. Med. Chem. Lett.* **2010**, *20*, 7124–7126.
- (54) Liu, T.; Wu, L. Y.; Kazak, M.; Berkman, C. E. Cell-Surface labeling and internalization by a fluorescent inhibitor of prostate-specific membrane antigen. *Prostate* **2008**, *68*, 955–964.
- (55) Nedrow-Byers, J. R.; Jabbes, M.; Jewett, C.; Ganguly, T.; He, H.; Liu, T.; Benny, P.; Bryan, J. N.; Berkman, C. E. A phosphoramidate-based prostate-specific membrane antigen-targeted SPECT agent. *Prostate* **2012**, *72*, 904–912.
- (56) Liu, T.; Wu, L. Y.; Choi, J. K.; Berkman, C. E. Targeted photodynamic therapy for prostate cancer: inducing apoptosis via activation of the caspase-8/–3 cascade pathway. *Int. J. Oncol.* **2010**, *36*, 777–784.
- (57) Bergers, G.; Benjamin, L. E. Tumorigenesis and the angiogenic switch. *Nat. Rev. Cancer* **2003**, *3*, 401–410.
- (58) Jain, R. K. Normalization of tumor vasculature: an emerging concept in antiangiogenic therapy. *Science* **2005**, *307*, 58–62.
- (59) Helmlinger, G.; Yuan, F.; Dellian, M.; Jain, R. K. Interstitial pH and pO<sub>2</sub> gradients in solid tumors in vivo: high-resolution measurements reveal a lack of correlation. *Nat. Med.* **1997**, *3*, 177–182.
- (60) Jain, R. K. Barriers to drug delivery in solid tumors. *Sci. Am.* **1994**, *271*, 58–65.
- (61) Staudacher, A. H.; Brown, M. P. Antibody drug conjugates and bystander killing: is antigen-dependent internalisation required? *Br. J. Cancer* **2017**, *117*, 1736–1742.
- (62) Ley, C. R.; Beattie, N. R.; Dannoon, S.; Regan, M.; VanBrocklin, H.; Berkman, C. E. Synthesis and evaluation of constrained phosphoramidate inhibitors of prostate-specific membrane antigen. *Bioorg. Med. Chem. Lett.* **2015**, *25*, 2536–2539.

## CANCER

# PSMA redirects cell survival signaling from the MAPK to the PI3K-AKT pathways to promote the progression of prostate cancer

Leslie Ann Caromile,<sup>1</sup> Kristina Dortche,<sup>1</sup> M. Mamunur Rahman,<sup>1</sup> Christina L. Grant,<sup>1</sup> Christopher Stoddard,<sup>2</sup> Fernando A. Ferrer,<sup>3</sup> Linda H. Shapiro<sup>1\*</sup>

2017 © The Authors,  
some rights reserved;  
exclusive licensee  
American Association  
for the Advancement  
of Science.

Increased abundance of the prostate-specific membrane antigen (PSMA) on prostate epithelium is a hallmark of advanced metastatic prostate cancer (PCa) and correlates negatively with prognosis. However, direct evidence that PSMA functionally contributes to PCa progression remains elusive. We generated mice bearing PSMA-positive or PSMA-negative PCa by crossing PSMA-deficient mice with transgenic PCa (TRAMP) models, enabling direct assessment of PCa incidence and progression in the presence or absence of PSMA. Compared with PSMA-positive tumors, PSMA-negative tumors were smaller, lower-grade, and more apoptotic with fewer blood vessels, consistent with the recognized proangiogenic function of PSMA. Relative to PSMA-positive tumors, tumors lacking PSMA had less than half the abundance of type 1 insulin-like growth factor receptor (IGF-1R), less activity in the survival pathway mediated by PI3K-AKT signaling, and more activity in the proliferative pathway mediated by MAPK-ERK1/2 signaling. Biochemically, PSMA interacted with the scaffolding protein RACK1, disrupting signaling between the  $\beta_1$  integrin and IGF-1R complex to the MAPK pathway, enabling activation of the AKT pathway instead. Manipulation of PSMA abundance in PCa cell lines recapitulated this signaling pathway switch. Analysis of published databases indicated that IGF-1R abundance, cell proliferation, and expression of transcripts for antiapoptotic markers positively correlated with PSMA abundance in patients, suggesting that this switch may be relevant to human PCa. Our findings suggest that increase in PSMA in prostate tumors contributes to progression by altering normal signal transduction pathways to drive PCa progression and that enhanced signaling through the IGF-1R/ $\beta_1$  integrin axis may occur in other tumors.

## INTRODUCTION

Prostate cancer (PCa) is the most commonly diagnosed cancer in men in the United States and the second leading cause of cancer deaths in American men over 50 [after lung cancer (1)]. Although the precise cause of PCa remains unknown, clinical and experimental observations suggest that hormonal, genetic, and environmental factors may each play a role. It is well established that androgens play a crucial role in PCa development. In most of the early cases, PCa can be effectively treated by either surgery or targeted pharmacological manipulation of the androgen receptor (AR) and its target genes (2). Unfortunately, once metastatic disease develops, this therapy is no longer effective, in part related to the loss or mutation of AR in late-stage PCa, suggesting an activation or shift to alternate prosurvival cancer signaling pathways (3). Although the relationship between these signaling pathways most likely varies within different tumors, elucidation of the global molecular mechanisms responsible for this prosurvival switch is necessary to improve treatment strategies for patients with advanced-stage PCa.

One common mechanism promoting the malignant cell behavior involves changes in the activation status of receptor tyrosine kinases (RTKs). The type 1 insulin-like growth factor receptor (IGF-1R) has often been implicated in cancer progression (4, 5), and increased abundance of IGF-1R have been observed in most primary and metastatic prostate tumors (6). Evidence suggests that increased and sustained IGF-1R signaling underlies persistent PCa survival and growth as tumors progress to androgen independence (7). However, results

from recent clinical trials targeting the IGF-1R pathway have been disappointing (8), suggesting that a more complex mechanism promotes malignant cell behavior. Alternatively, cross-talk between critical signal transduction pathways and aberrant activation of distinct pathways have both been implicated in cancer promotion (9), typified by the cross-talk between the IGF-1R and the  $\beta$  integrin signaling pathways, which has been implicated in breast cancer (10–21) and PCa (22–26), neuroblastoma (27, 28), and multiple myeloma (29), among others (30). Identification of the shared and unique participants of these pathways and their contribution to disease progression are necessary to improve therapeutic strategies for cancers of numerous etiologies.

PSMA is a 750–amino acid type II transmembrane peptidase enzyme that is encoded by the folate hydrolase 1 (*FOLH1*) gene. Although PSMA is also known as glutamate carboxypeptidase II, *N*-acetyl-L-aspartyl-L-glutamate peptidase I, and *N*-acetylaspartylglutamate peptidase, those studying PCa or general oncology commonly use the term PSMA, which will be used here. It has been shown that PSMA is present in low amounts on prostate epithelial cells and is progressively up-regulated during disease progression in prostate tumors, in which it correlates negatively with prognosis (31–33) and consequently may be a promising tool for the diagnosis, detection, localization, and treatment of PCa. Currently, PSMA is used as an immunoscintigraphic target in the clinic to direct therapy to androgen-independent prostate tumors. RNA aptamers selectively targeting PSMA enzymatic activity have also been successful in slowing primary tumor growth in murine models (34, 35). Although we have previously shown that endothelial-expressed PSMA regulates angiogenesis (36, 37) and retinal neovascularization (38) primarily via  $\beta_1$  integrin-mediated cell adhesion, an important functional role for PSMA in PCa has not been demonstrated. To directly investigate

<sup>1</sup>Center for Vascular Biology, University of Connecticut Health Center, Farmington, CT 06030, USA. <sup>2</sup>Department of Genetics and Developmental Biology, University of Connecticut Health Center, Farmington, CT 06030, USA. <sup>3</sup>Department of Urology, New York Medical College, Valhalla, NY 10595, USA.

\*Corresponding author. Email: lshapiro@uchc.edu

the role of PSMA in PCa progression, we crossed *FOLH1* global knockout mice (hereafter called PSMA knockout) (39) with the well-characterized transgenic adenocarcinoma of the mouse prostate (TRAMP) murine model (40, 41) to study PCa tumor progression in the absence of PSMA expression.

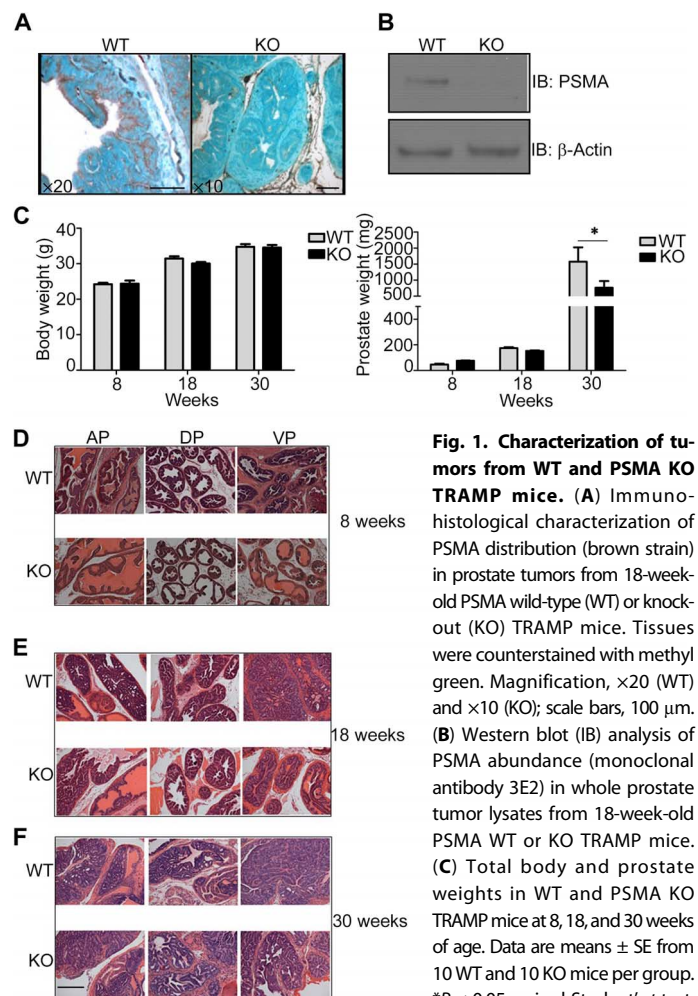
Here, we report that expression of PSMA in prostatic epithelial cells directly underlies prostate tumor progression *in vivo*. We found that tumors in wild-type animals were larger and of higher grade with a higher microvessel density as compared to tumors in the PSMA knockout animals, which is consistent with our previous results implicating PSMA as an angiogenic regulator (36, 37, 42). In addition, PSMA-positive tumor cells were viable at greater distances from the vasculature than their PSMA knockout counterparts, suggesting that cell-intrinsic survival components also contribute to tumor growth. Accordingly, wild-type tumors expressed relatively greater amounts of IGF-1R and exhibited greater activation of the phosphatidylinositol 3-kinase (PI3K)–AKT pathway, whereas tumors lacking PSMA not only had decreased IGF-1R expression but also had diverted signaling downstream of PI3K–AKT to the mitogen-activated protein kinase (MAPK)–extracellular signal–regulated kinases 1 and 2 (ERK1/2) pathway, consistent with a PSMA-dependent signaling switch. Moreover, manipulation of PSMA expression in mouse TRAMP-C1 cell lines and human PCa cell lines recapitulated this change in signaling. Analysis of publically available gene expression data sets from PCa samples confirmed that high PSMA expression was predictive of a high Gleason score. In addition, patient samples with high PSMA expression and high Gleason scores displayed a prosurvival gene expression signature with increased expression of the antiapoptotic marker survivin and IGF-1R, consistent with a role for PSMA in the regulation of signal transduction in human PCa disease as well. Therefore, in addition to its role as a PCa marker and target, our results indicate that increasing amounts of PSMA in prostate tumor epithelium serve to drive prosurvival mechanisms and thus identify it as a functional regulator of prostate tumor progression. These findings also suggest that PSMA-positive tumors may be more sensitive to PI3K pathway inhibitors and less sensitive to MAPK pathway inhibitors.

## RESULTS

Previous studies of PSMA in PCa progression have primarily involved manipulation of PSMA expression in established tumor cell lines. To genetically address the contribution of PSMA to PCa development and progression, we crossed PSMA knockout mice with TRAMP transgenic mice. The TRAMP murine model of PCa has been extensively characterized and closely mimics PCa progression seen in patients from onset of hyperplasia to adenoma and, eventually, to adenocarcinoma (40, 41). TRAMP mice uniformly and spontaneously develop autochthonous prostate tumors after the onset of puberty consequent to the expression of the SV40 T antigen from the rat probasin promoter (41, 43). Disease onset occurs by 8 weeks of age, adenoma occurs by 18 weeks, and most tumors are poorly differentiated and highly invasive by 30 weeks (40, 41). Considered within the range of their validity, TRAMP mouse models have been predictive of clinical outcome. To directly assess the contribution of PSMA to PCa initiation and progression, we initially determined that PSMA was expressed in tumors from the TRAMP model. F2 progeny of PSMA knockout or wild-type mice bred to TRAMP transgenic animals produced tumors that were either positive or negative for PSMA expression (Fig. 1A). Western blot analysis of tumor lysates derived from

PSMA knockout animals verified the complete loss of PSMA protein expression (Fig. 1B). Analysis of body and total prostate weights of wild-type and PSMA knockout animals at the established time points of 8, 18, and 30 weeks of age showed that although overall body weight at 18 weeks of age was significantly different between genotypes, this discrepancy was not seen at 8, 30, or >33 weeks of age (Fig. 1C). Conversely, the total prostate weights of wild-type mice were substantially higher than those of the PSMA knockout mice older than 30 weeks.

Considering the differences between mouse and human prostate tissue and the differences in rates at which lesions can progress in each lobe of the prostate (44), we assessed the dorsal, ventral, and anterior lobes separately at each time point using a double-blind, numerical scoring system based on histologically distinguishable patterns of growth and disease (45). Briefly, on the basis of a histological grading scheme for TRAMP mice developed by Suttie *et al.* (45), hematoxylin and eosin (H&E)–stained tissues were graded as hyperplasia (grades 1 to 3), adenoma (grades 4 to 5), or adenocarcinoma (grade 6). Within



of H&E-stained sections of anterior prostate (AP), ventral prostate (VP), and dorsal prostate (DP) lobes from PSMA WT and PSMA KO mice at 8 (D), 18 (E), and 30 (F) weeks of age.  $n = 30$  for each experimental group. Magnification,  $\times 25$ ; scale bar, 100  $\mu\text{m}$ .

each grade, a distribution was assigned as focal, multifocal, or diffuse (Table 1).

At 8 weeks of age (the initial time point), in the anterior lobe, the minimum lesion grade was the same for both the wild-type and PSMA knockout tumors (grade 2, focal), and the most severe grade was higher in the wild-type mouse tumor (grade 3, diffuse). In the dorsal lobe, the highest grade observed (grade 4, diffuse) was once again in the wild-type tumor, and the lowest grade (grade 2, multifocal) was observed in the PSMA knockout tumor. Finally, in the ventral lobe, the highest grade was seen in the wild-type tumor (grade 4, multi-

focal), and the lowest grade observed was identical for both experimental conditions (Fig. 1D).

At 18 weeks of age (the intermediate time point), in the anterior lobe, although the minimum lesion grade was the same for the wild type and PSMA knockout (grade 3, focal), the most severe grade was significantly higher in the wild-type mouse tumor (grade 5, multifocal) than in the PSMA knockout (grade 4, focal). In the dorsal lobe, the minimum lesion grade was slightly higher in the wild type (grade 3, diffuse) than in the PSMA knockout (grade 3, multifocal). However, the maximum grade was significantly higher in the wild type (grade 5,

**Table 1. Grade and distribution of prostate lesions.** Histopathological categorization of H&E-stained prostatic lobes from WT and PSMA KO tumors. Number of lesions in each lobe are assigned by grade [hyperplasia (grades 2 to 3), adenoma (grades 4 to 5), or adenocarcinoma (grade 6)] and distribution (focal, multifocal, or diffuse).

Treatment group and lobe	Grade 2			Grade 3			Grade 4			Grade 5			Grade 6		
	Focal	Multifocal	Diffuse												
<b>Anterior lobe</b>															
<b>Week 8</b>															
WT (n = 26)	3	8		3	7	5									
KO (n = 19)	4	7	3	2	2										
<b>Week 18</b>															
WT (n = 27)			3	2			8	5	5	1	3				
KO (n = 23)			7	8	4	4									
<b>Week 30</b>															
WT (n = 16)						4	3			5	2				2
KO (n = 16)				1		2	4	4		2					2
<b>Dorsal lobe</b>															
<b>Week 8</b>															
WT (n = 27)					7	12	5	2	1						
KO (n = 21)		3	5	3	7	2	1								
<b>Week 18</b>															
WT (n = 27)						1		13	9	2	22				
KO (n = 23)					1	8	6	5	3						
<b>Week 30</b>															
WT (n = 16)							4	3		5	2				
KO (n = 17)							2	4	2	1	2	4			
<b>Ventral lobe</b>															
<b>Week 8</b>															
WT (n = 29)		2	3	2	6	13	1	2							
KO (n = 21)		3	5	3	7	2	1								
<b>Week 18</b>															
WT (n = 27)					1	3	7	8	8						
KO (n = 23)					3	14	4	1	1						
<b>Week 30</b>															
WT (n = 18)						2	3	4	2	1	4			1	1
KO (n = 19)						1	6	3	1	2	3	1			2

Downloaded from https://www.science.org at University of Connecticut on October 29, 2021

multifocal) than in the PSMA knockout (grade 4 diffuse). Finally, in the ventral lobe, the maximum and minimum grades were identical for both conditions; however, the distribution of the grades was significantly different with most wild-type tumors having a higher grade (Fig. 1E).

At 30 weeks of age (the final time point), in the anterior lobe, the minimum grade of the wild type (grade 4, focal) remained slightly higher than that of the PSMA knockout (grade 3, diffuse). However, the highest grade was identical for both conditions (grade 6, diffuse). In both the dorsal lobe and anterior lobe, the maximum and minimum grades were identical (Fig. 1F).

To resolve the difference in grade and distribution between the wild type and PSMA knockout at the 8, 18, and 30 weeks of age, the data were combined and represented by a “distribution-adjusted lesion grade,” which was calculated by assigning a number to each successive rank (for example, 0 = normal; 1 = grade 1, focal; 2 = grade 2, multifocal; ... and so on, whereby 18 = grade 6, diffuse) (Table 2). Proliferative lesions were present in all mice by 8 weeks; however, the PSMA knockout clearly demonstrated less severe pathology at 8 and 18 weeks. There was no statistical difference in tumor score between wild-type and PSMA knockout tumors by 30 weeks, likely indicating that the tumors had progressed to a point beyond the ability to distinguish any differences. Therefore, we chose to focus our subsequent experiments on whole prostate tissues at the time point of 18 weeks of age.

To quantitatively confirm our observation that the lack of PSMA delayed tumor development, we measured expression of established markers of cancer progression. Survivin is a member of the inhibitor of apoptosis family that is highly abundant in most solid tumors where it supports tumor cell survival but is absent in normal, nonmalignant cells (46). Relevant to our study, increased survivin abundance has been associated with resistance to antiandrogen therapy in advanced PCa (46). Survivin prevents the proteolytic cleavage of procaspase-3 to its activated form to inhibit apoptosis, and thus, a reduction in full-length caspase-3 levels is an independent marker of tumor progression (46). Assessment of the 18-week-old tumor lysates showed significantly increased abundance of survivin (Fig. 2A) and concom-

itantly decreased cleaved caspase-3 (Fig. 2B) in the wild-type prostate tumors, consistent with increased disease progression and supporting our observation that PSMA promotes a more aggressive PCa phenotype.

We have previously shown that PSMA regulates endothelial activation in angiogenesis (36) and in retinal neovascularization (38). To assess the effects of PSMA on the formation of tumor vasculature, we quantified endothelial-specific CD31 abundance by immunohistochemistry in the 18-week-old tumors and saw a significant decrease in CD31 staining in prostate tumors from PSMA knockout mice in agreement with our previous studies (Fig. 2C). However, a closer examination revealed marked structural and morphological differences in vessel structure between genotypes. Vessels in wild-type tumors were irregularly branched, tortuous, random, and dilated, a phenotype consistent with tumor vessel angiogenesis. By contrast, vessels in tumors lacking PSMA appeared more regular and organized, a phenotype referred to as normalized, suggesting that PSMA also contributes to the dysregulated vessel growth characteristic of tumor angiogenesis. Tumor vessel “normalization” results in better perfusion, reduced hypoxia, and presumably increased tumor growth (47), which is in contrast to our findings. To functionally confirm that vasculature lacking PSMA is more normalized, we assessed relative hypoxia levels by measuring abundance of the enzyme carbonic anhydrase IX (CA9), which is strongly induced in response to hypoxia, particularly in hypoxic solid tumors that are refractory to conventional therapies (48). Consistent with our observation of more normalized blood vessels, lysates from PSMA knockout tumors exhibited significantly lower amounts of CA9 (Fig. 2D), indicating that these tumors are indeed less hypoxic than their wild-type counterparts. Further histologic examination indicated that both wild-type and PSMA knockout tumors contained defined areas of viable cells immediately adjacent to capillaries surrounded by a perimeter of necrotic cells (granular area). However, the viable cell area (measured as the distance from the capillary to the necrotic region) was more than 30% greater in the wild-type versus PSMA knockout tumors (Fig. 2E). Thus, wild-type cells apparently are able to remain viable at oxygen concentrations that are toxic for normal cells and can survive at greater distances from the vasculature than cells lacking PSMA despite increased tissue hypoxia. TUNEL (terminal deoxynucleotidyl transferase-mediated deoxyuridine triphosphate nick end labeling) staining indicated that cell death by apoptosis was markedly less in the wild-type compared to the PSMA knockout tumors (Fig. 2F), which is supported by an increased amount of cleaved poly(adenosine 5'-diphosphate-ribose) polymerase (PARP) Asp<sup>241</sup>, a marker of apoptosis (Fig. 2G) (9). Consequently, immunohistochemical analysis to assess cell proliferation exhibited decreased abundance of the cell proliferation marker Ki67 in PSMA knockout tumors (Fig. 2H). Together, these observations indicate that although vessels are more normalized and tumor tissues are less hypoxic in the absence of PSMA, PSMA expression in tumor cells appears to confer an intrinsic survival advantage that is more beneficial to tumor growth than a favorable vessel phenotype.

Tumor cells often escape apoptosis by modifying the expression or activation status of RTKs to induce hyperactivation of prosurvival signal transduction pathways and preserve cell integrity (49). To determine whether the presence of PSMA in advanced PCa may induce similar prosurvival mechanisms, we assayed the activation status of a panel of RTKs that are commonly altered in solid tumors (Fig. 3A) (50). Whereas protein abundance of the RTKs VEGFR2 (vascular endothelial growth factor receptor 2) and EGFR2 (epidermal growth

**Table 2. Prostate mean distribution-adjusted lesion grades.** The mean distribution-adjusted lesion grades for the WT and PSMA KO groups from Table 1 are summarized here. Data are means  $\pm$  SE.

Lobe	Age in weeks	WT	KO
<b>Anterior</b>	8	6.8 $\pm$ 0.20	5.7 $\pm$ 0.16
	18	10.4 $\pm$ 0.21	8.1 $\pm$ 0.17
	30	12.2 $\pm$ 0.26	13.3 $\pm$ 0.04*
<b>Dorsal</b>	8	8.5 $\pm$ 0.16	7.3 $\pm$ 0.03*
	18	11.7 $\pm$ 0.07	10.1 $\pm$ 0.05*
	30	13.3 $\pm$ 0.36	13.6 $\pm$ 0.21
<b>Ventral</b>	8	7.3 $\pm$ 0.15	6.4 $\pm$ 0.07
	18	10.7 $\pm$ 0.10	9.1 $\pm$ 0.03*
	30	12.3 $\pm$ 0.12	13.4 $\pm$ 0.15

\* $P < 0.05$ .

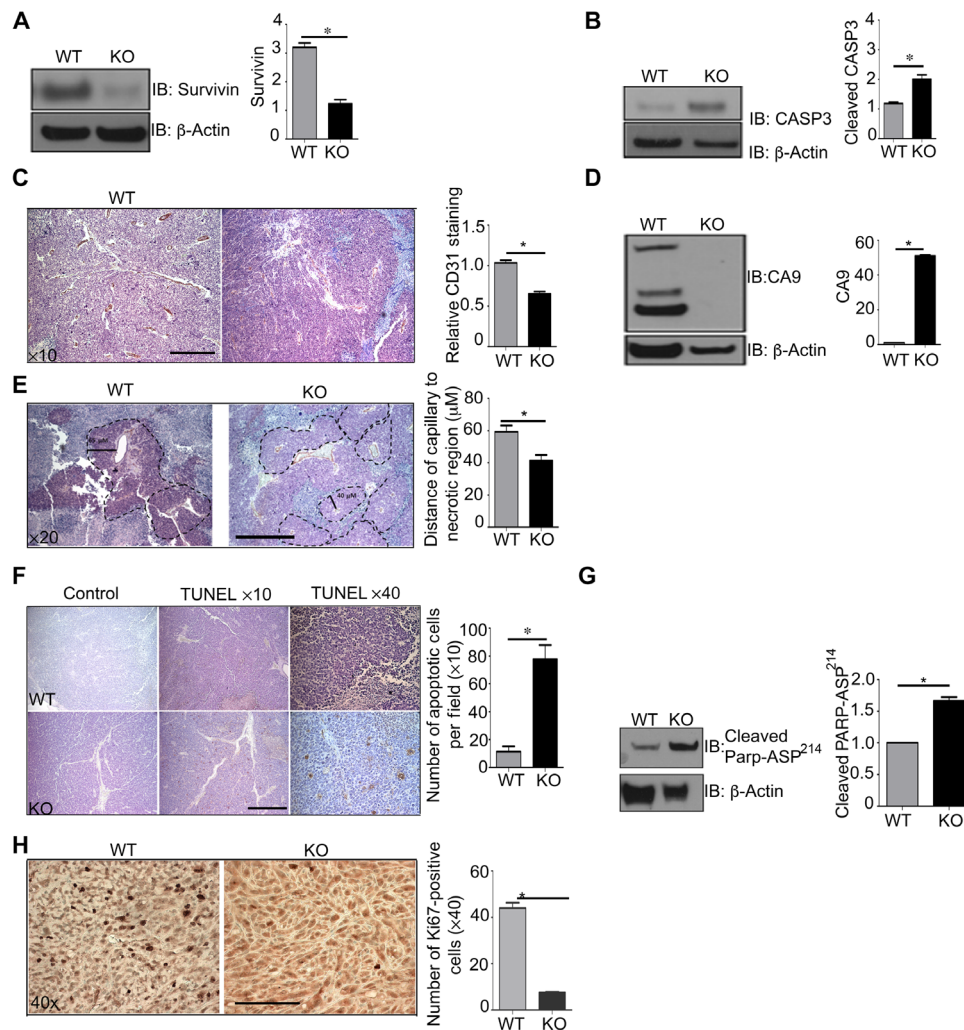


**Fig. 2. PSMA WT prostate tumors display a more vascularized, hypoxia-tolerant, antiapoptotic phenotype.** (A and B) Western blotting for survivin and caspase-3 (CASP3) in whole prostate tumor lysates from 18-week-old PSMA WT and KO TRAMP mice. (C) Immunohistochemical analysis of tumor vasculature by CD31 staining, quantified for CD31<sup>+</sup> pixel area sum from five nonoverlapping fields per sample using Image-Pro Plus software (hematoxylin counterstain). Scale bar, 50  $\mu$ m. (D) Western blot analysis for CA9, a marker of hypoxia, in whole prostate tumor lysate from 18-week-old PSMA WT and KO mouse tumors. (E) Thickness of viable layer of tumor cells from CD31-stained capillaries. PSMA WT (65  $\mu$ M) and KO (40  $\mu$ M). Tissue was counterstained with hematoxylin, and images are shown at  $\times 20$  magnification. Scale bar, 100  $\mu$ m. (F) Representative TUNEL stain to detect apoptotic cells (brown) in PSMA WT and KO tumor sections from 18-week-old mice. Sections were counterstained with hematoxylin. Analysis is representative of the number of apoptotic cells per field. Images are shown at  $\times 10$  and  $\times 40$  magnifications. Scale bar, 50  $\mu$ m. (G) Western blot analysis of cleaved PARP Asp<sup>214</sup>, a marker of apoptosis, in PSMA WT tumors compared to PSMA KO tumors. (H) Immunohistochemical analysis of cell proliferation (Ki67 staining) in PSMA WT and PSMA KO tumor sections. Scale bar, 100  $\mu$ m. All Western blots were normalized to  $\beta$ -actin and are presented as fold change relative to WT. Data are means  $\pm$  SE from  $n = 4$  animals for each experimental group, with at least three experimental replicates. \* $P < 0.05$ , paired Student's  $t$  test.

factor receptor 2) was unchanged in both the wild-type and PSMA knockout PCa tumors, wild-type PCa tumors displayed higher amounts of total IGF-1R, consistent with our prosurvival phenotype. In addition, elements of the PI3K-AKT prosurvival pathway PDK1-Ser<sup>241</sup>, and AKT-Thr<sup>308</sup> were stimulated and amounts of GSK-3 $\beta$ -Ser<sup>309</sup> were decreased (Fig. 3B). Surprisingly, signal transduction in the PSMA knockout prostate tumors was completely reversed, where the MAPK-ERK1/2 pathway is clearly enhanced, as illustrated by increased growth factor receptor-bound protein 2 (GRB2) adaptor pro-

tein levels and ERK phosphorylation in PSMA knockout tumors compared to wild type (Fig. 3C).

As a relatively slow-growing tumor, primary PCa can be present for years before detection, and latency to metastasis can also be quite protracted. However, a percentage of patients present with a more rapidly growing, aggressive form of PCa that has a markedly worse diagnosis. We observed that tumor progression and growth are delayed in PSMA knockout animals, although tumors from wild-type and PSMA knockout animals are histologically indistinguishable at the extended 30-week time point, suggesting either that the pathway switch we see at 18 weeks of age is eventually reversed, that a small percentage of cells do not switch and eventually outgrow the slower growing population, or that tumors with low levels of PSMA may correlate with the slower, less aggressive tumor type. To determine the signaling status of PSMA knockout tumors at 30 weeks of age, we assessed activation levels of the AKT versus ERK signaling pathways. Western blot analysis determined that AKT phosphorylation Thr<sup>308</sup> is maintained in the long term in PSMA wild-type tumors but not in PSMA knockout (Fig. 3D), consistent with a permanent pathway switch in the absence of PSMA and perhaps indicating that tumors presenting with low PSMA abundance may be a marker of the slower, less aggressive form of PCa.

To confirm that this pathway switch is strictly dependent on PSMA, we functionally manipulated PSMA by CRISPR (clustered regularly interspaced short palindromic repeats) deletion in both the human 22Rv1 and murine TRAMP-C1 cell lines (Fig. 4A and figs. S1 and S2) or small interfering RNA (siRNA) knockdown or by disrupting intracellular interactions with a PSMA-specific N-terminal blocking peptide in TRAMP-C1 cells (fig. S3) (36), which consistently resulted in effects on signaling via the AKT pathway (Fig. 4, A and B). Overexpression of human PSMA in the PSMA knockout human PC-3 PCa cell line altered signaling pathways similar to that we observed in wild-type tumors, demonstrating that these mechanisms are operative in human PCa (Fig. 4C). Together, our data suggest that in both the in vivo murine TRAMP model and the in vitro tumor cell lines, PSMA directly contributes to tumor progression by affecting IGF-1R signal transduction to result in a signaling pathway switch that promotes tumor survival, growth, and progression.

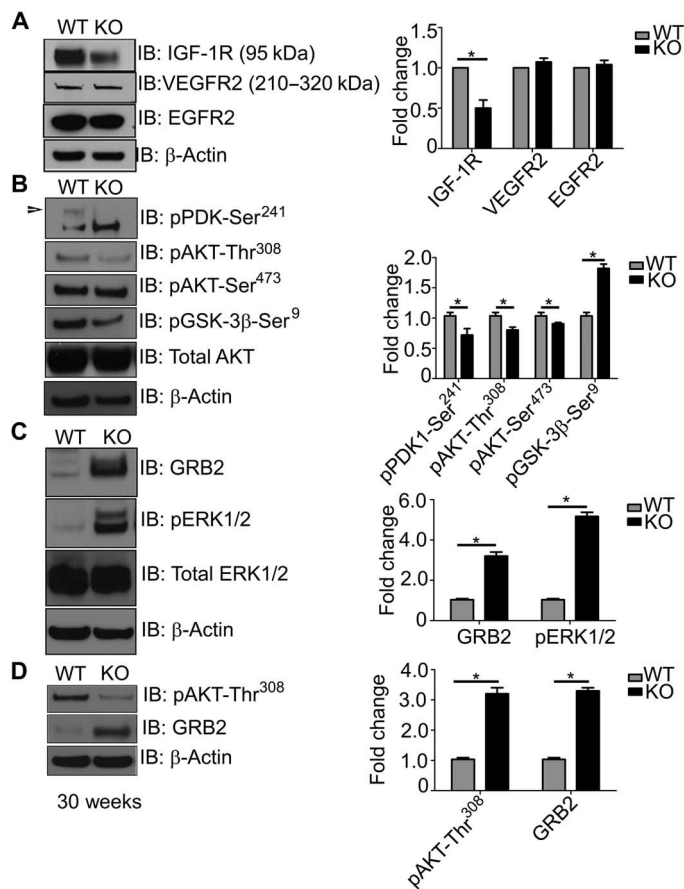


**Fig. 3. PSMA within the prostate tumor epithelium shifts cell signaling from an “active GRB2-ERK1/2 pathway–inactive PI3K-AKT pathway” state to an “active PI3K-AKT pathway–inactive GRB2-ERK1/2 pathway” state.** (A to C) Western blotting of whole prostate tumor lysates from 18-week-old PSMA WT or KO TRAMP mice for various RTKs (A), AKT pathway markers (B), and MAPK pathway markers (C). (D) Blotting for the indicated markers in tumors from 30-week-old PSMA WT and KO mice. Blots are representative of three experiments from  $n = 3$  WT and 3 KO mice, normalized to  $\beta$ -actin and presented as fold change relative to WT. \* $P < 0.05$ , paired Student's  $t$  test.

Aberrant or disrupted interactions between components of signaling pathways are frequently responsible for alterations in downstream signaling pathways during tumorigenesis (51). One such example is cooperation between IGF-1R and  $\beta_1$  integrin that regulates cancer cell growth, survival, and invasion (52). We have previously shown that PSMA regulates angiogenesis by modulating  $\beta_1$  integrin-dependent focal adhesion kinase (FAK)-Tyr<sup>925</sup> phosphorylation and signal transduction in endothelial cells (36, 37), and here, we demonstrate that PSMA affects IGF-1R signaling pathways in PCa cell lines (Fig. 5), suggesting that PSMA may affect IGF-1R/ $\beta_1$  integrin/FAK cross-talk. To further investigate PSMA in this capacity, we examined the aspects of the complex containing scaffolding protein RACK1 (receptor for activated C kinases) that facilitates cooperation between  $\beta_1$  integrin and RTKs (18, 19, 21, 53). Stable IGF-1R/RACK1/ $\beta_1$  integrin complex formation leads to activation of the ERK pathway, and disruption of this complex stimulates the AKT survival pathway (53–56), analogous to the PSMA-dependent pathway switch. Initial evaluation of potential PSMA effects on FAK status in PCa cells showed that whereas FAK is markedly phosphorylated on FAK-Tyr<sup>397</sup> in the wild-type

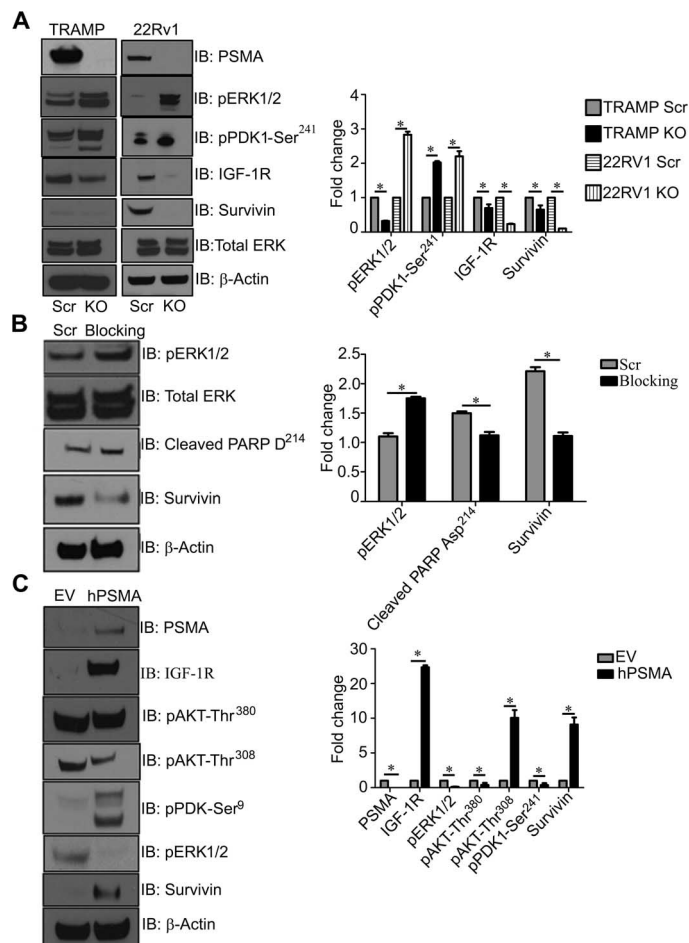


**Fig. 4. Manipulation of PSMA in both mouse TRAMP-C1 and human 22Rv1 and PC-3 PCa cell lines mimic pathway switch.** (A) CRISPR knockdown of PSMA in both the mouse TRAMP-C1 cell line (TRAMP-PSMA<sup>KO</sup>) and the human 22Rv1 cell line (22RV1-PSMA<sup>KO</sup>). Western blot analysis of both CRISPR cell lines to examine changes in PDK-Ser<sup>241</sup>, IGF-1R, survivin, and pERK1/2 compared to controls (Scr). (B) TRAMP-C1 cells transiently transfected with peptides blocking the PSMA NH<sub>2</sub>-terminal cytoplasmic tail. Western blot at 24 hours for pERK1/2, cleaved PARP Asp<sup>214</sup>, and survivin at 24 hours compared to the control (Scr). (C) Western blot analysis of PC-3 cells expressing human PSMA (hPSMA) and empty vector (EV) control cell lysates to investigate changes in the previously identified signaling pathways (PSMA, IGF-1R, AKT-Ser<sup>380</sup>, AKT-Thr<sup>308</sup>, PDK1-Ser<sup>241</sup>, pERK1/2, survivin, and  $\beta$ -actin). All data are representative images from the mean  $\pm$  SE of  $n = 3$  for each experimental condition and three experimental replicates normalized to  $\beta$ -actin and presented as fold change, where WT is equal to 1. \* $P < 0.05$ , paired Student's  $t$  test.

22Rv1 cell lines and tumors, elimination of PSMA expression in 22Rv1-Crispr-PSMA<sup>knockout</sup> cells or PSMA knockout tumors clearly switches FAK tyrosine phosphorylation to FAK-Tyr<sup>925</sup> (Fig. 5, A and B). This result confirms a role for PSMA in integrin activation in PCa cells and is consistent with observations of FAK-Tyr<sup>397</sup> hyperphosphorylation in cells where the IGF-1R/RACK1/ $\beta_1$  integrin complex is disrupted by IGF-1R mutation (21). Furthermore, immunoprecipitation of PSMA followed by Western blot analysis demonstrated that PSMA physically associates with RACK1 and IGF-1R in prostate cell lysates (Fig. 5, C and D) and that the association between RACK1 and  $\beta_1$  integrin is increased when PSMA is deleted (Fig. 5E). In further support of this notion, ligation of integrins by the addition of fibronectin, which is

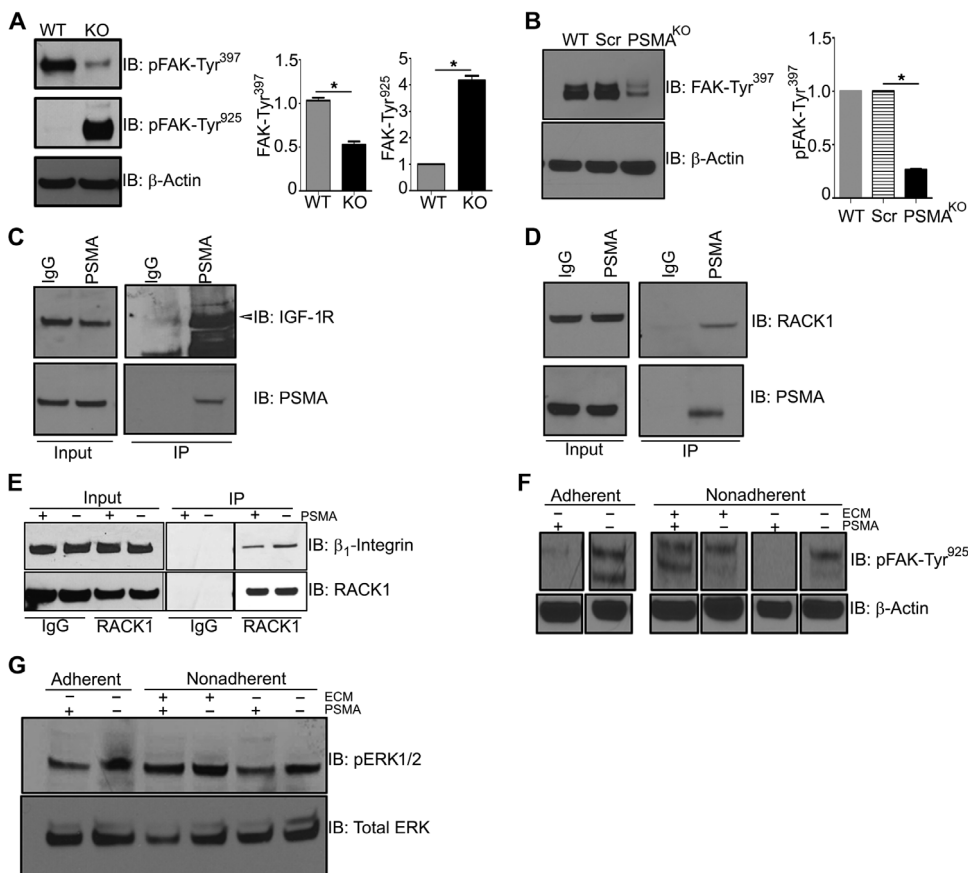


**Fig. 5. PSMA expression markedly alters FAK phosphorylation, and PSMA is in a complex with RACK1 and IGF-1R.** (A) Western analysis for FAK-Tyr<sup>397</sup> and FAK-Tyr<sup>925</sup> in tumor lysates from 18-week-old WT and KO mice. (B) Western blot analysis for FAK-Tyr<sup>397</sup> in parental WT, control scramble 22Rv1 cells (Scr), and 22Rv1-PSMA<sup>KO</sup> cells. (C) Immunoprecipitation (IP) of PSMA in WT 22Rv1 cells using PSMA monoclonal antibody or rabbit immunoglobulin G (IgG) control and Western blot for IGF-1R (arrow indicates band). Input refers to unbound fraction. (D) Immunoprecipitation of PSMA in WT 22Rv1 cells using PSMA rabbit monoclonal antibody or rabbit IgG control and Western blot for RACK1. (E) Immunoprecipitation of RACK1 in both 22Rv1-PSMA<sup>Scr</sup> and 22Rv1-PSMA<sup>KO</sup> cells and Western blot analysis for  $\beta_1$  integrin. (F and G) Both 22Rv1-PSMA<sup>Scr</sup> and 22Rv1-PSMA<sup>KO</sup> cells were put either not in suspension (adherent) or in suspension (nonadherent) for 2 hours and assayed by Western blot for the direct activation of FAK-Tyr<sup>925</sup> (F) and ERK (G) by addition of extracellular matrix (ECM) for 30 min. All data are representative images from the means  $\pm$  SE of  $n = 3$  for each experimental conditions and three experimental replicates normalized to  $\beta$ -actin and presented as fold change, where WT is equal to 1. \* $P < 0.05$ , paired Student's  $t$  test.

reported to enhance complex formation and FAK-Tyr<sup>925</sup> activation in breast cancer cells (18), leads to increased FAK-Tyr<sup>925</sup> and ERK activation in control 22Rv1 PCa cells expressing PSMA (Fig. 5, F and G). Together, these results support a model where the progressive up-regulation of PSMA expression in PCa tumors serves to alter the IGF-1R/RACK1/ $\beta_1$  integrin complex, leading to alterations in FAK phosphorylation, AKT activation, and enhanced PCa progression (Fig. 6). The dependence of TRAMP tumors on the AKT pathway is supported by studies in which systemic treatment of TRAMP transgenic mice with AKT inhibitors invariably inhibits tumor growth and progression (57–61).

To further investigate the potential link between PSMA expression levels and tumor progression in human PCa, we examined publicly available PCa gene expression data sets [National Center for Biotechnology Information (NCBI) Gene Expression Omnibus (GEO) ([www.ncbi.nlm.nih.gov/geo/](http://www.ncbi.nlm.nih.gov/geo/)) and SEEK (<http://seek.princeton.edu/>)] to determine (i) whether PSMA abundance is predictive of increased

Gleason score and (ii) whether samples with high PSMA and Gleason score display a more prosurvival gene expression phenotype, as we observed in mouse tumors (Fig. 7). A transcriptional analysis of 59 PCa and 39 matched benign tissue samples in the NCBI GEO data set GSE32571 compared tumor samples with a higher Gleason score (4 + 3 and higher) against those with a lower score (3 + 4 and below). Further analysis using GEO2R (data file S1) showed that high PSMA abundance was significantly associated with a higher Gleason score when compared to benign tissue (Fig. 7, A and B). Furthermore, changes in IGF-1R, survivin, and caspase-9, which is involved in the activation of caspases responsible for the initiation of apoptosis, support our murine data (Fig. 7, C and D). Together, these observations support the translational relevance of our findings regarding the role of PSMA in PCa progression and highlight that the identification of novel oncogenic and druggable pathways in patient subgroups with poor prognosis may promote the development of tumor-specific, targeted therapeutic approaches.

## DISCUSSION

The striking up-regulation of PSMA expression during PCa progression and its correlation with patient outcome have been recognized for many years (62). Numerous immunohistochemical investigations have demonstrated extensive PSMA expression in prostate adenocarcinomas and metastases (63–65), but its functional contribution to any aspect of PCa has remained enigmatic. Studies manipulating PSMA concentrations in PCa cell lines have produced contradictory results; one determined that the enzymatic activity of PSMA inhibited PCa cell invasion (66), whereas others found that PSMA expression increased PCa cell invasion in vitro (67). Neither study addressed the underlying mechanism. An interesting in vivo model that used transplanted prostate tissue from PSMA-overexpressing transgenic mice found that PSMA expression correlated with the development of small atypical glands representative of adenocarcinoma, but these PIN-like lesions never progressed to cancer and, again, molecular mechanism was not investigated (68). Here, we directly address whether the increased abundance of PSMA in advanced prostate tumors is indicative of a functional role for this cell surface peptidase in PCa progression. Using the well-characterized TRAMP model of PCa (69) and global PSMA knockout mice (39), we demonstrate that PSMA promotes dysregulation of IGF-1R signal transduction, resulting in a shift in downstream signal transduction pathways that promote PCa tumor progression in vivo.

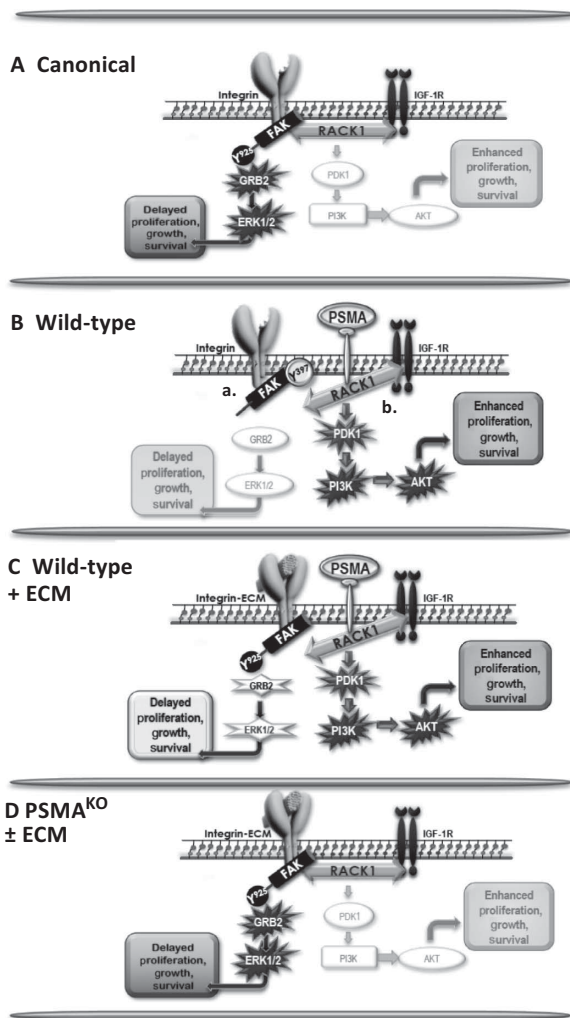


**Fig. 6. Schematic of PSMA regulation of PCa signaling.** (A) In the canonical pathway, a stable scaffolding complex containing  $\beta_1$  integrin, RACK1, and IGF-1R activates the FAK-Tyr<sup>925</sup>/GRB2/ERK pathway, leading to tumor cell proliferation, growth, and migration. (B) In WT cells, PSMA expression disrupts two pathways, both of which contribute to activation of the more aggressive, protumor PI3K-AKT pathway. PSMA physically associates with IGF-1R and RACK1, consistent with PSMA disrupting the scaffolding complex, which leads to FAK-Tyr<sup>397</sup> hyperphosphorylation (“a”), and PSMA expression reverses the phosphorylation of FAK-Tyr<sup>925</sup>, which is required for FAK/GRB2 interactions, thus inactivating ERK signal transduction (“b”). (C) Bypassing PSMA interference by directly activating FAK-Tyr<sup>925</sup> with extracellular matrix (ECM) rescues activation of FAK-Tyr<sup>925</sup> and the GRB2/ERK signaling pathway. (D) The absence of PSMA allows stable IGF-1R/RACK1/ $\beta_1$  integrin complex formation and activation of the FAK-GRB2-ERK canonical pathway, producing less aggressive tumors.

The IGF-1R has emerged as a molecule with important roles in cancer biology (7) and is overexpressed in a high percentage of primary and metastatic tumors, including PCa (4, 5, 7, 70). Most of the studies on IGF-1R signaling have focused on its role in the differential activation of two important intracellular signaling pathways: the MAPK-ERK pathway, which regulates cell proliferation, differentiation, and tissue homeostasis, or the PI3K-AKT cascade, which promotes cell survival, metabolism, antiapoptosis, and differentiation (6, 71). It is known that ligand binding to IGF-1R triggers the phosphorylation of multiple tyro-

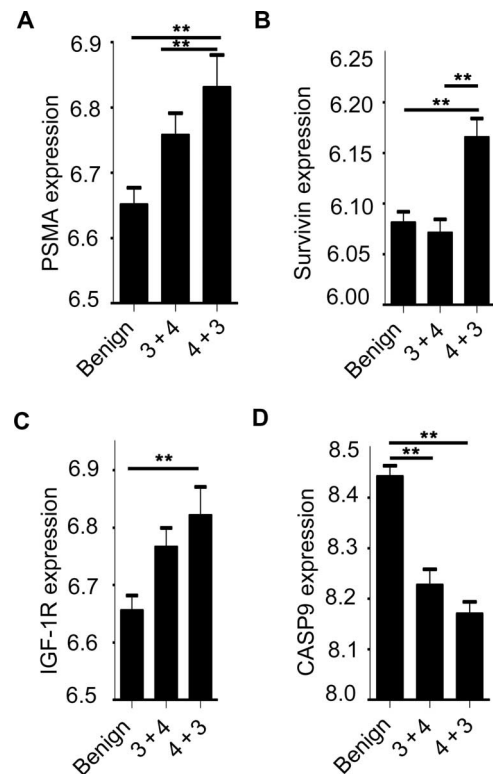


**Fig. 7. PSMA levels in human prostate tumors are significantly associated with an increase in Gleason score.** (A) GEO data set GSE32571 analyzed 59 PCa and 39 matched benign tissue samples for transcriptional differences between tumor samples with higher Gleason score (4 + 3 and higher) against samples of lower Gleason score (3 + 4 and lower). High PSMA gene expression is concurrent with high Gleason score in human tumor samples. (B and C) Abundances of survivin and IGF-1R are high in more aggressive tumors. (D) Abundance of caspase-9 (CASP9) decreases with tumor aggressiveness. Subgroup labels are along the bottom of the chart. Benign:  $n = 39$ ; “3 + 4”: tumors with a low Gleason score,  $n = 32$ ; “4 + 3”: tumors with a high Gleason score,  $n = 27$ . Groups that reach  $**P < 0.005$  are indicated on the graph. Gene expression on the y axis is presented as the relative expression of the gene of interest compared to all the other genes in the array. A distribution analysis of all selected samples determined that all selected samples were suitable for comparison. Data analysis was completed using GEO2R, for which the R script is provided in data file S1.

sine sites within the IGF-1R activation loop, creating a docking site for the signaling molecules IRS-1 and Shc. These interactions subsequently activate the PI3K-AKT and MAPK-ERK cascades through IGF-1R recruitment of either the P85 subunit of PI3K or the Ras-activating Grb2/SOS complex (72).

We see a high abundance of IGF-1R in wild-type tumors, which is markedly reduced upon loss of PSMA. A retrospective analysis of next-generation sequencing data from about 900 breast cancer samples showed that a large majority of tumors contained genetic alterations that resulted in either the activation of PI3K pathway or the repression of the MAPK pathway, but rarely contained both (73). A third group of tumors harbored amplifications or mutations resulting in increased expression of genes encoding the receptor-type tyrosine kinases IGF-1R, EGFR, or ERB-B2, which were accompanied by PI3K activation and MAPK repression, whereas the genes encoding components of the PI3K and MAPK pathways were intact. The authors interpreted this mutually exclusive, “mirror” pattern of genetic alterations to illustrate the intimate interregulation of the RTK, PI3K, and MAPK pathways

and hypothesized that the primary role of RTK up-regulation in tumors may be to regulate these kinases, thereby affecting the tumor cell balance among proliferation, self-renewal, and differentiation (73). Our study shows a very similar signaling signature in PCa with increased IGF-1R abundance, activation of the PI3K, and down-regulation of MAPK pathways in the presence of PSMA. However, in our model, rather than IGF-1R up-regulation by mutation or amplification, we demonstrate that IGF-1R abundance is PSMA-dependent and is potentially responsible for PI3K activation, thus controlling primary tumor advancement. Amounts of IGF-1R-mediated signaling do not change significantly during primary tumor progression in the TRAMP mice on the wild-type (PSMA<sup>+</sup>) background (74), and treatment of wild-type TRAMP mice with various AKT inhibitors reliably reduces tumor size and progression (57–61), further implicating PSMA as a driver of IGF-1R/AKT signaling and prostate tumor progression. Therefore, although the IGF-1R-dependent pathway switch we observe in advancing tumors is not unprecedented, its connection with this highly verified marker of PCa progression provides novel mechanisms, whereby PSMA expression promotes a more aggressive, apoptosis-resistant prostate tumor phenotype.

During cancer development, frequent cross-talk between receptor-driven signal transduction pathways often occurs and results in alterations in downstream signal transduction pathways (51). We have previously shown that PSMA regulates angiogenesis by modulating integrin signal transduction and  $\beta_1$  integrin-dependent FAK-Tyr<sup>925</sup> phosphorylation in endothelial cells (36, 37, 42) and show here that its expression alters FAK phosphorylation and IGF-1R signaling pathways in PCa cells (Fig. 6). A large body of evidence has suggested that cooperation between  $\beta_1$  integrin and RTKs regulates cancer cell growth, survival, and invasion in many tumor types (10–30, 52) and has been shown to involve the multifunctional scaffolding protein RACK1 (18–21). RACK1 physically interacts with multiple partners, thereby influencing their function by modifying stability, activity, or interactions with other proteins [reviewed in (75)]. Pertinent to this study, in breast and prostate tumor cells, RACK1 has been shown to promote migration and cell survival by scaffolding IGF-1R and  $\beta_1$  integrin to integrate signaling via recruitment of signaling proteins such as SHC and SHP2 (18–20, 26), whereas interruption of the IGF-1R/RACK1 interaction leads to activation of AKT (21). In prostate tumor cells, we find that RACK1 and IGF-1R associate with PSMA and that deletion of PSMA in PCa cell lines enhances the  $\beta_1$  integrin/RACK1 interaction, suggesting that PSMA may regulate integrin/IGF-1R cross-talk via its interaction with RACK1. Because binding of some proteins to RACK1 is competitive, our data are consistent with a model where the PSMA/RACK1 interaction disrupts or alters the IGF-1R/RACK1/ $\beta_1$  integrin complex, leading to aberrant cross-talk between  $\beta_1$  integrin and IGF-1R that favors PI3K-AKT activation in our PSMA wild-type tumor cells. Finally, although PSMA is expressed primarily in prostate and neuroendocrine cancers, the IGF-1R/ $\beta_1$  integrin axis has been implicated in many tumor types, and RACK1 has been demonstrated to interact with numerous, disparate proteins from cytoplasmic (PP2A, p85 PI3K, SHP-2, SRC, smoothed, Stat3, and TROP-2) to various cell surface proteins (PSMA, IGF-1R, and IR) (18–21, 23, 26, 53, 76). Thus, our findings regarding the regulation of signal transduction by interaction of PSMA with RACK1/IGF-1R will likely extend to other tumor types and cell surface molecules.

Historically, in oncology, PSMA has been studied as a reliable clinical biomarker for the diagnosis, detection, localization, and manage-

ment of PCa. A number of PSMA-targeted small and low-molecular weight inhibitors and antibodies have proven valuable in providing high image quality in diagnostic imaging and delivering high local doses of radiopharmaceuticals [reviewed in (77–79)]. Alternatively, targeting the PSMA-dependent mechanisms driving PCa tumor progression may provide a novel paradigm for the development of therapeutic strategies for treatment by targeting both progression and vascularization because we have shown that inhibition of PSMA with the inhibitor 2-PMPA impairs integrin activation, endothelial cell adhesion, and angiogenesis (36, 37, 42). Ligand engagement of PSMA induces its internalization, and therefore, it also presents an effective delivery system for therapeutic molecules (80). Recent preclinical characterization of PSMA-targeted RNA aptamers that bind to and block the enzymatic activity of PSMA has been described that specifically target therapies to primary tumors and disseminated PCa cell lines in vivo (35, 81, 82). Finally, TRAMP mice lacking PSMA develop more slowly growing tumors but eventually proceed to high-grade pathologies, likely because of their dependence on the weaker but still oncogenic Ras/MAPK pathway. Together with these observations, our study suggests the potential for design of combination therapies that exploit the PCa-dependent increase in PSMA expression, the proven ability of PSMA-targeting agents to deliver payloads, and the PSMA-dependent pathway switch by agents designed to deliver Ras/MAPK/ERK inhibitors or siRNA directly to PSMA-expressing tumor cells, thereby inducing the switch to the less aggressive pathway while silencing the tumors' escape mechanism. Such targeted, biology-based therapy has the potential to provide novel, less-toxic, and effective therapies that could have a broad positive impact on outcomes in PCa and in other tumors that rely on the IGF-1R/integrin axis for their oncogenicity.

## MATERIALS AND METHODS

### Mice

All procedures used in handling mice were approved by the Animal Care Committee of UCONN Health in compliance with Animal Welfare Assurance. TRAMP mice on a C57BL6 background have been described (83) and were obtained from The Jackson Laboratory. C57BL6 PSMA knockout mice have been described (84) and were a donation from W. Heston at the Cleveland Clinic. Sibling female TRAMP mice were mated to wild-type and PSMA knockout sibling males. The resultant female TRAMP-hemizygote PSMA heterozygote females were bred with PSMA knockout males to yield TRAMP-hemizygote PSMA knockout females, which were then bred to produce TRAMP-hemizygote PSMA knockout males for the study. In addition, mice from the original cohort were bred with PSMA wild-type males to obtain TRAMP-hemizygote PSMA wild-type males. Overall, male mice from the same cohort of animals (same original founders) hemizygous for the TRAMP transgene, either PSMA wild type or PSMA knockout (20 mice per genotype per time point; a total of 120 mice), were bred and held until they reach the desired time points (8, 18, and 30 weeks). Mice were provided food and water ad libitum. Littermates were compared in all experiments.

### Genotyping

Mice were genotyped for both PSMA and TRAMP by isolating DNA from tail biopsies [50 mM Tris (pH 8.8), 1 mM EDTA (pH 8.0), 0.5% Tween 20, and 3  $\mu$ g of proteinase K; 50°C overnight and then 100°C for 10 min]. Genotype for PSMA and the TRAMP transgene has been described previously (83, 84).

## Necropsy

Animals were euthanized by CO<sub>2</sub> asphyxiation, in accordance with the guidelines given by the Animal Care Committee of UCONN Health, followed by cervical dislocation to ensure death. Prostate was removed as part of the whole male urogenital system and then dissected away from nonprostatic tissue.

## Cell culture

TRAMP-C1, 22RV1, and PC-3 cells were obtained from the American Type Culture Collection (ATCC). Unless otherwise noted, TRAMP-C1 were cultured in Dulbecco's modified Eagle's medium supplemented with 5% fetal bovine serum (FBS), 5% Nu-Serum IV, 1% penicillin-streptomycin (pen-strep), bovine insulin (0.005 mg/ml), and 10 nM dehydroisoandrosterone. 22RV1 were cultured in RPMI supplemented with 10% FBS, and 1% pen-strep. PC-3 cells were cultured in F-12K supplemented with 10% FBS and 1% pen-strep. All cells were maintained at 37°C, 5% CO<sub>2</sub>.

## Apoptosis evaluation by TUNEL assay

For the evaluation of apoptosis, deparaffinized and rehydrated 6- $\mu$ m-thick sections of whole prostate tumor sections from PSMA wild-type and PSMA knockout mice at 18 weeks of age were incubated with proteinase K (20  $\mu$ g/ $\mu$ l) in 10 mM tris-HCl (pH 7.4) at 37°C for 20 min, and apoptotic cells were detected by the TUNEL method by using the ApopTag Peroxidase In Situ Apoptosis Detection system (EMD Millipore) according to the manufacturer's protocol. Negative controls were prepared by incubating slides without terminal deoxynucleotidyl transferase. Mouse small intestine was used as a positive control. To visualize the immunoreaction products, sections were incubated with a mixture of DAB (3,3'-diaminobenzidine) and H<sub>2</sub>O<sub>2</sub>. Slides were examined and TUNEL-positive cells were counted with hematoxylin. Images were acquired using a Zeiss LSM 510 META based on an Axiovert 200 microscope and processed using Zeiss AxioVision software.

## Antibodies

Antibody against PSMA for immunohistochemistry was purchased from Zymed (517-3294). PSMA monoclonal antibody 3E2 was a kind gift from Memorial Sloan Kettering. Rabbit monoclonal PSMA (D718E; cat. no. 12815) and RACK1 (D59D5; cat. no. 5432) were purchased from Cell Signaling Technologies (CST). Antibody against CD31/PECAM-1 was purchased from Santa Cruz Biotechnology (SCB; sc-1506). Antibody against Ki67 was purchased from Abcam (15580). Antibody against GRB2 was purchased from SCB (sc-503). The following antibodies were purchased from CST: IGF-1R (cat. no. 9750),  $\beta_1$  intergrin (cat. no. 34971), survivin (cat. no. 71G4B7), caspase-3 (cat. no. 9665), CA9 (cat. no. 5648), PDK1-Ser<sup>241</sup> (cat. no. 3438), AKT-Thr<sup>308</sup> (cat. no. 13038), AKT-Ser<sup>473</sup> (cat. no. 4060), GSK-3 $\beta$ -Ser<sup>9</sup> (cat. no. 5558), total AKT (cat. no. 4691), pERK1/2 (cat. no. 197G2), total ERK (cat. no. 9102), and  $\beta$ -actin (cat. no. 3700).

## Western blot analysis

Mouse prostate tumor tissues were removed, weighed, and then washed three times in cold phosphate-buffered saline (PBS). A portion of the tumor was incubated in 1 $\times$  RBC lysis buffer for 10 min (Thermo Fisher Scientific), and the remaining portion of the tumor was saved for RNA extraction and/or paraffin embedding. Samples were then centrifuged at 1000 rpm for 2 min, and the supernatant was removed. The tumor tissue was then homogenized with a PowerGen 125 tissue homogenizer (Thermo Fisher Scientific) in lysis buffer containing 50 mM tris (pH 7.4), 150 mM NaCl, 1% NP-40, plus the tyrosine phosphatase

inhibitor Na<sub>3</sub>VO<sub>4</sub> (1 mM), and the protease inhibitors phenylmethylsulfonyl fluoride (PMSF) (1 mM), pepstatin (1 mM), and aprotinin (1.5 mg/ml). After incubation at 4°C for 20 min, nuclear and cellular debris were removed by microcentrifugation at 14,000 rpm for 10 min at 4°C. Total protein concentrations were determined by the BCA Assay kit (Thermo Fisher Scientific), and 30 to 50  $\mu$ g of each sample was electrophoresed on a 4 to 20% tris-Hepes SDS gradient gel (Pierce) and then electroblotted onto Protran nitrocellulose membranes (Thermo Fisher Scientific) using a semidry transfer apparatus. Membranes were blocked with tris-buffered saline, 5% bovine serum albumin (BSA) for 30 min, washed, and incubated with indicated primary and secondary antibodies for 12 hours and 30 min, respectively. The membranes were washed extensively with tris-buffered saline and 0.1% Tween 20 after secondary antibody incubation and detected using the ECL Western blotting kit (Thermo Fisher Scientific) according to the manufacturer's suggested protocol.

## Immunohistochemistry

Mouse prostate tissues were fixed overnight in 4% paraformaldehyde at 4°C and were paraffin-processed. Slides containing 6- $\mu$ m-thick sections were deparaffinized and rehydrated. Antigen retrieval was conducted using 10 mM sodium citrate (pH 6.0) in a pressure cooker. Endogenous peroxidase activity was quenched by incubating slides for 15 min in 0.3% H<sub>2</sub>O<sub>2</sub>. Slides were blocked in 1% BSA for 30 min at room temperature in a humidified chamber and then incubated with the specified primary antibody overnight in a humidified chamber. Slides were washed in PBS. Biotinylated secondary antibody (Vector Laboratories) in 1% BSA was applied, and slides were incubated for 1 hour at room temperature in a humidified chamber. Slides were washed again, and Vectastain Elite ABC kit (Vector Laboratories) was applied for 30 min. Slides were developed with NovaRED (Sigma-Aldrich) and counterstained with hematoxylin (Vector Laboratories) and then dehydrated and mounted under Cytoseal 60. Images were acquired using a Zeiss LSM510 META based on an Axiovert 200 microscope and processed using the Zeiss AxioVision software.

## PSMA knockdown in TRAMP-C1 by siRNA

siRNA constructs were designed from the mouse *Folh1* GenBank sequence BC119604.1 using the Oligoengine 2.0 software and cloned into the mammalian expression vector pSUPER.retro.puro at Bg III/Hind III (OligoEngine) according to the manufacturer's directions. To generate the retrovirus, plasmid DNA (10  $\mu$ g) was transfected into the Phoenix Amphotropic retrovirus packaging cell line (ATCC) by lipid transfection. Medium containing virus was collected 48 hours after transfection. TRAMP-C1 cells were infected and selected in puromycin (5  $\mu$ g/ml; Sigma-Aldrich). Reduction of PSMA transcript level was evaluated by reverse transcription polymerase chain reaction (PCR) and real-time PCR followed by Western blot evaluation of PSMA protein expression.

PSMA siRNA primers were as follows: 581, 5'-GATCCCCGAA-GATCAGTTGTTCTGGGTTCAAGAGACCCAGAACAACCT-GATCTTCTTTTTTA-3' (forward) and 5'-AGCTTAAAAAG-AAGATCAGTTGTTCTGGGTTCTTGAACCCAGAACAACCT-GATCTTCGGG-3' (reverse); 472, 5'-GATCCCCATGTAGTGCCAC-CATACAGTTC AAGAGACTGTATGGTGGCACTACATTTTTTA-3' (forward) and 5'-AGCTTAAAAAATGTAGTGCCACCATA-CAGTCTTGAACCTGTATGGTGGCACTACATGGG-3' (reverse); 348, 5'-GATCCCCGCTTGTCTGTCTATCCAATTCAAGAGATTG-GATAGGACAGCAAGACTTTTTTA-3' (forward) and 5'-AGCT-TAAAAAGTCTTGTCTGTCTATCCAATCTTGAATTGGATAG-GACAGCAAGACGGG-3' (reverse).

## CRISPR knockout of PSMA in PCa cell lines TRAMP-C1 and 22RV1

PSMA CRISPR/Cas9 constructs were created in both TRAMP-C1 and 22RV1 cell lines using the lentiCRISPRv2 plasmid #52961 (Addgene) (85, 86). To guard against genome-wide off-target effects and still maintain high target specificity, 20-base pair (bp) guide RNA (gRNA) was designed through the CRISPR Design (<http://crispr.mit.edu>) using the target sequence from either the mouse *Folh1* GenBank sequence BC119604.1 or the human *FOLH1* GenBank sequence NG\_029170.1 as input; scramble gRNA was also designed as a control: gRNA for PSMA 22RV1, 5'-TCACGAAACCGACTCGGCTG-3'; gRNA scramble 22RV1, 5'-CAGTCGGGCGTCATCATGAT-3'; gRNA for PSMA TRAMP, 5'-GCAGGACAGAGACTCCGCGG-3'; and gRNA scramble TRAMP, 5'-CAGTCGGGCGTCATCATGAT-3'. In the genome, gRNA sequences were flanked on the 3' end by a 3-bp NGG protospacer adjacent motif sequence. The gRNAs were phosphorylated, annealed, and cloned into a dephosphorylated lentiCRISPRv2 at BSMB1 according to the manufacturer's directions (Addgene). To generate the lentivirus, the plasmid lentiCRISPRv2 containing either the human or the mouse PSMA or scramble gRNA was cotransfected (Lipofectamine 2000, Thermo Fisher Scientific) into HEK293(F)T cells along with the packaging plasmids pMD2.G (#12259, Addgene) and psPAX2 (#12260, Addgene). The culture medium containing virus was collected 48 h after transfection. 22RV1 and TRAMP-C1 cells were infected and selected in puromycin (2 or 5 µg/ml, respectively) (Sigma-Aldrich). Validation of genetic modification in individual TRAMP-CRISPR-PSMA<sup>knockout</sup> and 22RV1-CRISPR-PSMA<sup>knockout</sup> clones was assessed by PCR amplification of the targeted loci and subsequent sequencing. Chromatographs were compared to wild-type cells using TIDE (Tracking of Indels by Decomposition; <https://tide-calculator.nki.nl/>) analysis to identify the mutations in the two alleles (figs. S1 and S2) (87).

## TaqMan (real-time quantitative reverse transcription PCR) analysis

Total RNA from cultured cells was isolated using RNeasy (Qiagen). RNA was reverse-transcribed by standard methods using reverse transcriptase (Invitrogen). For TaqMan real-time PCR, PSMA and 18S primers, TaqMan Gene Expression Assay probe, and primer sets were purchased from Applied Biosystems. An Applied Biosystems Prism 7500 Fast Real-time PCR system (Applied Biosystems) was used with the default thermal cycling program (95°C for 20 s, followed by 40 cycles at 95°C for 3 s and 60°C for 30 s). Reactions were performed in triplicate and normalized to the level of 18S RNA transcript.

## Primers

PSMA primers were as follows: forward IntA, 5'-ATTCAATCCTGCT-CAGACCC-3'; forward Neo-S, 5'-AGCAGGCATGCTGGGGATGC-3'; reverse S49, 5'-GTAGAAGAGGAAGTCTGAGGA-3'. TRAMP primers were as follows: forward TRAMP SV5, 5'-CAGAGCAGA-ATTGTGGAGTGG-3'; reverse TRAMP SV1, 5'-GGACAAACCA-CAACTAGAATGCAGTG-3'.

## PSMA blocking peptide

A peptide containing the C-terminal domain of PSMA was synthesized by Invitrogen. A C-terminal free acid and an N-terminal free amine were added to the completed peptides to aid in transfection. Mouse PSMA, MWNALQDRDSAIEVLGHRQR; scramble, ESAMTWVRLRNP-TADRLAH. For peptide transfections, 1 mg of the PSMA and scrambled peptides were transfected into  $2 \times 10^5$  to  $4 \times 10^5$  TRAMP C-1 cells using

BioPORTER (Qiagen) protein delivery system according to the manufacturer's recommendations. Cotransfection of a positive control fluorescein isothiocyanate (FITC)-containing protein ensured appropriate transfection efficiency (fig. S4). Cells were incubated for 24 hours, washed in PBS, and lysed in 1% NP-40, 150 mM NaCl, 50 mM tris-HCl (pH 7.4) buffer plus the tyrosine phosphatase inhibitor Na<sub>3</sub>VO<sub>4</sub> (1 mM), and the protease inhibitors PMSF (1 mM), pepstatin (1 mM), and aprotinin (1.5 mg/ml). After incubation at 4°C for 20 min, nuclear and cellular debris were removed by microcentrifugation at 14,000 rpm for 10 min at 4°C.

## Stimulation of adherent and nonadherent cells

For analysis of signaling responses affected by the ligation of integrins in 22RV1-CRISPR-PSMA<sup>knockout</sup> adherent cells, the cells and scramble control were washed with PBS and starved from serum for 4 hours before being stimulated with culture medium containing 10% FBS. For analysis of signaling responses affected by the ligation of integrins in nonadherent cells, confluent 22RV1-CRISPR-PSMA<sup>knockout</sup> cells and scramble control were detached with trypsin and then washed with PBS. Cells were resuspended in serum-free medium containing 5% ECM Gel (Sigma-Aldrich) and maintained in suspension for 4 hours before stimulation with culture medium containing 10% FBS.

## Preparation of cellular protein extracts and immunoprecipitation

To study the interaction of PSMA, RACK-1, IGFR-1B, and β<sub>1</sub> integrin, cellular protein extracts from either 22RV1-CRISPR-PSMA<sup>knockout</sup>, scramble, or wild-type cells were prepared by washing cells with PBS and lysed in buffer consisting of tris-HCl (pH 7.4), 150 mM NaCl, 1% NP-40 plus the tyrosine phosphatase inhibitor Na<sub>3</sub>VO<sub>4</sub> (1 mM), and the protease inhibitors PMSF (1 mM), pepstatin (1 mM), and aprotinin (1.5 mg/ml). After incubation at 4°C for 20 min, nuclear and cellular debris were removed by microcentrifugation at 14,000 rpm for 10 min at 4°C. Protein (700 µg) was immunoprecipitated with either 1 µg of RACK1 (D59D5) or PSMA 3E2 antibodies and immunoglobulin G antibodies, with 5 µg of goat anti-rabbit immunoglobulin G Fab fragment as a control (Cell Signaling Technologies), and attached to protein G Dynabeads (Invitrogen) at 4°C with either of the prepared beads overnight. Beads were washed while attached to a DynaMag and eluted according to the manufacturer's directions (Invitrogen).

## Statistical analysis

All experiments in this study were repeated for a minimum of three independent experiments. Differences between means were analyzed using either the two-tailed Student's *t* test or analysis of variance (ANOVA), where appropriate, and significance was set at a *P* < 0.05.

## SUPPLEMENTARY MATERIALS

[www.sciencesignaling.org/cgi/content/full/10/470/eaag3326/DC1](http://www.sciencesignaling.org/cgi/content/full/10/470/eaag3326/DC1)

Fig. S1. CRISPR knockout of PSMA in 22RV1 cells.

Fig. S2. CRISPR knockout of PSMA in TRAMP-C1 cells.

Fig. S3. PSMA knockdown increases the phosphorylation of ERK1/2 and decreases that of PDK in TRAMP-C1 cells.

Fig. S4. Cotransfection of TRAMP-C1 cells with FITC and PSMA blocking peptide.

Data file S1. R script document for analysis of GEO data set GSE32571.

## REFERENCES AND NOTES

1. R. Siegel, C. DeSantis, K. Virgo, K. Stein, A. Mariotto, T. Smith, D. Cooper, T. Gansler, C. Lerro, S. Fedewa, C. Lin, C. Leach, R. S. Cannady, H. Cho, S. Scoppa, M. Hachey, R. Kirch, A. Jemal, E. Ward, Cancer treatment and survivorship statistics, 2012. *CA Cancer J. Clin.* **62**, 220–241 (2012).

2. Y. Chen, C. L. Sawyers, H. I. Scher, Targeting the androgen receptor pathway in prostate cancer. *Curr. Opin. Pharmacol.* **8**, 440–448 (2008).
3. M. P. Roudier, L. D. True, C. S. Higano, H. Vessella, W. Ellis, P. Lange, R. L. Vessella, Phenotypic heterogeneity of end-stage prostate carcinoma metastatic to bone. *Hum. Pathol.* **34**, 646–653 (2003).
4. H. E. Jones, L. Goddard, J. M. W. Gee, S. Hiscox, M. Rubini, D. Barrow, J. M. Knowlden, S. Williams, A. E. Wakeling, R. I. Nicholson, Insulin-like growth factor-I receptor signalling and acquired resistance to gefitinib (ZD1839; Iressa) in human breast and prostate cancer cells. *Endocr. Relat. Cancer* **11**, 793–814 (2004).
5. G. S. Warshamana-Greene, J. Litz, E. Buchdunger, C. Garcia-Echeverria, F. Hofmann, G. W. Krystal, The insulin-like growth factor-I receptor kinase inhibitor, NVP-ADW742, sensitizes small cell lung cancer cell lines to the effects of chemotherapy. *Clin. Cancer Res.* **11**, 1563–1571 (2005).
6. G. O. Hellawell, G. D. H. Turner, D. R. Davies, R. Poulson, S. F. Brewster, V. M. Macaulay, Expression of the type 1 insulin-like growth factor receptor is up-regulated in primary prostate cancer and commonly persists in metastatic disease. *Cancer Res.* **62**, 2942–2950 (2002).
7. S. L. Krueckl, R. A. Sikes, N. M. Edlund, R. H. Bell, A. Hurtado-Coll, L. Fazli, M. E. Gleave, M. E. Cox, Increased insulin-like growth factor I receptor expression and signaling are components of androgen-independent progression in a lineage-derived prostate cancer progression model. *Cancer Res.* **64**, 8620–8629 (2004).
8. H. X. Chen, E. Sharon, IGF-1R as an anti-cancer target—Trials and tribulations. *Chin. J. Cancer* **32**, 242–252 (2013).
9. S.-W. Yu, S. A. Andrabi, H. Wang, N. S. Kim, G. G. Poirier, T. M. Dawson, V. L. Dawson, Apoptosis-inducing factor mediates poly(ADP-ribose) (PAR) polymer-induced cell death. *Proc. Natl. Acad. Sci. U.S.A.* **103**, 18314–18319 (2006).
10. G. Loughran, N. C. Healy, P. A. Kiely, M. Huigsloot, N. L. Kedersha, R. O'Connor, Mystique is a new insulin-like growth factor-I-regulated PDZ-LIM domain protein that promotes cell attachment and migration and suppresses Anchorage-independent growth. *Mol. Biol. Cell* **16**, 1811–1822 (2005).
11. R. K. Deevi, O. T. Cox, R. O'Connor, Essential function for PDLIM2 in cell polarization in three-dimensional cultures by feedback regulation of the  $\beta$ 1-integrin-RhoA signaling axis. *Neoplasia* **16**, 422–431 (2014).
12. A. Sureshbabu, H. Okajima, D. Yamanaka, E. Tonner, S. Shastri, J. Maycock, M. Szymanowska, J. Shand, S.-I. Takahashi, J. Beattie, G. Allan, D. Flint, IGF1R5 induces cell adhesion, increases cell survival and inhibits cell migration in MCF-7 human breast cancer cells. *J. Cell Sci.* **125**, 1693–1705 (2012).
13. X. Zhang, S. Kamaraju, F. Hakuno, T. Kabuta, S.-I. Takahashi, D. Sachdev, D. Yee, Motility response to insulin-like growth factor-I (IGF-I) in MCF-7 cells is associated with IRS-2 activation and integrin expression. *Breast Cancer Res. Treat.* **83**, 161–170 (2004).
14. C. Huang, C. C. Park, S. G. Hilsenbeck, R. Ward, M. F. Rimawi, Y.-c. Wang, J. Shou, M. J. Bissell, C. K. Osborne, R. Schiff,  $\beta$ 1 integrin mediates an alternative survival pathway in breast cancer cells resistant to lapatinib. *Breast Cancer Res.* **13**, R84 (2011).
15. C. C. Park, H. J. Zhang, E. S. Yao, C. J. Park, M. J. Bissell,  $\beta$ 1 integrin inhibition dramatically enhances radiotherapy efficacy in human breast cancer xenografts. *Cancer Res.* **68**, 4398–4405 (2008).
16. K. J. Martin, D. R. Patrick, M. J. Bissell, M. V. Fournier, Prognostic breast cancer signature identified from 3D culture model accurately predicts clinical outcome across independent datasets. *PLOS ONE* **3**, e2994 (2008).
17. C. C. Park, H. Zhang, M. Pallavicini, J. W. Gray, F. Baehner, C. J. Park, M. J. Bissell,  $\beta$ 1 integrin inhibitory antibody induces apoptosis of breast cancer cells, inhibits growth, and distinguishes malignant from normal phenotype in three dimensional cultures and in vivo. *Cancer Res.* **66**, 1526–1535 (2006).
18. P. A. Kiely, D. O'Gorman, K. Luong, D. Ron, R. O'Connor, Insulin-like growth factor I controls a mutually exclusive association of RACK1 with protein phosphatase 2A and  $\beta$ 1 integrin to promote cell migration. *Mol. Cell Biol.* **26**, 4041–4051 (2006).
19. U. Hermanto, C. S. Zong, W. Li, L.-H. Wang, RACK1, an insulin-like growth factor I (IGF-I) receptor-interacting protein, modulates IGF-I-dependent integrin signaling and promotes cell spreading and contact with extracellular matrix. *Mol. Cell Biol.* **22**, 2345–2365 (2002).
20. L. Lynch, P. I. Vodyanik, D. Boettiger, M. A. Guvakova, Insulin-like growth factor I controls adhesion strength mediated by  $\alpha$ 5 $\beta$ 1 integrins in motile carcinoma cells. *Mol. Biol. Cell* **16**, 51–63 (2005).
21. P. A. Kiely, M. Leahy, D. O'Gorman, R. O'Connor, RACK1-mediated integration of adhesion and insulin-like growth factor I (IGF-I) signaling and cell migration are defective in cells expressing an IGF-I receptor mutated at tyrosines 1250 and 1251. *J. Biol. Chem.* **280**, 7624–7633 (2005).
22. H. L. Goel, A. Sayeed, M. Breen, M. J. Zarif, D. S. Garlick, I. Leav, R. J. Davis, T. J. FitzGerald, A. Morrione, C.-C. Hsieh, Q. Liu, A. P. Dicker, D. C. Altieri, L. R. Languino,  $\beta$ 1 integrins mediate resistance to ionizing radiation in vivo by inhibiting c-Jun amino terminal kinase 1. *J. Cell. Physiol.* **228**, 1601–1609 (2013).
23. M. Trerotola, J. Li, S. Alberti, L. R. Languino, Trop-2 inhibits prostate cancer cell adhesion to fibronectin through the  $\beta$ 1 integrin-RACK1 axis. *J. Cell. Physiol.* **227**, 3670–3677 (2012).
24. A. Sayeed, N. Alam, M. Trerotola, L. R. Languino, Insulin-like growth factor 1 stimulation of androgen receptor activity requires  $\beta$ 1A integrins. *J. Cell. Physiol.* **227**, 751 (2012).
25. H. L. Goel, J. M. Underwood, J. A. Nickerson, C.-C. Hsieh, L. R. Languino,  $\beta$ 1 Integrins mediate cell proliferation in three-dimensional cultures by regulating expression of the sonic hedgehog effector protein, Gli1. *J. Cell. Physiol.* **224**, 210–217 (2010).
26. H. L. Goel, M. Breen, J. Zhang, I. Das, S. Aznavoorian-Cheshire, N. M. Greenberg, A. Elgavish, L. R. Languino,  $\beta$ 1A integrin expression is required for type 1 insulin-like growth factor receptor mitogenic and transforming activities and localization to focal contacts. *Cancer Res.* **65**, 6692–6700 (2005).
27. A. Meyer, C. M. van Golen, B. Kim, K. L. van Golen, E. L. Feldman, Integrin expression regulates neuroblastoma attachment and migration. *Neoplasia* **6**, 332–342 (2004).
28. C. M. van Golen, M. E. Soules, A. R. Grauman, E. L. Feldman, N-Myc overexpression leads to decreased  $\beta$ 1 integrin expression and increased apoptosis in human neuroblastoma cells. *Oncogene* **22**, 2664–2673 (2003).
29. Y.-T. Tai, K. Podar, L. Catley, Y.-H. Tseng, M. Akiyama, R. Shringarpure, R. Burger, T. Hideshima, D. Chauhan, N. Mitsiades, P. Richardson, N. C. Munshi, C. R. Kahn, C. Mitsiades, K. C. Anderson, Insulin-like growth factor-1 induces adhesion and migration in human multiple myeloma cells via activation of  $\beta$ 1-integrin and phosphatidylinositol 3'-kinase/AKT signaling. *Cancer Res.* **63**, 5850–5858 (2003).
30. M. Edderkaoui, P. Hong, J. K. Lee, S. J. Pandol, A. S. Gukovskaya, Insulin-like growth factor-I receptor mediates the prosurvival effect of fibronectin. *J. Biol. Chem.* **282**, 26646–26655 (2007).
31. W. D. W. Heston, Characterization and glutamyl preferring carboxypeptidase function of prostate specific membrane antigen: A novel folate hydrolase. *Urology* **49**, 104–112 (1997).
32. R. S. Israeli, C. T. Powell, W. R. Fair, W. D. W. Heston, Molecular cloning of a complementary DNA encoding a prostate-specific membrane antigen. *Cancer Res.* **53**, 227–230 (1993).
33. J. T. Pinto, B. P. Suffoletto, T. M. Berzin, C. H. Qiao, S. Lin, W. P. Tong, F. May, B. Mukherjee, W. D. Heston, Prostate-specific membrane antigen: A novel folate hydrolase in human prostatic carcinoma cells. *Clin. Cancer Res.* **2**, 1445–1451 (1996).
34. M. Eder, M. Eisenhut, J. Babich, U. Haberkorn, PSMA as a target for radiolabelled small molecules. *Eur. J. Nucl. Med. Mol. Imaging* **40**, 819–823 (2013).
35. J. P. Dassie, L. I. Hernandez, G. S. Thomas, M. E. Long, W. M. Rockey, C. A. Howell, Y. Chen, F. J. Hernandez, X. Y. Liu, M. E. Wilson, L.-A. Allen, D. A. Vaena, D. K. Meyerholz, P. H. Giangrande, Targeted inhibition of prostate cancer metastases with an RNA aptamer to prostate-specific membrane antigen. *Mol. Ther.* **22**, 1910–1922 (2014).
36. R. E. Conway, N. Petrovic, Z. Li, W. Heston, D. Wu, L. H. Shapiro, Prostate-specific membrane antigen regulates angiogenesis by modulating integrin signal transduction. *Mol. Cell Biol.* **26**, 5310–5324 (2006).
37. R. E. Conway, K. Joiner, A. Patterson, D. Bourgeois, R. Rampp, B. C. Hannah, S. McReynolds, J. M. Elder, H. Gilfilen, L. H. Shapiro, Prostate specific membrane antigen produces pro-angiogenic laminin peptides downstream of matrix metalloprotease-2. *Angiogenesis* **16**, 847–860 (2013).
38. C. L. Grant, L. A. Caromile, K. Durrani, M. M. Rahman, K. P. Claffey, G.-H. Fong, L. H. Shapiro, Prostate specific membrane antigen (PSMA) regulates angiogenesis independently of VEGF during ocular neovascularization. *PLOS ONE* **7**, e41285 (2012).
39. D. J. Bacich, E. Ramadan, D. S. O'Keefe, N. Bukhari, I. Wegorzewska, O. Ojefifo, R. Olszewski, C. C. Wrenn, T. Bzdega, B. Wroblewska, W. D. W. Heston, J. H. Neale, Deletion of the glutamate carboxypeptidase II gene in mice reveals a second enzyme activity that hydrolyzes N-acetylaspartylglutamate. *J. Neurochem.* **83**, 20–29 (2002).
40. J. R. Gingrich, R. J. Barrios, B. A. Foster, N. M. Greenberg, Pathologic progression of autochthonous prostate cancer in the TRAMP model. *Prostate Cancer Prostatic Dis.* **2**, 70–75 (1999).
41. N. M. Greenberg, F. DeMayo, M. J. Finegold, D. Medina, W. D. Tilley, J. O. Aspinall, G. R. Cunha, A. A. Donjacour, R. J. Matusik, J. M. Rosen, Prostate cancer in a transgenic mouse. *Proc. Natl. Acad. Sci. U.S.A.* **92**, 3439–3443 (1995).
42. R. E. Conway, C. Rojas, J. Alt, Z. Nováková, S. M. Richardson, T. C. Rodrick, J. L. Fuentes, N. H. Richardson, J. Attalla, S. Stewart, B. Fahmy, C. Barinka, M. Ghosh, L. H. Shapiro, B. S. Slusher, Prostate-specific membrane antigen (PSMA)-mediated laminin proteolysis generates a pro-angiogenic peptide. *Angiogenesis* **19**, 487–500 (2016).
43. J. R. Gingrich, R. J. Barrios, R. A. Morton, B. F. Boyce, F. J. DeMayo, M. J. Finegold, R. Angelopoulos, J. M. Rosen, N. M. Greenberg, Metastatic prostate cancer in a transgenic mouse. *Cancer Res.* **56**, 4096–4102 (1996).
44. C. Rojas, S. T. Frazier, J. Flanary, B. S. Slusher, Kinetics and inhibition of glutamate carboxypeptidase II using a microplate assay. *Anal. Biochem.* **310**, 50–54 (2002).

45. A. Suttie, A. Nyska, J. K. Haseman, G. J. Moser, T. R. Hackett, T. L. Goldsworthy, A grading scheme for the assessment of proliferative lesions of the mouse prostate in the TRAMP model. *Toxicol. Pathol.* **31**, 31–38 (2003).
46. M. Zhang, D. E. Latham, M. A. Delaney, A. Chakravarti, Survivin mediates resistance to antiandrogen therapy in prostate cancer. *Oncogene* **24**, 2474–2482 (2005).
47. R. K. Jain, Normalization of tumor vasculature: An emerging concept in antiangiogenic therapy. *Science* **307**, 58–62 (2005).
48. H.-J. Shin, S. B. Rho, D. C. Jung, I.-O. Han, E.-S. Oh, J.-Y. Kim, Carbonic anhydrase IX (CA9) modulates tumor-associated cell migration and invasion. *J. Cell Sci.* **124**, 1077–1087 (2011).
49. Y.-T. Oh, D. W. C. Chen, G. J. Dougherty, W. H. McBride, Adenoviral interleukin-3 gene-radiation therapy for prostate cancer in mouse model. *Int. J. Radiat. Oncol. Biol. Phys.* **59**, 579–583 (2004).
50. K. Takeuchi, F. Ito, Receptor tyrosine kinases and targeted cancer therapeutics. *Biol. Pharm. Bull.* **34**, 1774–1780 (2011).
51. A. M. Xu, P. H. Huang, Receptor tyrosine kinase coactivation networks in cancer. *Cancer Res.* **70**, 3857–3860 (2010).
52. Y. H. Soung, J. L. Clifford, J. Chung, Crosstalk between integrin and receptor tyrosine kinase signaling in breast carcinoma progression. *BMB Rep.* **43**, 311–318 (2010).
53. P. A. Kiely, A. Sant, R. O'Connor, RACK1 is an insulin-like growth factor 1 (IGF-1) receptor-interacting protein that can regulate IGF-1-mediated Akt activation and protection from cell death. *J. Biol. Chem.* **277**, 22581–22589 (2002).
54. W. Zhang, C. S. Zong, U. Hermanto, P. Lopez-Bergami, Z. Ronai, L.-H. Wang, RACK1 recruits STAT3 specifically to insulin and insulin-like growth factor 1 receptors for activation, which is important for regulating anchorage-independent growth. *Mol. Cell. Biol.* **26**, 413–424 (2006).
55. H. S. Lee, S. J. Millward-Sadler, M. O. Wright, G. Nuki, R. Al-Jamal, D. M. Salter, Activation of Integrin-RACK1/PKCo signalling in human articular chondrocyte mechanotransduction. *Osteoarthritis Cartilage* **10**, 890–897 (2002).
56. J. Liliental, D. D. Chang, RACK1, a receptor for activated protein kinase C, interacts with integrin  $\beta$  subunit. *J. Biol. Chem.* **273**, 2379–2383 (1998).
57. S. Shukla, N. Bhaskaran, M. A. Babcook, P. Fu, G. T. MacLennan, S. Gupta, Apigenin inhibits prostate cancer progression in TRAMP mice via targeting PI3K/Akt/FoxO pathway. *Carcinogenesis* **35**, 452–460 (2014).
58. S. Shukla, G. T. MacLennan, S. R. Marengo, M. I. Resnick, S. Gupta, Constitutive activation of PI3K-Akt and NF- $\kappa$ B during prostate cancer progression in autochthonous transgenic mouse model. *Prostate* **64**, 224–239 (2005).
59. H. Hu, Y. Chai, L. Wang, J. Zhang, H. J. Lee, S.-H. Kim, J. Lü, Pentagalloylglucose induces autophagy and caspase-independent programmed deaths in human PC-3 and mouse TRAMP-C2 prostate cancer cells. *Mol. Cancer Ther.* **8**, 2833–2843 (2009).
60. A. M. Sargeant, R. D. Klein, R. C. Rengel, S. K. Clinton, S. K. Kulp, Y. Kashida, M. Yamaguchi, X. Wang, C.-S. Chen, Chemopreventive and bioenergetic signaling effects of PDK1/Akt pathway inhibition in a transgenic mouse model of prostate cancer. *Toxicol. Pathol.* **35**, 549–561 (2007).
61. M. Shimizu, Y. Shirakami, H. Moriwaki, Targeting receptor tyrosine kinases for chemoprevention by green tea catechin, EGCG. *Int. J. Mol. Sci.* **9**, 1034–1049 (2008).
62. G. E. Wynant, G. P. Murphy, J. S. Horoszewicz, C. E. Neal, B. D. Collier, E. Mitchell, G. Purnell, I. Tyson, A. Heal, H. Abdel-Nabi, G. Winzelberg, Immunoscintigraphy of prostatic cancer: Preliminary results with  $^{111}\text{In}$ -labeled monoclonal antibody 7E11-C5.3 (CYT-356). *Prostate* **18**, 229–241 (1991).
63. D. G. Bostwick, A. Pacelli, M. Blute, P. Roche, G. P. Murphy, Prostate specific membrane antigen expression in prostatic intraepithelial neoplasia and adenocarcinoma: A study of 184 cases. *Cancer* **82**, 2256–2261 (1998).
64. P. Wolf, N. Freudenberg, P. Bühler, K. Alt, W. Schultze-Seemann, U. Wetterauer, U. Elsässer-Beile, Three conformational antibodies specific for different PSMA epitopes are promising diagnostic and therapeutic tools for prostate cancer. *Prostate* **70**, 562–569 (2010).
65. D. A. Silver, I. Pellicer, W. R. Fair, W. D. Heston, C. Cordon-Cardo, Prostate-specific membrane antigen expression in normal and malignant human tissues. *Clin. Cancer Res.* **3**, 81–85 (1997).
66. A. Ghosh, X. Wang, E. Klein, W. D. W. Heston, Novel role of prostate-specific membrane antigen in suppressing prostate cancer invasiveness. *Cancer Res.* **65**, 727–731 (2005).
67. V. Yao, D. J. Bacich, Prostate specific membrane antigen (PSMA) expression gives prostate cancer cells a growth advantage in a physiologically relevant folate environment in vitro. *Prostate* **66**, 867–875 (2006).
68. V. Yao, A. Parwani, C. Maier, W. D. Heston, D. J. Bacich, Moderate expression of prostate-specific membrane antigen, a tissue differentiation antigen and folate hydrolase, facilitates prostate carcinogenesis. *Cancer Res.* **68**, 9070–9077 (2008).
69. A. A. Hurwitz, B. A. Foster, J. P. Allison, N. M. Greenberg, E. D. Kwon, The TRAMP mouse as a model for prostate cancer. *Curr. Protoc. Immunol.* **Chapter 20**, Unit 20.5 (2001).
70. I. Heidegger, P. Massoner, N. Sampson, H. Klocker, The insulin-like growth factor (IGF) axis as an anticancer target in prostate cancer. *Cancer Lett.* **367**, 113–121 (2015).
71. M. Pollak, Insulin and insulin-like growth factor signalling in neoplasia. *Nat. Rev. Cancer* **8**, 915–928 (2008).
72. A. Belfiore, R. Malaguamera, Insulin receptor and cancer. *Endocr. Relat. Cancer* **18**, R125–R147 (2011).
73. A. Guille, M. Chaffanet, D. Birnbaum, Signaling pathway switch in breast cancer. *Cancer Cell Int.* **13**, 66 (2013).
74. P. J. Kaplan, S. Mohan, B. A. Foster, N. M. Greenberg, The insulin-like growth factor axis and prostate cancer: Lessons from the transgenic adenocarcinoma of mouse prostate (TRAMP) model. *Cancer Res.* **59**, 2203–2209 (1999).
75. J.-J. Li, D. Xie, RACK1, a versatile hub in cancer. *Oncogene* **34**, 1890–1898 (2015).
76. S. Shi, Y.-Z. Deng, J.-S. Zhao, X.-D. Ji, J. Shi, Y.-X. Feng, G. Li, J.-J. Li, D. Zhu, H. P. Koeffler, Y. Zhao, D. Xie, RACK1 promotes non-small-cell lung cancer tumorigenicity through activating sonic hedgehog signaling pathway. *J. Biol. Chem.* **287**, 7845–7858 (2012).
77. U. Haberkorn, M. Eder, K. Kopka, J. W. Babich, M. Eisenhut, New strategies in prostate cancer: Prostate-specific membrane antigen (PSMA) ligands for diagnosis and therapy. *Clin. Cancer Res.* **22**, 9–15 (2016).
78. K. L. S. Chatalic, S. Heskamp, M. Konijnenberg, J. D. M. Molkenboer-Kuening, G. M. Franssen, M. C. Clahsen-van Groningen, M. Schottelius, H.-J. Wester, W. M. van Weerden, O. C. Boerman, M. de Jong, Towards personalized treatment of prostate cancer: PSMA I&T, a promising prostate-specific membrane antigen-targeted theranostic agent. *Theranostics* **6**, 849–861 (2016).
79. T. Ganguly, S. Dannoon, M. R. Hopkins, S. Murphy, H. Cahaya, J. E. Blecha, S. Jivan, C. R. Drake, C. Barinka, E. F. Jones, H. F. VanBrocklin, C. E. Berkman, A high-affinity [ $^{18}\text{F}$ ]-labeled phosphoramidate peptidomimetic PSMA-targeted inhibitor for PET imaging of prostate cancer. *Nucl. Med. Biol.* **42**, 780–787 (2015).
80. S. A. Rajasekaran, G. Anilkumar, E. Oshima, J. U. Bowie, H. Liu, W. Heston, N. H. Bander, A. K. Rajasekaran, A novel cytoplasmic tail MXXXL motif mediates the internalization of prostate-specific membrane antigen. *Mol. Biol. Cell* **14**, 4835–4845 (2003).
81. J. P. Dassie, X.-y. Liu, G. S. Thomas, R. M. Whitaker, K. W. Thiel, K. R. Stockdale, D. K. Meyerholz, A. P. McCaffrey, J. O. McNamara II, P. H. Giangrande, Systemic administration of optimized aptamer-siRNA chimeras promotes regression of PSMA-expressing tumors. *Nat. Biotechnol.* **27**, 839–846 (2009).
82. J. P. Dassie, P. H. Giangrande, Current progress on aptamer-targeted oligonucleotide therapeutics. *Ther. Deliv.* **4**, 1527–1546 (2013).
83. J. J. Christiansen, S. A. Rajasekaran, P. Moy, A. Butch, L. Goodglick, Z. Gu, R. E. Reiter, N. H. Bander, A. K. Rajasekaran, Polarity of prostate specific membrane antigen, prostate stem cell antigen, and prostate specific antigen in prostate tissue and in a cultured epithelial cell line. *Prostate* **55**, 9–19 (2003).
84. C. H. Tsai, J.-H. Hong, K.-F. Hsieh, H.-W. Hsiao, W.-L. Chuang, C.-C. Lee, W. H. McBride, C.-S. Chiang, Tetracycline-regulated intratumoral expression of interleukin-3 enhances the efficacy of radiation therapy for murine prostate cancer. *Cancer Gene Ther.* **13**, 1082–1092 (2006).
85. N. E. Sanjana, O. Shalem, F. Zhang, Improved vectors and genome-wide libraries for CRISPR screening. *Nat. Methods* **11**, 783–784 (2014).
86. O. Shalem, N. E. Sanjana, E. Hartenian, X. Shi, D. A. Scott, T. S. Mikkelsen, D. Heckl, B. L. Ebert, D. E. Root, J. G. Doench, F. Zhang, Genome-scale CRISPR-Cas9 knockout screening in human cells. *Science* **343**, 84–87 (2014).
87. E. K. Brinkman, T. Chen, M. Amendola, B. van Steensel, Easy quantitative assessment of genome editing by sequence trace decomposition. *Nucleic Acids Res.* **42**, e168 (2014).

**Acknowledgments:** We thank the UCONN Health Histology Core for the processing and sectioning of samples as well as for the use of their microscopes, and the UCONN Health Human Genome Editing Core for CRISPR construction and sequencing. **Funding:** This work was supported by NIH NCI Mentored Research Scientist Development Award to Promote Diversity (K01CA188412) to L.A.C. and the Prostate Cancer Foundation and the Department of Defense Prostate Cancer Program (PC073976) to L.H.S. The funders had no role in the study design, data collection and analysis, decision to publish, or preparation of the manuscript. **Author contributions:** L.A.C. and L.H.S. designed the project; L.A.C., K.D., M.M.R., and C.L.G. performed experiments; C.S. was responsible for the CRISPR construction and sequencing; F.A.F. provided clinical and urological expertise; and L.A.C. and L.H.S. wrote the manuscript. **Competing interests:** The authors declare that they have no competing interests.

Submitted 27 June 2016  
Accepted 24 February 2017  
Published 14 March 2017  
10.1126/scisignal.aag3326

**Citation:** L. A. Caromile, K. Dortche, M. M. Rahman, C. L. Grant, C. Stoddard, F. A. Ferrer, L. H. Shapiro, PSMA redirects cell survival signaling from the MAPK to the PI3K-AKT pathways to promote the progression of prostate cancer. *Sci. Signal.* **10**, eaag3326 (2017).

## PSMA redirects cell survival signaling from the MAPK to the PI3K-AKT pathways to promote the progression of prostate cancer

Leslie Ann Caromile Kristina Dortche M. Mamunur Rahman Christina L. Grant Christopher Stoddard Fernando A. Ferrer Linda H. Shapiro

*Sci. Signal.*, 10 (470), eaag3326. • DOI: 10.1126/scisignal.aag3326

### PSMA is more than a diagnostic marker

Detection of prostate-specific membrane antigen (PSMA) diagnoses aggressive prostate cancer and predicts poor prognosis in patients. Using mouse models and tumor cell cultures, Caromile *et al.* found that the presence of PSMA on the surface of prostate tumor cells directs proliferative signaling through one pathway over another by disrupting the interaction of a receptor tyrosine kinase complex with an intracellular scaffolding protein. The findings suggest that patients with PSMA-positive tumors may benefit from PI3K-AKT pathway inhibitors and reveal a tumorigenic role for this traditionally diagnostic marker.

### View the article online

<https://www.science.org/doi/10.1126/scisignal.aag3326>

### Permissions

<https://www.science.org/help/reprints-and-permissions>

Use of this article is subject to the [Terms of service](#)

# UConn

## SCHOOL OF MEDICINE

**Position:** Postdoctoral Position in Prostate Cancer Health Disparities

**Employer:** University of Connecticut Health Center (UConn Health)

**Department:** Center for Vascular Biology, Department of Cell Biology

**Location:** Farmington, CT USA

**This postdoctoral position is available in the laboratory of Dr. Leslie Caromile, PhD.**

**Position description:** Dr. Leslie Caromile has partnered with physician scientists in the Division of Urology at University of Connecticut Health Center to advance our understanding and improve diagnosis of individuals with aggressive prostate cancer. The Caromile laboratory is seeking a highly-motivated postdoctoral candidate committed to a translational project that examines the molecular underpinnings of prostate cancer health disparities. The successful applicant will apply detailed molecular, biochemical, cellular, genomic and bioinformatic approaches to functionally annotate and assess risk of previously identified germline coding SNP's within specific prostate cancer oncogenic signaling pathways. Experiments will also use primary patient samples, *in vitro* cell culture, *in vivo* transgenic and xenograft cancer models. Laboratories are located at the University of Connecticut Health Center (<http://www.uchc.edu>), a state-of-the-art research facility with a diverse graduate/medical/dental program and an attractive campus centrally located between New York and Boston Access. The candidate will have access to extensive core facilities including the Center for Genome Innovation, the Center for Cell Analysis and Modeling as well as flow cytometry and a transgenic mouse core thus offering the trainee wide latitude in the design and pursuit of their research questions. The University of Connecticut Health Center is dedicated to building a diverse community and offers a wide array of training opportunities for early career scientists.

**Qualifications:** Successful candidates should have or be very close to obtaining a PhD within the biomedical sciences from an accredited university or have less than 2 years postdoctoral experience. Applicants should have a strong background in cancer research, as well as proven expertise in molecular/cellular biology, biochemistry, genomics and bioinformatics. A demonstrated record of scientific accomplishment evidenced by at least one first-author paper, a strong work ethic, and strong intellectual commitments to cancer research and to the individual research project, are essential. The successful candidate should possess excellent interpersonal and organizational skills, and stellar communication skills with fluency in both spoken and written English.

**To apply:** Suitably qualified candidates are encouraged to submit their CV, cover letter, and names and contact information of three references to **Dr. Leslie Caromile** at [caromile@uchc.edu](mailto:caromile@uchc.edu).

Salary will be commensurate with research experience.